

Master's thesis

Haptic shared control improves teleoperated task performance towards performance in direct control

H.Boessenkool

Delft, 26th of January 2011

Report Number: 1126
Student Number: 1230581

Delft University of Technology
Faculty of 3mE
Department of BioMechanical Engineering

Haptic shared control improves tele-operated task performance towards performance in direct control

Henri Boessenkool

Committee:

Prof. Dr. F.C.T. van der Helm	Department of BioMechanical Engineering, 3mE
Dr. Ir. D.A. Abbink	Department of BioMechanical Engineering, 3mE
Prof. Ir. R.H. Munnig Schmidt	Department of Precision and Microsystems Engineering, Mechatronic System Design, 3ME
Dr. Ir. C.J.M. Heemskerk	Heemskerk Innovative Technology B.V.

Coaches:

Dr. Ir. D.A. Abbink
Dr. Ir. C.J.M. Heemskerk

Preface

You are about to read the results of the study I conducted in favour of my Master's thesis. This study was about haptic shared control in tele-manipulation. During this study I worked on the design and testing of a new haptic shared control application. I enjoyed working on this subject which is on the frontline of tele-manipulation research; until now most research focused on transparency to improve task performance, while this study shows that haptic shared control is a more effective approach. It was interesting to see how haptic shared control is able to bring together the inventiveness and complexity of human and the extensive possibilities of robotic devices.

The various sides that were involved made this study nice to accomplish. One part of this study was the design of shared control and the adaption of the test setup, including the very practical aspects of implementing sensors and other hardware. Next to this, a human factor experiment was involved, which included the testing of subjects. Finally the measured data had to be processed and analyzed and a report had to be written.

The focus of this study is a human factors experiment, which is described in detail in a research paper. The appendices provide background information and give a broad overview of the accomplished work. These appendices allow future students and researchers to gain detailed insight in the challenges faced during this study.

The experimental setup is described in Appendix A. Appendix B shows the work done on modelling of the effects of shared control. Appendix C contains a description of the shared control design and implementation. The shared control experiment is described in Appendix D, including an extensive overview of the results. Appendix E contains a submitted conference paper, presenting a brief overview of the results. Finally, Appendix F shows some interesting insights gained during this research.

An USB-stick containing used literature, software, raw measurement data and other information that could be of interest, was submitted to the Biomechanical Engineering depository and is available on request.

I want to thank all people who contributed to this study. Special thanks to my coaches; David and Cock, thanks for all inspiring discussions and your efforts commenting and reviewing my work. Finally I want to thank my wife Juliët; thanks for your support especially during the last straws.

Haptic shared control improves tele-operated task performance towards performance in direct control

Henri Boessenkool^{1,2}, David A. Abbink¹, Cock J.M. Heemskerk² and Frans C.T. van der Helm¹

Abstract— In tele-operation, haptic feedback from the remote environment to the human is often limited, which has been shown to negatively influence the performance and required time of tasks. The conventional research focus is on improving the quality of the haptic feedback (transparency), which may have led to significant improvement, but is still imperfect, with many unresolved issues. The present study presents an alternative approach to improve tele-operated tasks: by offering haptic shared control in which both operator and support system apply the required forces at the input (master) device. It is hypothesized that virtual forces from well-designed shared control will improve required time and accuracy, with less control effort, and that these benefits exist for perfect transparency but even more so for imperfect transparency. In an experimental study haptic shared control was designed to aid operators ($n=9$) with performing a simple bolt-spanner task using a planar (2D, 3DOF) tele-operator setup. Haptic shared control was compared to normal operation for three types of control: the baseline condition of direct control at the master (perfect transparency), teleoperation with a simple PERR controller, and a PERR controller with feedback gains set to zero (no transparency). The experimental results provided evidence for the hypotheses, showing that all tested tele-manipulation tasks benefit from haptic shared control, for all three levels of transparency. Essentially, the presence of haptic shared control allows for a worse transparency without compromising accuracy or required time, and can even improve accuracy and required time during perfect transparency. Subjective results indicated that the shared control was perceived as helpful and beneficial.

Index Terms—Tele-operation, haptic guidance, haptic shared control, transparency, task performance, human factors experiment

1 INTRODUCTION

Human beings are intelligent and dexterous and are able to perform many complex (manipulation) tasks like surgery, (dis-)assembly and maintenance. Though many complex tasks can be taken over by robots, one of the unique abilities of humans remains their ability to deal well with unexpected circumstances and changing environments. There are circumstances where the abilities of both human and robots are needed. One might think of complex tasks that need to be executed in unpredictable environments where human can not directly interact, due to for example the hostile nature of the environment (such as deep sea and nuclear or toxic environments) or due to dimension constraints (such as micro-assembly or minimal invasive surgery). In such cases issues like safety, responsibility [30], and costs restrict the usability of full automation, and the human-in-the-loop approach using tele-manipulation robots is commonly used [13], [27]. Figure 1 shows a schematic representation of the total system of human operator, telemanipulator and environment, which will be referred to as the Connected Tele-manipulator System (CTS)[9].

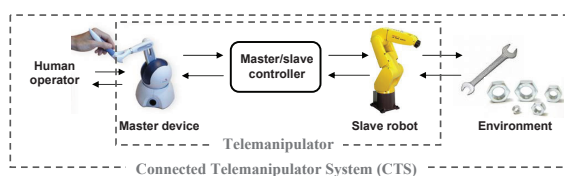


Fig. 1. The five components of the Connected Tele-manipulation System (CTS), adapted from [9]

Tele-manipulation robots essentially extend the human's sensorimotor facilities to a remote location, which should give the sensation of actually being at that location performing the task (telepresence

[29]). Good telepresence is achieved by accurate visual and audio representation of the (interaction with the) remote location, but also by translating the human's interaction forces on the master device to interaction forces between the remote environment and slave robot, and vice versa.

One of the main challenges in the field remains the accurate rendition of these forces, often called transparency. Previous research showed that providing force feedback from the environment to the human improves task performance [12],[17] and reduces cognitive workload [31]. However, the quality of the provided force feedback is often limited due to technical issues. Great efforts have been made over the past decades to improve transparency, and although substantial progress has been made [19],[21],[11],[7] and [9], optimal transparency is not yet realized. Another approach is then not to focus on achieving optimal transparency but to focus on optimal task performance. This approach was initially used by Rosenberg [28], presenting virtual fixtures which worked as a virtual ruler assisting a tele-manipulated peg-in-hole task. The addition of artificial guiding forces resulted in a large improvement in task performance. This research laid foundation for further research in haptic shared control, combining automation and manual control. The main application of shared control that is found in current literature is on operational assistance; guiding to a certain reference position [28],[22],[8], protecting areas [25],[6] and disturbance reduction [4],[23]. An example is the continuous haptic guiding during car following [4] and curve negotiation [23] proposed by Abbink and Mulder. These studies show that haptic shared control solutions look very promising for tele-manipulation. Most of this research is however limited to 1 or 2 degrees of freedom and/or focused on motions in free air. Furthermore continuous guiding seems promising, but is not often applied yet.

A promising way to improve tele-operated task performance is the extension of the haptic shared control approaches, as found in literature described above, to a continuous cooperation between operator and support system. Ideally haptic shared control should be implemented in such a way that the control can shift smoothly between operator and support system, optimizing the human-machine interaction.

A metaphor of haptic shared control is horse-riding [15]. The rider is in control, and guides the horse. But the horse can find a way by itself in case the rider loosens his or her control for a moment. Through the forces on the reins, control authority is switched smoothly back and forth between horse and rider.

¹ Department of BioMechanical Engineering, Faculty of 3mE, Delft University of Technology, Mekelweg 2, Delft, The Netherlands, (contact: d.a.abbink@tudelft.nl)

² Heemskerk Innovative Technology, Jonckerweg 20, 2201 DZ Noordwijk, The Netherlands, (contact: c.heemskerk@heemskerk-innovative.nl)

To implement continuous haptic shared control on more degrees of freedom, this research proposes a haptic shared control for telemanipulation based on the principle used by Abbink and Mulder [5]. The haptic shared control system is an intelligent system which calculates the ideal control action based on sensor information (e.g. about the slave robot, and the environment it interacts with). This ideal control action is presented as a force on the master device, so the operator continuously feels the optimal control action. The system will help the operator to execute this optimal action, but the operator can always resist the assisting forces if he does not agree with the system. A general scheme of the proposed haptic shared control is illustrated in figure 2.

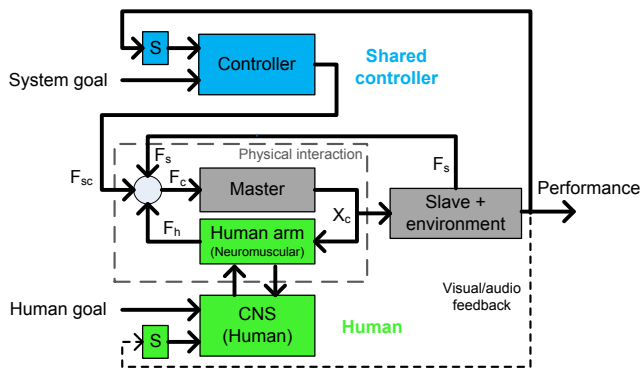


Fig. 2. A schematic representation of haptic shared control. The guiding system receives feedback by sensors (S) and uses a control model to continuously calculate the optimal guiding force F_{sc} , which is presented at the master side. The control input to the master (X_c) is affected by the feedback forces from the slave (F_c) and may now be simultaneously influenced by both the human (F_h) and the shared control system (F_{sc}) [adapted from [5]].

When designing a haptic shared control system, it is important to understand that human tune their visual and haptic feedback differently and use a different control strategy for every different type of motion. The design of a proper haptic shared control system should consider these different types of motion. Based on Aliaga [7] Wildenbeest proposed four fundamental types of motion [32]. For each of these fundamental motion types a different guiding strategy was proposed:

1. *Free Air Movement*. The slave robot has no interaction with the environment. Proposed guiding strategy for haptic shared control: Guiding of tool position and orientation to the *ideal* path.
2. *Contact Transition*. The slave robot moves close to a surface and makes contact. Proposed guiding strategy for haptic shared control: Position and orientation guiding. Guiding prevents hard collision by an artificial damping.
3. *Constrained Position Movement*. One or more degrees of freedom of the slave robot are constrained (e.g. moving over a surface, coaxial sliding of pipes). Proposed guiding strategy for haptic shared control: Guiding of tool position and orientation.
4. *Constrained Force Movement*. A motion in which forces/torques have to be controlled in one or more degrees of freedom (e.g. polishing a pipe, cutting human tissue). Proposed guiding strategy for haptic shared control: Guiding places rotation/compliance center at the bolt origin (guiding forces only perpendicular to the force movement).

Figure 2 shows that both human and the haptic shared control system have a *goal* input. Ideally, the haptic shared control system should be able to figure out the human goal (intention and strategy) and adapt to this goal. The shared control system used in the current

Table 1. Hypotheses about the effect of shared control on task performance for different levels of transparency. Direct control is taken as baseline (denoted as '0').

	Ideal	Transparency	No
F1:	Direct Control	Teleoperation - Force Feedback	Teleoperation - No Force Feedback
No Shared Control	0	-	--
Shared Control	+	+	+

study deviates from the system shown in figure 2 in that the shared control system determines the goal (e.g. the ideal path), and shows this visually to the human. This "ideal" path is chosen and is not optimized to human motions.

The main objective of this research was to provide evidence that appropriately designed haptic shared control results in larger improvements in human-in-the-loop task performance than improving transparency. To test this, an experiment was designed using a simple bolt-and-spanner task [32], containing the four fundamental motion types. The subjects had to execute the task for three different levels of transparency: Direct Control (perfect transparency), tele-manipulation with force feedback and tele-manipulation without force feedback (no transparency). These conditions were tested with and without haptic shared control. It was hypothesized that reducing transparency will degrade task performance, while appropriate haptic shared control will increase task performance with respect to Direct Control, independent of the level of transparency (see table 1). Since Direct Control is the golden standard in transparency-oriented research, it is defined here as baseline condition. Moreover it is expected that the hypotheses for the total task will be reflected in time performance for the four individual subtasks. Since all subtasks contain movement, the use of haptic shared control is expected to improved time performance for all subtasks. The level of transparency is expected to have no influence on time performance during Free Air Movement, since Free Air Movement is mainly a visual task.

2 METHODS

2.1 Subjects

The proposed shared control was tested on a group of 9 male subjects. The mean age of the subjects was 26.1 (1.05) year. All subjects were right handed and master students of the department Mechanical Engineering at the Delft University of Technology. None of the subjects had experience with teleoperators. The subjects participated voluntarily and did not receive a financial compensation for their efforts.

2.2 Task description

The subjects were asked to take place in front of the master device and hold the interface of the master device like a normal spanner. Subsequently the following bolt-and-spanner task had to be executed (see also figure 3); start at the lower y-limit, move to points 1, 2 and 3, move to the bolt, slide the spanner over the bolt, and rotate the bolt to the visible reference angle. The subjects were asked to perform this task as fast as possible. The locations of the target points were respectively: $(x, y, \theta) = (0m, 0m, 0^\circ)$, $(0m, 0.02m, 0^\circ)$, $(-0.06m, 0.07m, 0^\circ)$, $(0.06m, 0.08m, 65^\circ)$ and the bolt position $(x, y) = (0m, 0.12m)$.

These instructions were handed out to the subjects and were verbally explained in addition by the experiment leader before the start of the experiment.

2.3 Experimental setup

The haptic shared control experiment was performed using a 3-DOF planar telemanipulation system. The system consists of a parallel

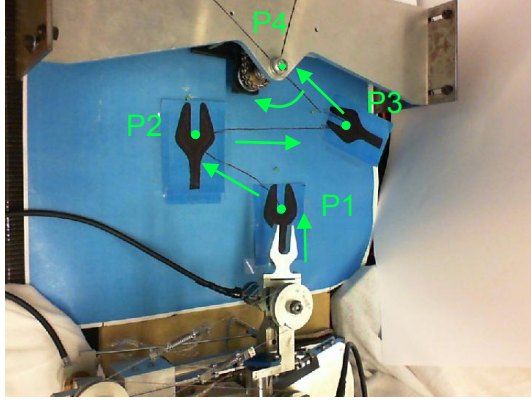


Fig. 3. Cameraview (tilted) from the environment at the slave side

force-redundant master device (see fig. 4) and a serial slave device (see fig. 5)

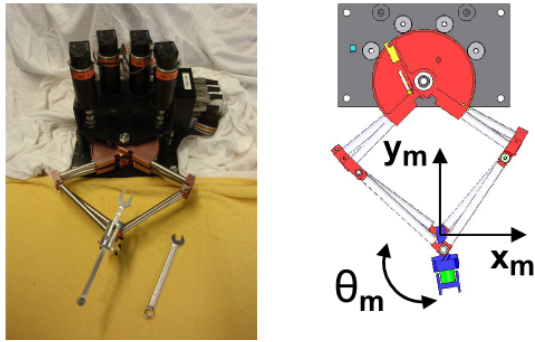


Fig. 4. A picture (left) and a schematic drawing (right) of the master device

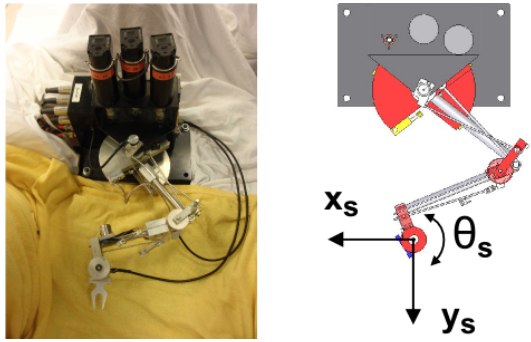


Fig. 5. A picture (left) and a schematic drawing (right) of the slave device

The controller ran on a Mathworks xPC Target real time operating system at 1kHz. The positional accuracy was 0.03mm and the minimal time delay between master and slave was estimated at 1.5ms (1ms measurement interval and 0.5 due to the zero-order hold of the analogy output [10]). The design of this telemanipulator is discussed in detail by Christiansson [9].

The device performance and stability was evaluated in by Wildenbeest [32] using the two-port network modeling framework [16]. The column *Force Feedback* in table 2 shows a summary of the most important analytic performance metrics for the tele-operator in PERR mode. The other two columns show the deduced values for the other transparency modes.

The setup was equipped to perform a bolt and spanner task. Both master and slave were equipped with a spanner interface. The slave

Table 2. Numerical Performance Metrics for the different levels of transparency

	Ideal <—	Transparency	—> No
	<i>Direct Control</i>	<i>Teleoperation - Force Feedback</i>	<i>Teleoperation - No Force Feedback</i>
Analytic Metrics			
free air m [kg]	0.23	0.52	0.23
free air b [Ns/m]	4.5	11	4.5
free air k [N/m]	0	0.027	0
stiff contact m [kg]	~inf	0.23	0.23
stiff contact b [Ns/m]	~inf	4.5	4.5
stiff contact k [N/m]	~inf	400	0
transparency error [-]	0	68	~ inf
Zwidth [-]	~ inf	31	~ 0

device was actuated using the series-elastic-actuation principle which provides the ability of estimating interaction forces at the slave side. Furthermore an accelerometer was mounted at the tip of the slave to measure the high frequency contact forces.

The (remote) environment consisted of a construction with an M6 bolt (figure 3). This construction could be placed at the slave or the master side. The torque required to rotate the bolt was artificially created by a friction force induced by a spring. The tightening torques to overcome static and dynamic friction were estimated to be respectively 35.7 (2.0) Nmm and 31.6 (6.0) Nmm. The rotation of the bolt was measured with an angle sensor.

2.4 Haptic shared control design

The haptic shared control design could be based on two fundamentally different types of guiding; *attractive* guiding [22],[23], creating guiding forces towards an ideal path and *repulsive* guiding [28],[6], preventing users to enter forbidden regions by presenting repulsive forces. Attractive motion guiding can be done in a *passive* or in an *active* way: passive guiding will not induce a motion by itself, active guidance however actively pushes the master to the (sub)goal and will induce a motion when the operator releases the master. A variety of shared control designs, partly based on the literature that was discussed above, was implemented and tested during a pilot experiment. Passive guiding based on an ideal path showed the best performance and was chosen for this experiment. This chosen guiding is not necessarily the optimal guiding and neither totally optimized, though suitable for a proof of principle.

The haptic shared control used for the experiments is described below per subtask:

1. *Free Air Movement.* A smooth path between the target points was chosen as ideal path (see red line in figure 3). The guiding forces were based on the 'look ahead' path error (E_2 in figure 6) [23], which is defined as the path error at an estimated position in future based on the current velocity vector and a look ahead time of 0.1s.

$$F_{shared-control} = -\vec{E}_2 * k_2 \quad (1)$$

The shared control stiffness was $k_2 = 120[N/m]$. Within a radius of 0.04m of the target points 1 to 3, guiding of the tool orientation was linear increased to a stiffness of 0.5 [Nm/rad].

2. *Contact Transition.* Within a radius of 0.05m of the bolt, the tool orientation guiding was linear increased to a stiffness of 0.5 [Nm/rad]. An artificial damping prevented hard collision.
3. *Constrained Position Movement.* The spanner was guided to the right orientation with a stiffness of 0.5 [Nm/rad]. Furthermore a snap-feature was introduced close to the bolt.
4. *Constrained Force Movement.* The presented guiding force was only perpendicular to the force movement. The snap-feature was

Table 3. The six experimental conditions

	Ideal ←	Transparency	→ No
F1:	<i>Direct Control</i>	<i>Teleoperation - Force Feedback</i>	<i>Teleoperation - No Force Feedback</i>
F2:			
<i>No Shared Control</i>	DC	FF	NoFF
<i>Shared Control</i>	DC-SC	FF-SC	NoFF-SC

active to ensure that the spanner stayed on the bolt head. In the *No Force Feedback* (NoFF) condition, the shared control system introduced a virtual rotation/compliance centre at the bolt origin.

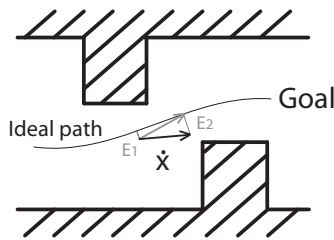


Fig. 6. Shared control design for free air movement. $E1$ shows the current path error and $E2$ the look ahead path error based on the current velocity \dot{x} and a defined look-ahead-time. The guiding force is based on the look ahead path error ($E2$), adapted from [23].

2.5 Experiment design

2.5.1 Experimental conditions

The two main factors of the experiment were two different types of haptic information: (F1) the 'level of transparency', and (F2) 'with/without haptic shared control'. These factors were combined into six experimental condition (see table 3). For statistical analyses a third factor 'subjects' (F3) was introduced to consider the variation between subjects.

Transparency was defined as how transparent the interaction forces were transmitted to the operator. The two extremes of these factor were *Direct Control* (DC), which gives perfect transparency, and *No Force Feedback* (NoFF), which gives no transparency. A third condition in between was *Force Feedback* (FF) using a classical PERR-controller. The FF and the NoFF conditions were tested in tele-manipulation configuration. The NoFF condition was tested by setting the PERR slave-to-master PD-gains to zero. For the DC condition, the environment was placed at the master side and the task was executed hands on using the spanner mounted at the master.

The experiment contained 8 repetitions of each of the six conditions per subject. Every subject started with the *Force Feedback* (FF) condition, to have a reference for the subjective measures. The remaining conditions were presented randomly to minimize learning effects during the experiment. The all trials were analysed for the total task, but also for the four fundamental subtasks; Free Air Movement, Contact Transition Movement, Constrained position Movement and Constrained Force Movement.

All subjects did have training sessions for each new condition in advance of the actual experiment.

2.5.2 Controlled variables

Visual feedback Visual feedback from the remote environment is very important during tele-manipulation tasks and is usually achieved by camera views. Yet in many cases the often hazardous environments limit the quality and available dept information, which increase the difficulty of the task for the human operator.

For all conditions of the experiment, the subjects were dependent on visual feedback from the (remote) environment by a camera view (see figure 3). This camera view had a limited resolution (960 x 544 pixels) and was displayed on a 14 inch laptop screen next to the setup. The camera was placed under an angle of 45 degrees with respect to the horizontal and could be placed at the slave or master side. This tilt of the camera was done to make the task more difficult (and realistic) by introducing dept effects.

Task instruction Upon executing a task human always have a (subconscious) preference for certain control strategies. In most cases, this control strategy has to do with a trade-off between energy consumption, accuracy and/or time. During the training trials preceding the experiments the subjects got an explicit instruction to perform the task with one of the two following control strategies:

1. *Accurate*; perform the task as accurate as possible. This would lead to optimisation of strategy towards low forces and positional accuracy.
2. *Fast*; perform the task as fast as possible. This would lead to optimisation of strategy towards time duration.

During the pilot study it appeared that testing both strategies on each subject resulted in a high burden on the subjects. Hence, during the actual experiments the subjects were instructed to perform the task *as fast as possible* for all conditions.

2.6 Measured variables & Metrics

To analyse the effect of shared control on tele-operated task performance, a vast amount of variables were recorded during the measurements, all sampled at 1 kHz. Based on the recorded data, a number of metrics were calculated to determine the performance. These metrics can be separated into two categories explained below:

Task performance metrics:

- t_{tc} Time-to-complete; the time it takes for a subject to complete the (sub)task.
- err_{int} Integrated path error; integration of the error with the ideal path.
- $F_{e,av}$ Average contact force; average of the measured interaction force with the environment.

Control effort metric:

- n_{rev} Reversal rate; number of steering corrections done by the human operator. The reversal rate can be seen as a measure for control effort of the subject to control the system.

Furthermore, the following subjective measures were tracked for all six conditions:

- Self reported workload using the NASA Task Load Index (NASA-TLX) [18]. A scale from 0 to 100 represents the amount of mental workload.
- The subjects were asked to grade their own performance with respect to accuracy and with respect to time performance. A 14 point scale from 1 to 8 was used; 1 represented 'very bad' and 8 represented 'very good'.
- The subjects were asked to rate the helpfulness of the shared control. A 16 point scale from -4 to 4 was used; -4 represented 'totally opposing' and 4 represented 'very helpful'.

2.7 Data analysis

A multi-variate analysis of variance (ANOVA) was used to evaluate the differences between the two experimental factors (F1 and F2) and between the subjects (F3). Because of the large variance between subjects, a multi-way ANOVA was considered as most suitable for further analyses. A two-way ANOVA was used to analyse the effects of shared control separately for the three different *transparency* conditions. The two factors in this two-way ANOVA were the experimental factor *haptic shared control* (F2), and the *between-subject variation* (F3).

Table 4. ANOVA results from the three factors on the four performance metrics. In the table, (●●●), (●●), (●) denote the significance of $p \leq 0.001$, $p \leq 0.01$ and $p \leq 0.05$ respectively, and (-) denotes no significance

	F1 Transparency	F2 SC	F3 SubjectV
ttc	●●●	●●●	●●●
err_{int}	-	●●●	-
$F_{e,av}$	-	-	●●
$n_{rev} - x$	-	●●●	●●●

Normality assumption was checked on all dependent variables ($p = 0.05$) to ensure the applicability of the statistical tests. Results were regarded as statistical significant when $p \leq 0.05$. In figures 7,8,11 and 13 and ANOVA tables 4,5 and 6 the marks (●●●), (●●), (●) denote the significance of $p \leq 0.001$, $p \leq 0.01$ and $p \leq 0.05$ respectively, and (-) denotes no significance

3 RESULTS

The experimental results for the entire bolt-and-spanner task were compared using a three-way ANOVA, taking into account the two experimental factors *transparency* (F1) and *haptic shared control* (F2), and also the *between-subject variation* (F3). The main results of the analysis are shown in table 4. The first column shows that transparency only influenced time-to-complete (ttc). Column two shows that shared control influenced time-to-complete (ttc), integrated path error (err_{int}) and the reversal rate (n_{rev}), but does not influence average contact force ($F_{e,av}$). The last column, representing the subjects, shows a large variation between subjects.

Note that average contact force ($F_{e,av}$) was only measured and analysed for the teleoperated conditions (FF and NoFF).

The performance metrics as defined in section 2.6 are separately presented in the upcoming paragraphs, followed by an analysis per subtask and subjective measures.

3.1 Effect of transparency and Haptic Shared Control on task performance

Figure 7 shows the time-to-complete for the entire task. The data is presented in box plots; the central mark is the median, the edges of the box are the 25th and 75th percentiles and the whiskers extend to the most extreme datapoint within 1.5 times interquartile range. With respect to transparency, it shows that the baseline (DC/perfect transparency) yields the shortest time to complete. Compared to DC, the FF and NoFF conditions showed an increased time-to-complete of respectively 24% ($p=0.0013$) and 48% ($p=0.0104$). Haptic shared control resulted in an improved time-to-complete of 19.7% ($p = 0.006$), 24.2% ($p = 0.0002$) and 31.9% ($p = 0.008$) for respectively the DC, FF and NoFF condition (see table 5). Subject did not show a significant difference ($p=0.692$) in time performance between perfect transparency (DC) and shared control without transparency (NoFF-SC).

The effect of haptic shared control on positional accuracy is shown in figure 9. This figure shows the DC motion trajectories of a typical subject. Compared to normal control, shared control showed less deviation and a lower nominal path error. Trajectory plots for FF and NoFF showed comparable results, indicating that transparency does not influence positional accuracy. Results for metric integrated path error are shown in figure 8. Transparency had no significant effect on path error, providing haptic shared control improved path error with 38% to 56% (see table 5).

The average force exerted on the environment during contact transition and constrained position motion is shown in figure 10. No significant difference was found between transparency and/or shared control conditions (see table 5).

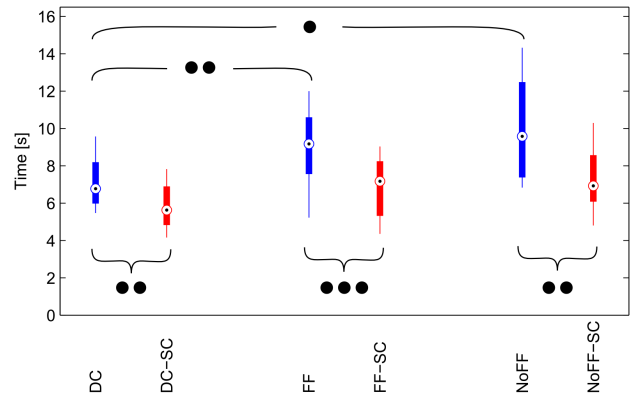


Fig. 7. Time-to-complete for the entire bolt-and-spanner task (9 subjects, 8 repetitions), shown for six conditions

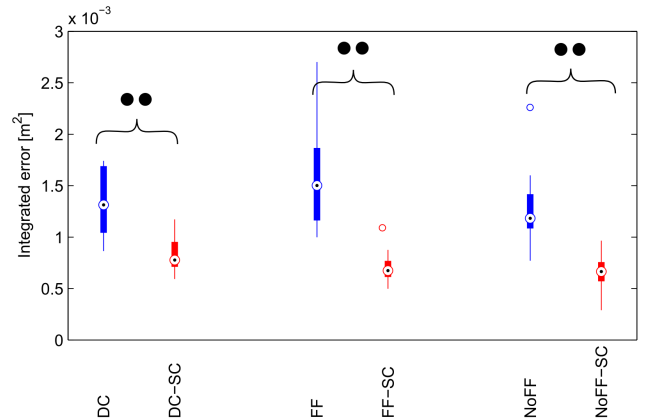


Fig. 8. Integrated error subtask Free Air Motion (9 subjects, 8 repetitions), shown for six conditions

3.2 Effect of transparency and Haptic Shared Control on control effort

Reversal rates for the entire bolt-and-spanner task are shown in figure 11 as control effort measure. Presented are the reversal rates in x-direction, but same trends were found in y- and rotational direction. Comparable to the results of integrated path error, no significant differences between the transparency conditions were found. Shared control resulted for all transparency conditions in significant decrease of the reversal rate (see table 5).

3.3 Influence of fundamental subtasks

The results above showed the effects of transparency and haptic shared control for the entire bolt-and-spanner task. Question remains how these effects are related to the four fundamental subtasks. Figure 12

Table 5. ANOVA results from the factor shared control (F2), shown for each transparency condition (F1)

F1:	DC	FF	NoFF
	F2: SC	F2: SC	F2: SC
ttc	●●	●●●	●●
err_{int}	●●	●●	●●
$F_{e,av}$	x	-	-
$n_{rev} - x$	●●	●●	●

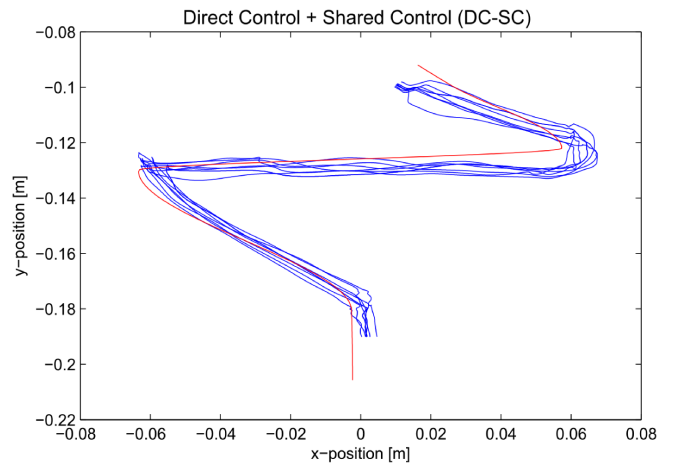
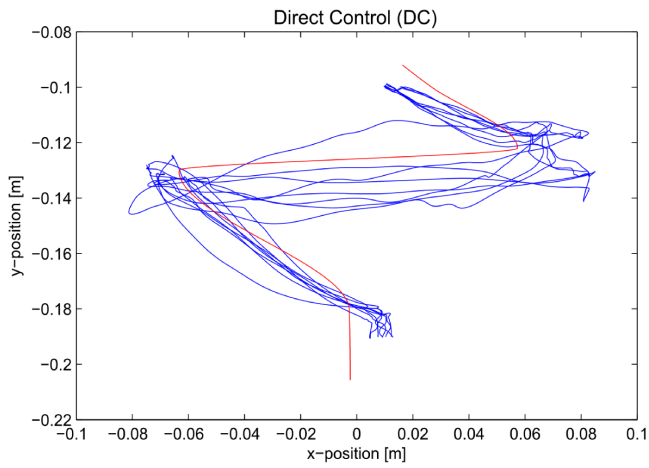


Fig. 9. Comparison of trajectories (2 x 8 repetitions) from a typical subject, both perfect transparency conditions (DC). Haptic shared control (right) results in a significant lower path deviation

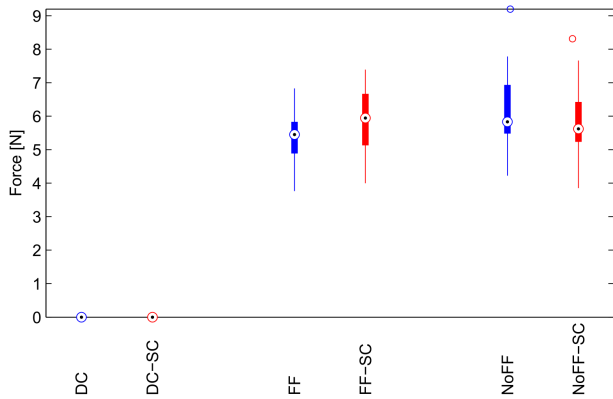


Fig. 10. Average contact force during Contact Transition and Constrained Position Motion (9 subjects, 8 repetitions), shown for the four teleoperated conditions

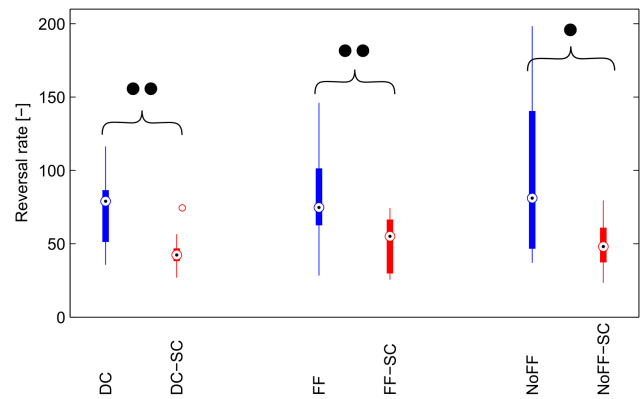


Fig. 11. Reversal rate entire bolt-and-spanner task (9 subjects, 8 repetitions), shown for six conditions

shows a bar chart of the time-to-complete, per fundamental subtask. The general trends found for the total task are reflected in the subtasks. Compared to DC, the time to complete increased for decreasing transparency for each subtask. Table 6 shows the effects of haptic shared control on time-to-complete per subtask. The subtasks Free Air Movement (FAM) and Constrained Position Movement (CPM) showed significant improvement in time performance for all transparency conditions. Contact Transition Movement (CTM) showed significant improvements for DC and FF, but not for NoFF ($p=0.1432$). Constrained Force Movement (CFM) showed only significant improvement for DC and not for FF ($p=0.132$) and NoFF ($p=0.0625$).

3.4 Subjective measures

The TLX-scores for each of the six conditions were compared (figure 13). On average the workload for DC, FF and NoFF was rated at respectively 52, 52 and 64. Haptic shared control resulted in a decreased workload of 28% ($p=0.005$), 18% ($p=0.138$) and 39% ($p=0.002$) for DC, FF and NoFF respectively. Seven out of nine subjects reported a decreased workload for all transparency conditions when shared control was added. Two subjects reported a slightly higher workload for the FF-SC condition.

Eight out of nine subjects rated the helpfulness of haptic shared control positive for all conditions, with an average grade of 2.4, 2.5 and 2.5 (range -4 to 4) for DC, FF and NoFF respectively. The only

Table 6. ANOVA results from the factor shared control ($F2$) for time-to-complete per subtask, shown for each transparency condition ($F1$)

F1:	DC	FF	NoFF
	$F2-SC$	$F2-SC$	$F2-SC$
<i>ttc - FAM</i>	•	•••	•••
<i>ttc - CTM</i>	•	•	-
<i>ttc - CPM</i>	••	•	•
<i>ttc - CFM</i>	•	-	-

negative rating was a -0.3 for DC-SC. The mean of self reported time performance (how fast do you think you performed the task?) were 5.9, 5.6 and 4.5 (range 0 to 8) for DC, FF and NoFF respectively. The means for self reported accuracy were 3.9, 4.9 and 3.3 (range 0 to 8). Eight out of nine subjects rated their time performance higher when haptic shared control was added, for accuracy this was seven out of nine subjects.

4 DISCUSSION

The experimental results showed that the tele-manipulation task benefits from haptic shared control, for all three levels of transparency. In fact, the presence of haptic shared control allowed for a worse transparency without compromising required time, accuracy, exerted

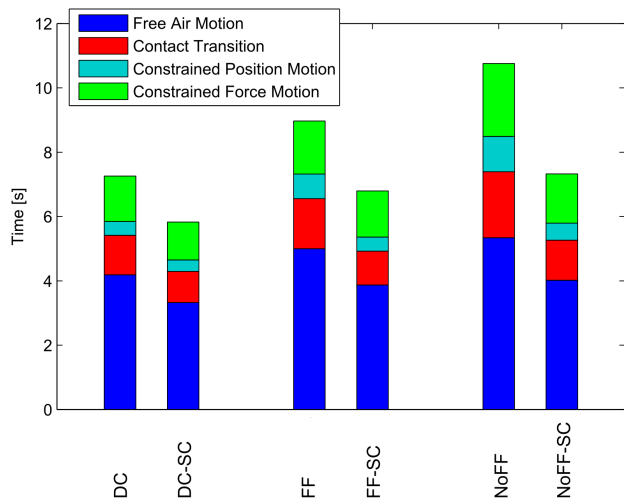


Fig. 12. Time-to-complete for the entire bolt-and-spanner task (9 subjects, 8 repetitions), separated for the four fundamental subtasks

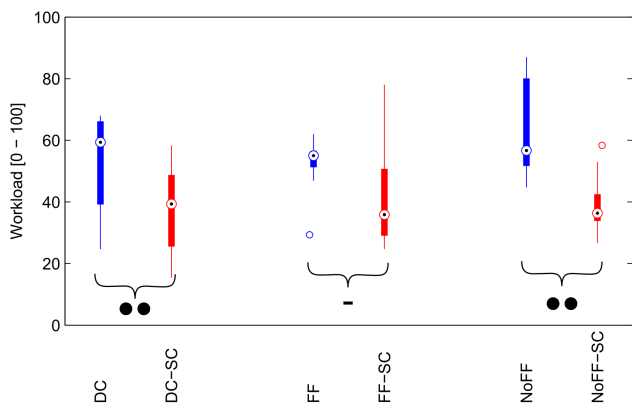


Fig. 13. Self reported workload; NASA TLX test (9 subjects)

forces and control effort. Moreover haptic shared control could even improve required time, accuracy and control effort during perfect transparency.

The association between time-performance and transparency was as expected; a lower transparency yields to a higher time-to-complete. These findings correspond with existing literature. For example Draper [12] and Hannaford [17] reported an improved performance when providing force reflection. The relative small difference between the NoFF and FF condition represents the limited force feedback quality of the used tele-manipulator. This was due to the simple PERR controller that was used. The difference in performance between FF and DC shows the room for improvement when focussing on improvement of telemanipulator transparency. Shared control resulted in an improved time-to-complete for all transparency conditions. These effects were higher for imperfect transparency. Even without any force feedback from the environment shared control resulted in task execution approximately as fast as in Direct Control.

For positional accuracy no difference was found under different transparency conditions. This can be explained by the fact that free air motion is mainly a visual task as no contact is involved. The addition of shared control substantially improved the positional accuracy for all three transparency conditions (as shown in figure 9).

Although an improved time performance was found with shared control, the average force exerted on the environment was not mea-

sured to be higher. The artificial damping and orientation guiding added by the shared control system allows for higher speeds without compromising exerted forces during the contact transition motion and the constrained position motion.

It is interesting to note that the effects mentioned above were also present in pilot experiments with the task instruction to "perform as accurately as possible".

It was expected that less transparency would result in a higher control effort of the human operator, since less force feedback was expected to make the task more difficult. The found differences in reversal rate were not significant, however the increased variation between subjects for the FF and NoFF conditions indicates a higher control effort for at least a part the subjects. Shared control resulted in a decreased control effort for all transparency conditions. Comparable results were found for self reported mental workload. The decreased mental workload found during haptic shared control is important to notice, since it has been shown that mental workload directly influences the human's ability to perform tasks [31]. Optimization of mental workload could reduce human error, improve system safety, increase productivity and increase operator satisfaction [33].

Subjective measures show that the subjects perceived shared control to be helpful and beneficial for improving accuracy and speed. This is of great importance since human like to experience the beneficial effects of a system, before they start using it.

When examining the four different subtasks in detail, all subtasks showed a decreased time performance during worse transparency conditions. This decrease in time performance was not expected to be found for the Free Air Movement subtask, since Free Air Movement is mainly a visual task, not requiring force reflexion. It is possible that the addition of extra slave dynamics in de FF and NoFF condition resulted in the decreased time performance.

The largest improvement of haptic shared control in time-to-complete can be found during Free Air Movement (FAM, from P1 to P3) and Constrained Position Motion (CPM, sliding over the bolt head). This is not surprising since the execution of these two subtasks highly depend on the right position and orientation of the spanner, both guided by shared control.

It is remarkable that haptic shared control during Constrained Force Movement (CFM) does not show an improvement for the NoFF condition. Several subjects mentioned the difficulty of this subtasks without shared control, as they had to rotate around a 'virtual' point. These subjects mentioned a beneficial effect of shared control, but this effect is not represented in the measured time-to-complete. The beneficial effects are probably better represented in other metrics like lower contact forces and a lower operator workload.

Haptic shared control is a special way of assisting, since it not directly controls the output (e.g. the slave robot), but indirectly influences the output by applying forces at the input device (e.g. master device). This approach is focused on the human-in-the-loop, allowing the operator to be fully aware of the guiding and the system status.

The proposed haptic shared control requires the availability of information about the environment, the task and the human intention, since the control system needs to define an ideal path. In most tele-manipulation situations this environmental information could be deduced from a virtual (CAD) model or be obtained by sensors, and since tele-manipulation is mostly used in controlled environments with closely monitored task sequences, the general task sequences are known. Operator intention and operator motion planning also play an important part, but is much harder to track. The experimental results showed the importance of including human intention and motion planning into a haptic shared control design. A limitation of the used shared control implementation was the fact that 9-14% of the executed trials contained counteracting control behaviour between the human and the shared control system. These counteracting actions were caused by a mismatch of intentions between the human and the control system: e.g. in some cases subjects intended to move

from point 2 to point 3, while the shared control system expected a movement from point 2 to point 1. The subjects were able to detect and solve these conflicts with guiding forces quite fast, and note that even with this limitation shared control resulted in an improved performance.

The experimental task was a two dimensional three degree of freedom (3DOF) bolt-and-spanner task, containing two translations and one rotation. Performing this similar task in a three dimensional environment using a 6DOF tele-manipulator would make the task considerably harder, mainly due to the need of three dimensional visual information. 3D vision is still a subject of research and is often not practically realizable in tele-manipulation situations. In conventional tele-operation a combination of different (perpendicular) camera views is used to deduce the depth information. In that situation an operator has to track multiple camera views simultaneously, which is quite hard. The problem of receiving depth information when going from 2D to 3D is inherent to the visual channel. The same transition from 2D to 3D does not have such an implication for the haptic channel. Since shared control supports the operator via the haptic channel, improvements by shared control are expected to be even higher for 3D 6DOF manipulation, than for the tested planar situation.

It is interesting to look into more detail on the different roles of transparency and haptic shared control with respect to execution of tasks. In this experimental setup haptic shared control could totally replace transparency; with no transparency subjects were still able to reach a performance comparable to DC. This result implies that tasks containing movement do not require transparency, but can be improved more effectively by addition of haptic shared control. However, shared control should ideally be combined with transparency for two reasons. First of all, real force tasks require a certain level of transparency, since human need at least an indication of the exerted forces. The force task used in this experiment is actually not a real force task, as there is movement involved. During a real force task the amount and direction of the exerted force can not be approximately deduced from a resulting motion, as was the case during the experiment. Secondly, unexpected situations also require transparency, as the operator will not be able to trust on shared control.

An interesting possibility of the haptic shared control, as proposed earlier [5], is the option to gradually shift between human control and automation [2]. A low stiffness of the shared control system allows the operator to easily over-rule the guiding forces, whereas a high controller stiffness forces the operator to a certain path or even a motion. In this way the shared control stiffness system defines the autonomy level of the shared control system. Marayong [22] showed experimental results which indicate that the level of operator support should be adjusted to the task. In normal situations a low compliance of the guiding was found optimal, however for tasks such as off-path targeting and obstacle avoidance a higher compliance resulted in the best task performance. To support an operator during tele-manipulation tasks the gradual scaling of the amount of shared control depending on the task, as well as the operator's intention and possibly the criticality of the situation are very promising. To develop shared control to such a level, a thorough understanding of human motion control and the human dynamics is required. Knowledge about the physical behaviour of the human arm is important to optimize shared control, as the human arm admittance influences the response to forces. A way to measure and include the highly adaptable human neuromuscular dynamics in a haptic design is proposed by [26] and [3].

Future research could further improve haptic shared control by resolving the conflicting guiding force issues discussed above. This could be done by focusing on a better matching of the guiding to natural control behaviour of the human. Available research in the field of human motion as [14], providing a mathematical model about coordination of arm movement and [24] which focussed on the prediction of movement profiles, can provide more insight in path planning and

control intention of humans. Furthermore it is important to include neuromuscular analyses in the shared control design process, as a better insight in human control behaviour and human response to forces is essential to optimize haptic shared control towards the human operator.

5 CONCLUSION

Haptic shared control was investigated as a means of supporting operators with performing a tele-operated bolt-and-spanner task. The effect of the designed shared control system was investigated for three different levels of tele-operator transparency. For all three levels of transparency, shared control allowed subjects to significantly and substantially improve their time-to-complete and accuracy without needing to exert more force. Control effort and mental workload decreased with shared control and subjective measures showed that shared control was perceived as helpful and beneficial.

For the experimental conditions studied, shared control influenced task performance and control effort much more than transparency: even with the worst possible transparency, shared control allowed subjects to perform just as well as with perfect transparency, as provided by direct control. The experimental results imply that - at least for tasks that contain movement - focusing on haptic shared control may be more beneficial to operators than focussing on improving transparency.

REFERENCES

- [1] D. Aarno, S. Ekvall, and D. Kragi. Adaptive virtual fixtures for machine-assisted teleoperation tasks. In *Proceedings - IEEE International Conference on Robotics and Automation*, 2005.
- [2] D. Abbink and M. Mulder. Exploring the dimensions of haptic feedback support in manual control. *Journal of Computing and Information Science in Engineering*, 9(1), 2009.
- [3] D. A. Abbink. *Neuromuscular analysis of haptic gas pedal feedback during car following*. PhD thesis, TU Delft, 2006.
- [4] D. A. Abbink, E. R. Boer, and M. Mulder. Motivation for continuous haptic gas pedal feedback to support car following. In *IEEE Intelligent Vehicles Symposium, Proceedings*, pages 283–290, 2008.
- [5] D. A. Abbink and M. Mulder. Neuromuscular analysis as a guideline in designing shared control. *Advances in Haptics*, 109:499–516, 2010.
- [6] J. J. Abbott and A. M. Okamura. Virtual fixture architectures for telemanipulation. 2003.
- [7] I. Aliaga, . Rubio, and E. Sinchez. Experimental quantitative comparison of different control architectures for master-slave teleoperation. *IEEE Transactions on Control Systems Technology*, 12(1):2–11, 2004.
- [8] A. Bettini, P. Marayong, S. Lang, A. M. Okamura, and G. D. Hager. Vision-assisted control for manipulation using virtual fixtures. *Ieee Transactions on Robotics and Automation*, 20(6):953–966, 2004.
- [9] G. Christiansson. *Hard Master Soft Slave Haptic Teleoperation*. PhD thesis, Delft University of Technology, 2007.
- [10] G. Christiansson. The low-stiffness teleoperator slave - a trade-off between performance and stability. *International Journal of Robotics Research*, 26(3):287–301, 2007.
- [11] R. W. Daniel and R. R. McAree. Fundamental limits of performance for force reflecting teleoperation. *International Journal of Robotics Research*, 17(8):811–830, 1998.
- [12] J. V. Draper, W. E. Moore, J. Herndon, and W. B. S. Effects of force reflection on servomanipulatro task performance. In *International topical meeting on remote systems an robotics in hostile environments, Pasco, WA, pp. 654-660*, 1986.
- [13] P. Fischer, R. Daniel, and K. V. Siva. Specification and design of input devices for teleoperation. 1990.
- [14] T. Flash and N. Hogan. The coordination of arm movements: An experimentally confirmed mathematical model. *Journal of Neuroscience*, 5(7):1688–1703, 1985.
- [15] K. H. Goodrich, P. C. Schutte, F. O. Flemisch, and R. A. Williams. Application of the h-mode, a design and interaction concept for highly automated vehicles, to aircraft. In *AIAA/IEEE Digital Avionics Systems Conference - Proceedings*, 2006.
- [16] B. Hannaford. A design framework for teleoperators with kinesthetic feedback. *IEEE Trans. on Robotics and Automation*, 5(4):426–434, 1989.

- [17] B. Hannaford, L. Wood, D. A. McAfee, and H. Zak. Performance evaluation of a six-axis generalized force-reflecting teleoperator. *IEEE Trans. Syst., Man, Cybern.*, 1991.
- [18] S. Hart and L. Staveland. Development of nasa-tlx (task load index): Results of empirical and theoretical research. In P. Hancock and N. Meshkati (Eds.), *Human mental workload*, pages 139–183, 1988.
- [19] J. Dudragne. A generalized bilateral control applied to master-slave manipulators. In *Proc of the 20th ISIR*, pages 435–442, 1989.
- [20] D. Kragic, P. Marayong, M. Li, A. Okamura, and G. Hager. Human-machine collaborative systems for microsurgical applications. *International Journal of Robotics Research*, 24(9):731–741, 2005.
- [21] D. A. Lawrence. Stability and transparency in bilateral teleoperation. *IEEE Transactions on Robotics and Automation*, 9(5):624–637, 1993.
- [22] P. Marayong, A. Bettini, and A. Okamura. Effect of virtual fixture compliance on human-machine cooperative manipulation. In *IEEE International Conference on Intelligent Robots and Systems*, 2002.
- [23] M. Mulder, D. A. Abbink, and E. R. Boer. The effect of haptic guidance on curve negotiation behavior of young, experienced drivers. In *Conference Proceedings - IEEE International Conference on Systems, Man and Cybernetics*, pages 804–809, 2008.
- [24] H. Nagasaki. Asymmetric velocity and acceleration profiles of human arm movements. *Experimental Brain Research*, 74(2):319–327, 1989.
- [25] S. Park, R. D. Howe, and D. F. Torchiana. Virtual fixtures for robotic cardiac surgery. *Fourth International Conference on Medical Image Computing and Computer-Assisted Intervention*, pages 1419–1420, 2001.
- [26] R. Pintelon and J. Schoukens. *System Identification: A Frequency Domain Approach*. IEEE, New York, 2001.
- [27] A. C. Rolfe. A perspective on fusion relevant remote handling techniques. *Fusion Engineering and Design*, 82(15-24):1917–1923, 2007.
- [28] L. B. Rosenberg. Virtual fixtures: Perceptual tools for telerobotic manipulation. In *Virtual Reality Annual International Symposium, 1993.*, 1993 *IEEE*, 1993.
- [29] T. B. Sheridan. Telerobotics. *Automatica*, 25(4):487–507, 1989.
- [30] T. B. Sheridan. *Humans and Automation: System Design and Research Issues*. WileyBlackwell, 2002.
- [31] H. S. Vitesse, J. A. Jacko, and V. K. Emery. Multimodal feedback: An assessment of performance and mental workload. *Ergonomics*, 46(1-3):68–87, 2003.
- [32] J. Wildenbeest. Improving the quality of haptic feedback yields only marginal improvements in teleoperated task performance. Master's thesis, Delft University of Technology, 2010.
- [33] B. Xie and G. Salvendy. Prediction of mental workload in single and multiple tasks environments. *International Journal of Cognitive Ergonomics*, 4:213–242, 2000.

Appendices belonging to the Master's thesis:

**Haptic shared control improves tele-operated
task performance towards performance in direct
control**

H.Boessenkool

Content

Appendix A – Experimental setup	5
A1 – Telemanipulator	6
A1.1 – Master device	7
A1.2 – Slave device	13
A1.3 – Controller	14
A1.4 Numerical performance metrics	21
A2 – Analysis force-torque sensor for experimental setup	23
A2.1 – Requirements force sensor	23
A2.2 – Load estimations force sensor	23
A2.3 – Possible sensor options:	28
A2.4 – Evaluation	29
A3 – Task environment	33
A4 – The camera system	36
A5 – Short guideline to run the setup	37
Appendix B – Simulation of the CTS	38
B1 – Human operator model	41
B1.1 – Human cortex model	41
B1.2 – Human neuromuscular arm model	43
B2 – Contact dynamics model	45
B3 – Tele-manipulator model	45
B4 – Environment model	46
B5 – Shared control model	46
B6 – Shared control 2D, 3DOF implementation	47
B7 – Results & recommendations	48
Appendix C – Shared control designs & implementation	50
C1 – Design of haptic shared control	50
C2 – Implementation of shared control	54
Appendix D – Shared control experiment	56
D1 – Experiment task	56
D1.1 – Task instruction test subjects	56
D1.2 – Selection of motion types	59
D2 – Description of evaluation metrics	62
D3 – Data management	69
D4 – Results	71
D4.1 – Total task	72
D4.2 – Free Air Movement (FAM)	74
D4.3 – Contact Transition Motion (CTM)	80
D4.4 – Constrained position Motion (CPM)	84
D4.5 – Constrained Force Motion (CFM)	88
D4.6 – Subjective measures	90
D4.7 – Additional results	93
Appendix E – Conference paper WHC	96
Appendix F – Epilogue	97
References	98

Appendix A – Experimental setup

The experimental setup consisted of a telemanipulator, a task environment and a camera system. These components will be discussed in more detail in the coming paragraphs. An overview of the experimental setup is shown in *Figure 1*.

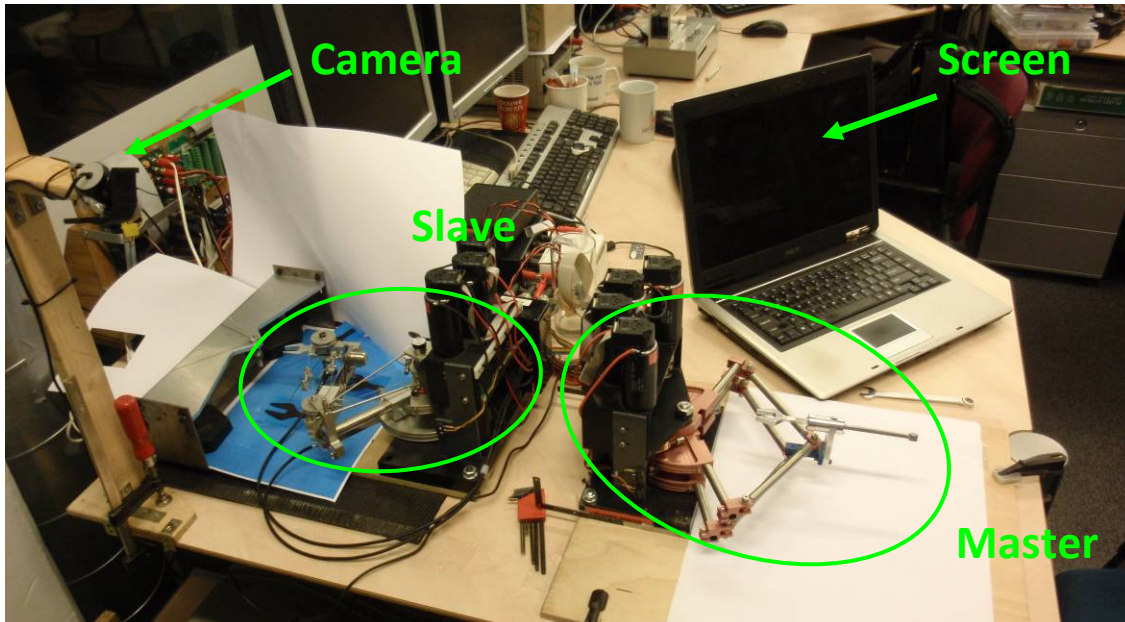


Figure 1: An overview of the experimental setup; the telemanipulator, the task environment and the camera system

A1 – Telemanipulator

The telemanipulator used for the experiments is a 3-DOF planar telemanipulation system design by G.Christiansson (Christiansson, 2007b), called Munin. The system consists of a parallel force-redundant master device (see *Figure 2*) and a serial slave device (see *Figure 3*).

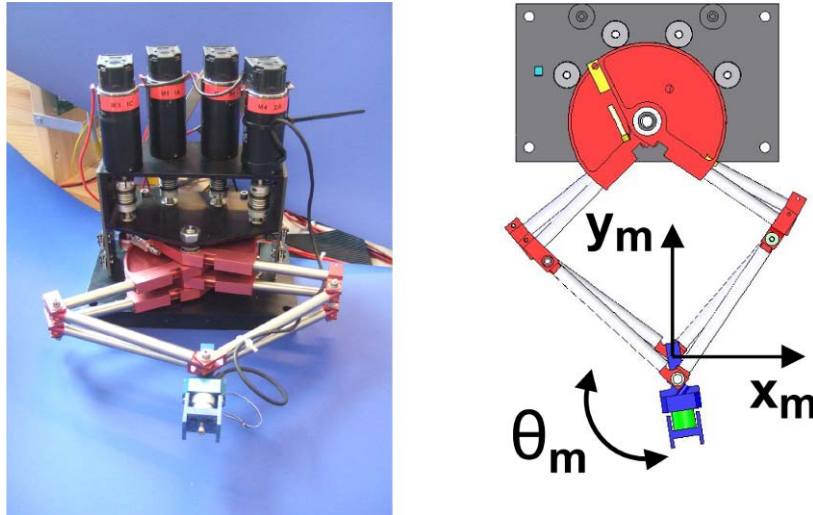


Figure 2: The Munin master device, by G.Christiansson

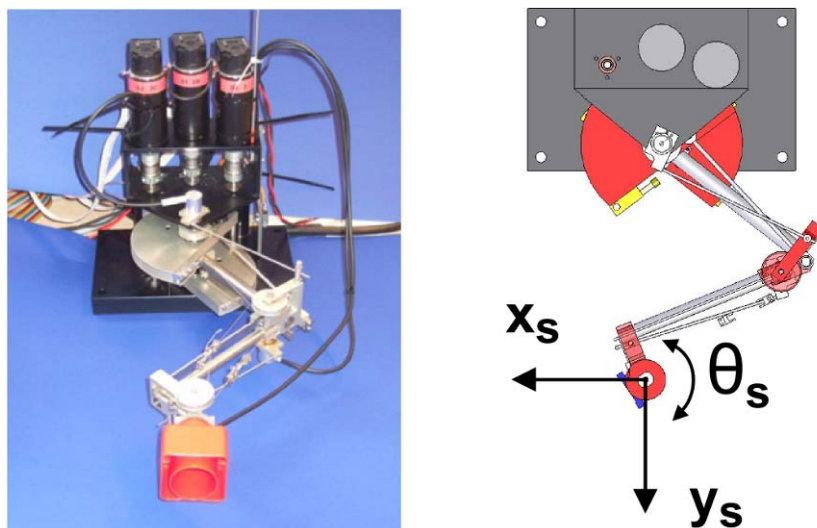


Figure 3: The Munin slave device, by G.Christiansson

The device was designed to evaluate the ‘hard-master soft-slave tele-operator’ concept [Christiansson, 2007a]. This concept aims to optimize task performance by adjusting the tele-operator design to the properties and capabilities of human and the properties of the environment.

Other studies added components to the slave device to make it more stiff, to make the tele-operator useful for more generic research in tele-operation.

Wildenbeest [Wildenbeest, 2010] made some other modifications to the tele-operator to be able to investigate the influence of the quality of haptic feedback on tele-operated task performance. The main hardware modifications made by Wildenbeest involved the increase

of the rotational stiffness of the slave, addition of an accelerometer at the slave endpoint and the change of the master and slave end-effectors into a spanner interface. The status of the tele-manipulator at this point was the basis for the current research.

In order to make the tele-operator suitable for the shared control experiments, the following changes and improvements of the telemanipulator were required:

- Master:
 - Force measurement at master endpoint (Paragraph A1.1).
- Controller:
 - Recalculate master dynamics to improve positional accuracy (Paragraph A1.3).
 - Solve not-homogeneous stiffness problems in workspace master (Paragraph A1.3).
- Implementation of shared control (Appendix C).

Some of these modifications were done in cooperation with Wildenbeest, since our projects were partly running in parallel.

The three components of the tele-operator; master, slave and controller, will be discussed in more detail in the next paragraphs.

A1.1 - Master device

The master device with the 10mm spanner interface (compatible with M6 bolts) can be seen in *Figure 4*. The workspace of the master is approximately 15x15 cm. The master is actuated by 4 brushed Maxon DC motors (RE35, Graphite brushes, 90W). The used amplifier is a Aerotech BL10-40 Linear Amplifier (current mode).

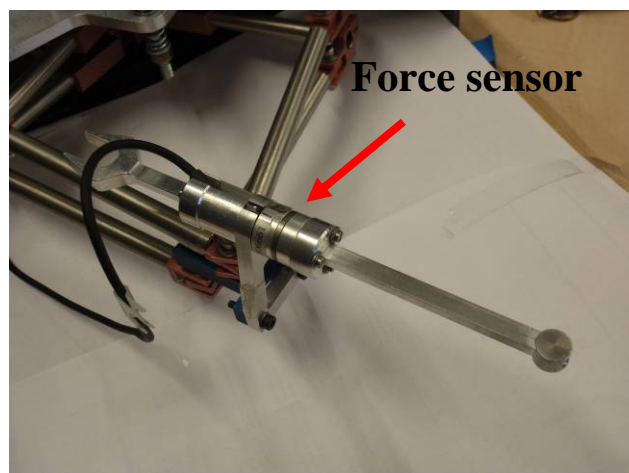
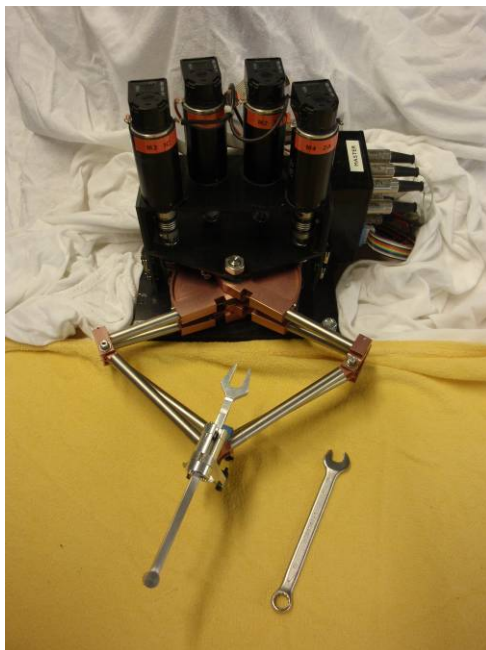


Figure 4: Master device with spanner interface (left). A close-up of the spanner interface, including a force sensor to measure the human input forces (right).

Force measurement at master endpoint – Force sensor

The interaction between master and human is an important issue during haptic shared control experiments. Therefore, it is interesting to measure these interaction forces.

The spanner interface was designed to include an 6 dof ATI Nano 17 force sensor (see *Figure 4*) and an ATI Nano 17 SI-12-0.12 sensor was implemented to measure the interaction forces between human and master.

The data acquisition was done using the real-time tele-operator controller to be able to log the force data real-time and synchronized with other data. The implementation was done according to the scheme shown in *Figure 5*.

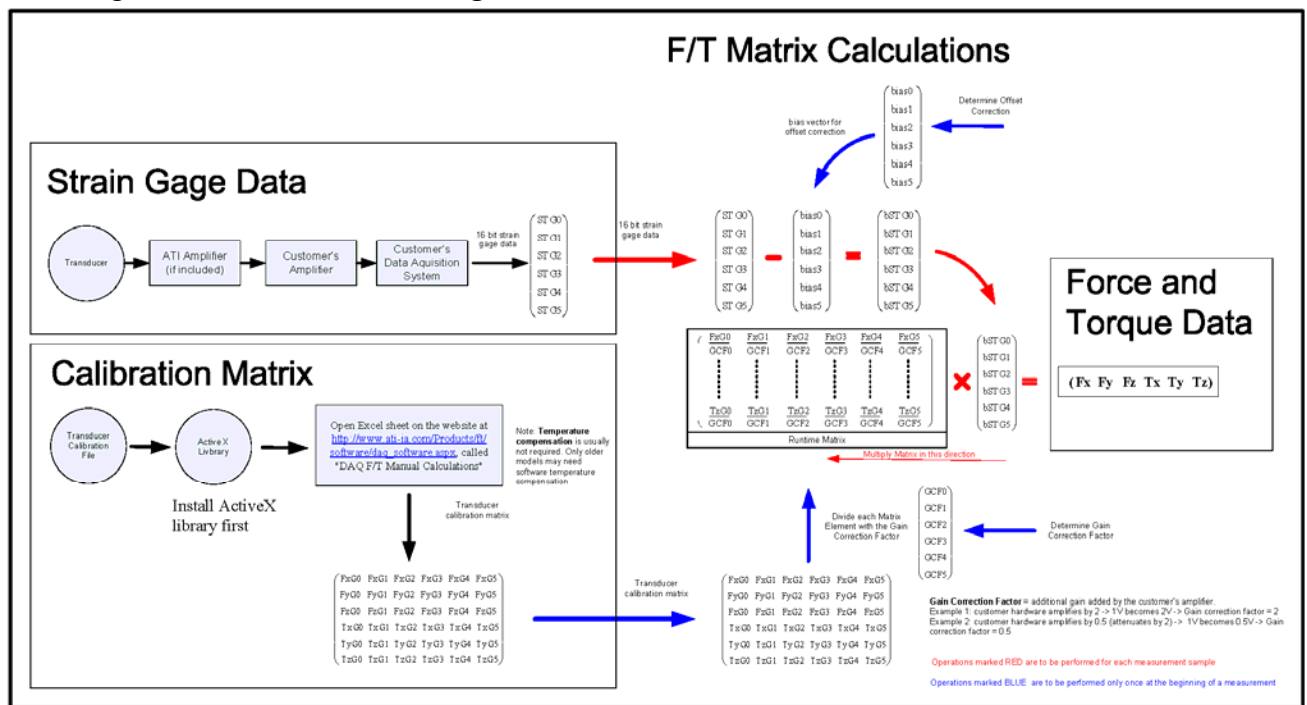


Figure 5: Implementation scheme of the ATI 6 dof force sensors [source: ATI]

To avoid bias, the offset of the sensor signal was corrected during each initialisation of the tele-operator by taking the average of 500 samples and subtracting that from the biased signal.

The sensor was calibrated using a weight of 127,51g (1,251N). Only the x- and y-force and the z-torque were calibrated as the setup is a planar setup. The following measurements were used for the calibration:

X-axis – Mean steady state x-force: -1.19N

Measured force x-axis (y-axis sensor)

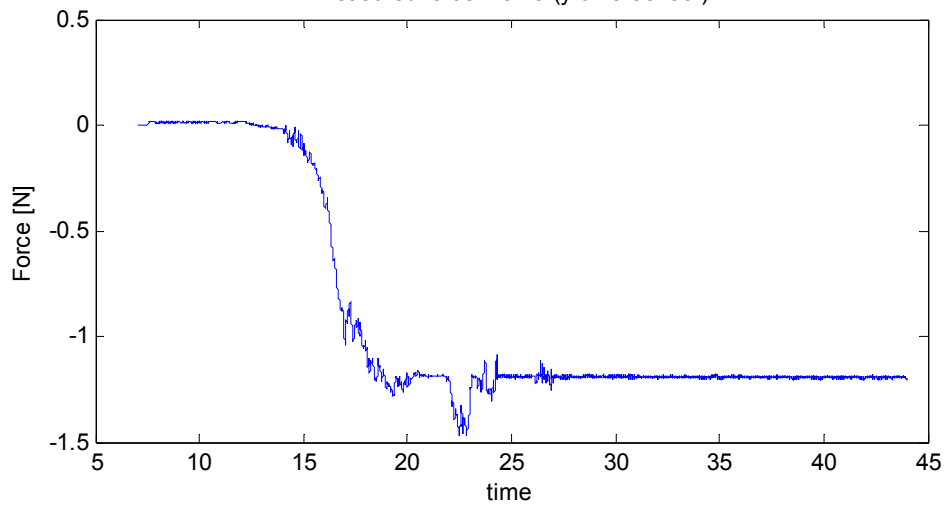


Figure 6: Calibration measurement x-axis force sensor.

Y-axis – Mean steady state y-force: -1.21N

Measured force y-axis (z-axis sensor)

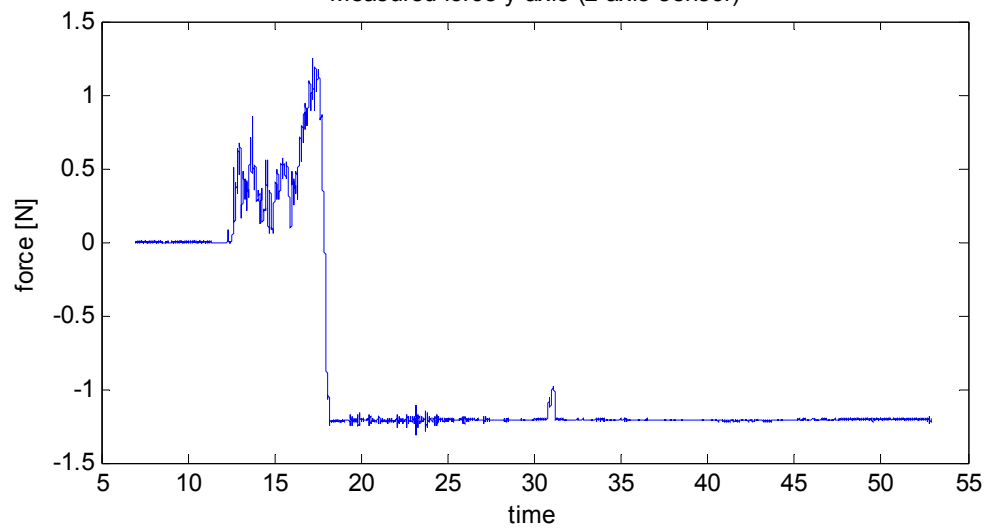


Figure 7: Calibration measurement y-axis force sensor.

Rotation-axis – Mean steady state torque: -39.05Nmm
Moment arm: 36,4mm; moment by weight: -45.54Nmm
Measured torque rot-axis (x-axis sensor)

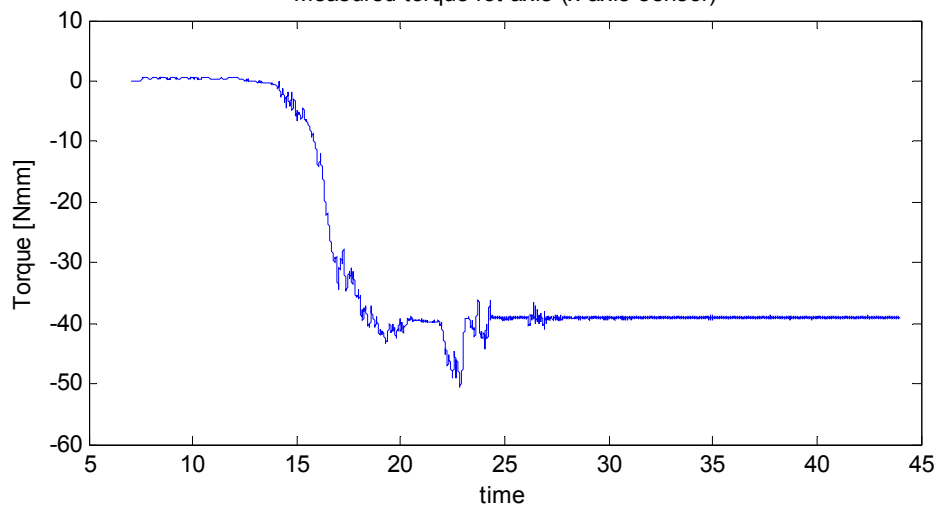


Figure 8: Calibration measurement torque x-axis, force sensor.

After these calibration steps the force sensor was ready to use. After some pilot tests it appeared that the applied torques were much higher than expected, resulting in an overload of the force sensor. A force analysis was done earlier to check the applicability of the sensor, however during assembly it was decided to place the sensor on a different place without redoing the force analysis. At the original sensor location the sensor measured the interaction forces of the master and the master task environment, at the current location the interaction forces with the human could be measured. Our pilot tests showed that this sensor was not suitable for this experiment in the current configuration.

As the current sensor location was essential for the experiment, a new analysis of forces was done and a suitable new sensor was selected (Paragraph A2). Unfortunately, the order time of this new sensor (10-12 weeks) was beyond the time frame of this project. To still have an indication of the interaction forces, we came up with plan B; using the calculated controller forces as indication of the real forces. This method is described in the next paragraph.

Force measurement at master endpoint – Controller forces

Without the use of a force sensor, the controller output signals can be used as an indication of the forces at the master side. A drawback of this method is that interaction forces are not directly measured; only in a static situation the controller force is a good estimation of the interaction forces. However, the controller forces do give information about the forces during the telemanipulation task. An advantage is that the calculated haptic shared control forces and the total output forces can be recorded separately.

The controller output (force) signals are only a useful estimate of the real forces on the master device in case the following requirements are met:

- The amplifier should be linear (in current mode).
⇒ The specifications of the Aerotech BL10-40 Linear Amplifier used in our experimental setup showed a linear response.
- The relation between the mechanical torque and the electrical current should be linear.

⇒ The specifications of the Maxon RE35 brushed DC motor used in our experimental setup showed the following relation between the mechanical torque (M) and the electrical current (I): $M = k_m \cdot I$, where k_m = the torque constant.

The controller output signals were calibrated using a Nano 17 force sensor as follows: The master was programmed to go to a reference position. Around this reference position a high controller stiffness was situated. To calibrate the controller forces, the controller output forces was limited to a certain value. By pushing the master from it's reference position, the force limit could be reached; beyond this point, the controller output was the maximal (limited) force. With the force sensor mounted at the master, it was possible to measure this maximal (limited) force (static situation).

This procedure resulted in measurements as shown in the figure below. For calibration, the absolute mean of the four repetitions was used.

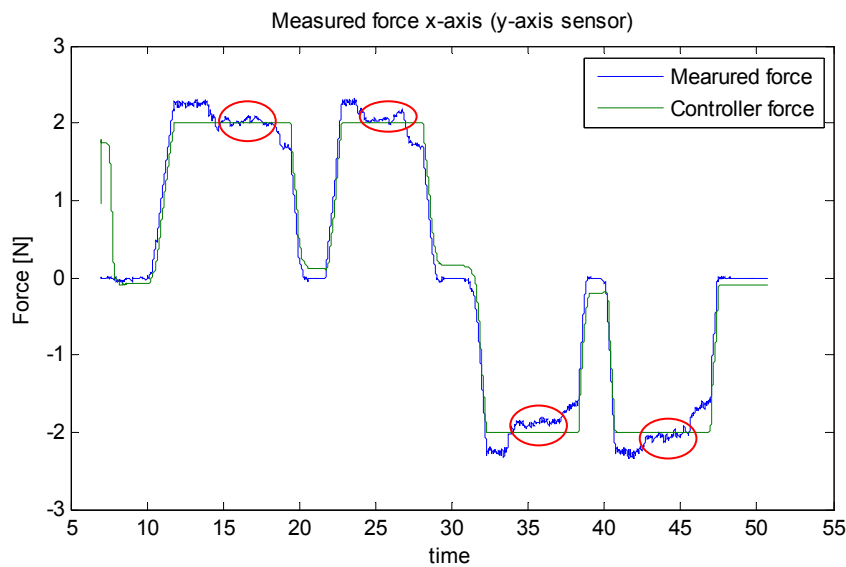


Figure 9: (Measured) force profiles (four repetitions). Red encircled the static situation: these intervals are used for the calibration.

To check the assumption that the relation between ‘controller forces’ and ‘real forces’ is more or less constant over workspace, the calibration was done for two points in the workspace; point 1 (at the y-axis) and point 2 (offset from the y-axis) (see Table 1).

Table 1: Calibration of controller forces is done for two points in the workspace

	x-position [m]	y-position [m]
Point 1	0.00	-0.23
Point 2	-0.06	-0.18

In the figures below, the calibration measurements are shown for the x, y and the rotation forces at point 1 and 2. It can be seen that the measured x and y forces came very close to the controller forces. Therefore no correction factor was required for the x and y forces; the controller forces were a good estimate of the static forces at the master.

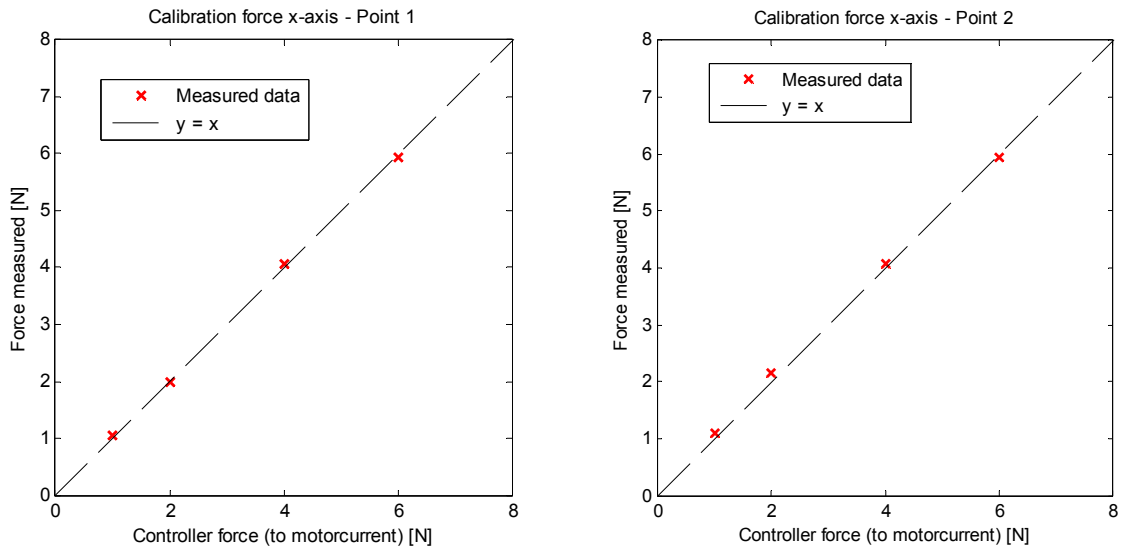


Figure 10: Calibration measurements x-axis controller forces; point 1 (left), point 2 (right).

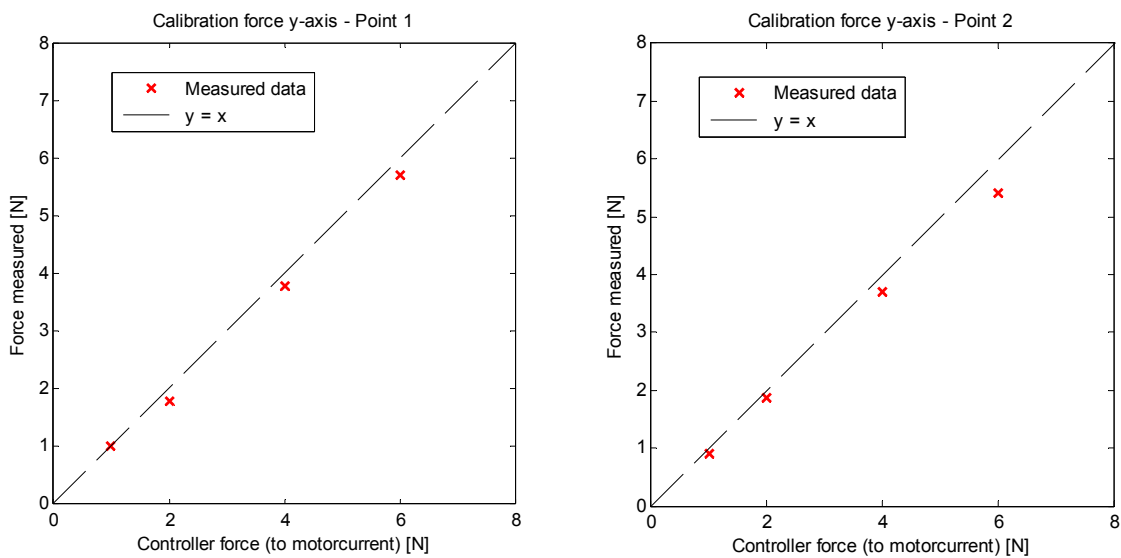


Figure 11: Calibration measurements y-axis controller forces; point 1 (left), point 2 (right).

De measured torques showed some deviation from the controller forces. Linear fits for the measured forces at point 1 and 2 are: $F_{measured1} = 1.084*x + 8.121$ and $F_{measured2} = 1.071*x + 4.628$. Therefore a correction factor of the torque was: $\mathbf{T_{master} = T_{controller} * 1.077 + 6}$

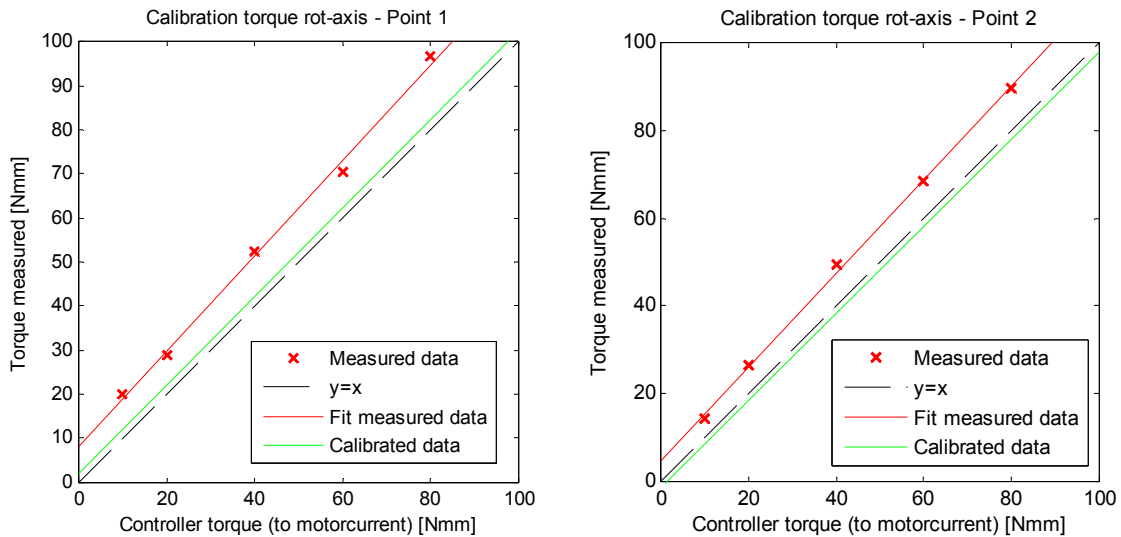


Figure 12: Calibration measurements controller torques; point 1 (left), point 2 (right).

A1.2 - Slave device

The slave device with the 10mm spanner interface (compatible with M6 bolts) is shown in *Figure 13*. The workspace of the slave was approximately 15x15cm. The slave was actuated by 3 brushed Maxon DC motors (RE35, Graphite brushes, 90W). The used amplifier was a Aerotech BL10-40 Linear Amplifier (current mode).

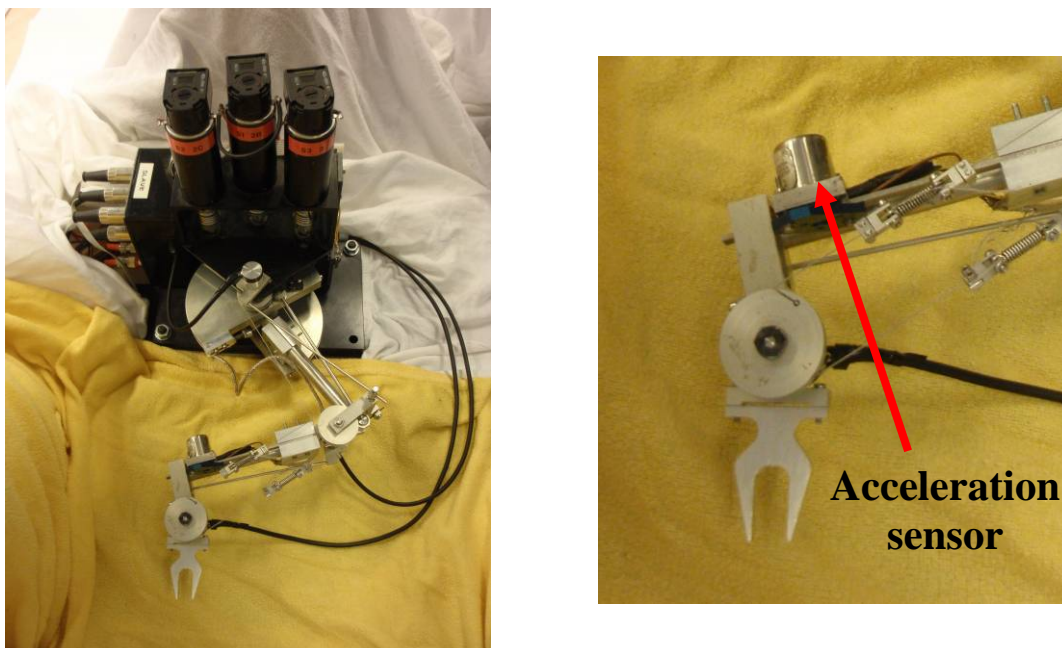


Figure 13: Slave device with spanner interface (left). A close-up of the spanner interface, including the acceleration sensor to measure the impact forces at the slave environment (right).

The slave device was actuated using the *series-elastic-actuation* principle [Pratt and Williamson,1995]. This way of actuation offers the opportunity to measure the interaction forces between slave and environment.

To estimate the impact forces caused by the interaction with the environment an acceleration sensor was placed at the tip of the slave.

A1.3 – Controller

The master and the slave device were connected by a controller. Numerous sorts of controller architectures exist, all different in performance characteristics [Aliaga, 2004]. Examples are position-position control, position-force control and four-channel control.

We used the most basic one; a PERR controller (also called position-position controller or position error control). The force feedback obtained using a PERR controller has a relatively low bandwidth, as the force feedback is deduced from position errors of the master and the slave; the high frequencies are damped out by the master's and slave's inertia. This controller type is preferred in a lot of hazardous environments (space/nuclear/deep-sea), as it is robust, reliable and not requiring expensive and fragile force sensors.

The two main reasons to choose the PERR controller in our research were:

- The low bandwidth force feedback complements the experimental conditions with regard to transparency. In the range from *ideal transparency* (direct control; condition 1) to *no transparency* (condition 3), the PERR controller fulfils the moderate transparency condition (condition 2).
- This research is initiated by ITER related remote handling research performed at FOM Rijnhuizen. Based on experience from ITER's predecessor JET (Oxford, UK), the remote handling at ITER will likely be done using PERR-controlled tele-manipulators. ITER remote handling is one of the candidates that could rely benefit from a shared control strategy.

Figure 14 shows the control scheme of a PERR controller. The position of the two devices are measured, and the controller strives to decrease position errors as much as possible. There are two position servos, one for the master and one for the slave. Each one gets the reference position from the current value of the other. The two servo loops consist of a position (P) and a velocity (D) gain.

The P and D gains used for this experiment were manually tuned:

P-gains master and slave: $K_P = [K_{P,x} \ K_{P,y} \ K_{P,rot}] = [400 \ 400 \ 0.4]$

D-gains master and slave: $K_D = [K_{D,x} \ K_{D,y} \ K_{D,rot}] = [0.02 \ 0.02 \ 0.002]$

The shared control forces were added at the master side.

The controller runs on a Mathworks xPC Target real time operating system at 1 kHz. The implemented control model in Matlab Simulink is shown in *Figure 15*

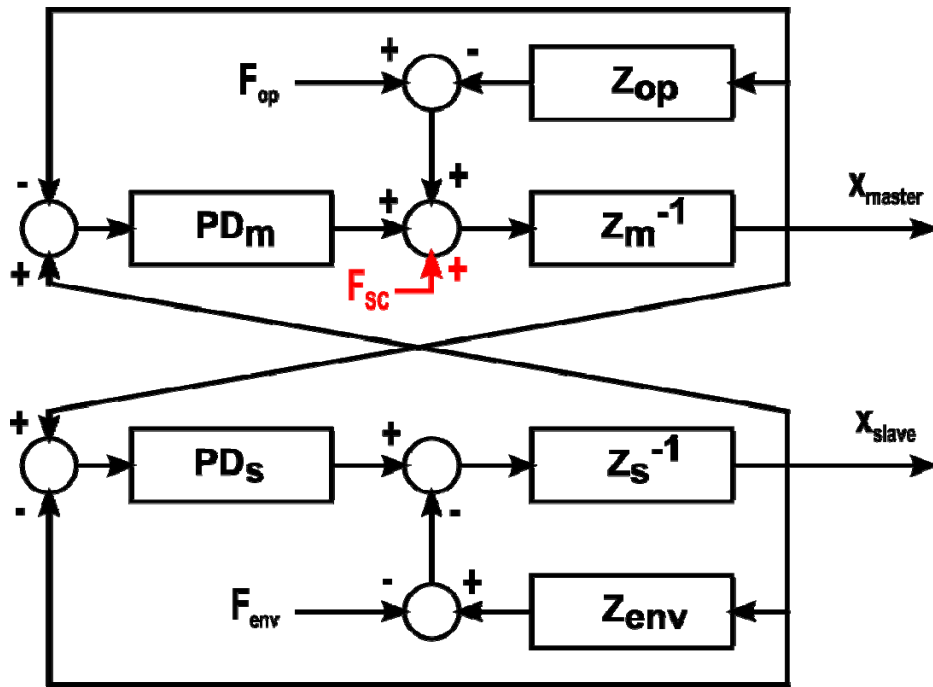


Figure 14: Block diagram of a PERR controller. X_{master} and X_{slave} are the positions/rotations of the master and slave, PD_m and PD_s are the master and slave PD controllers, Z_{op} , Z_m , Z_s and Z_{env} are respectively the impedances of the operator, the master, the slave and the environment. F_m and F_s are the interaction forces with the human and the environment. The shared control forces F_{sc} are added at the master side. [modified from Wildenbeest]

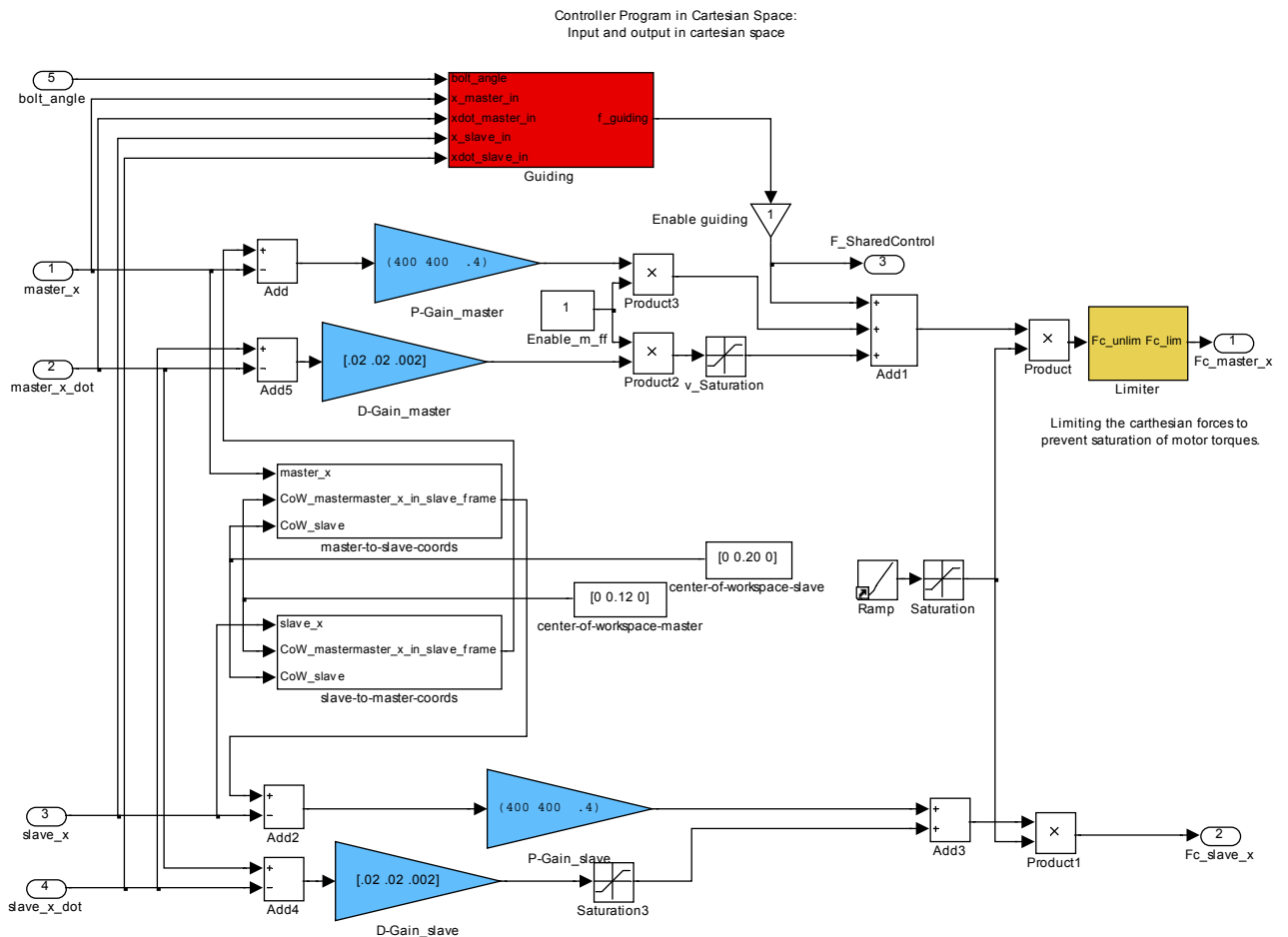


Figure 15: The PERR controller implemented in Matlab Simulink. The P- and D-gains are shown in blue, the Cartesian force limiter in yellow and the designed shared control module in red.

The PERR controller was implemented in Cartesian space. Therefore a transformation of parameters was required (see *Figure 16*): First the measured motor angles (q_m, q_s) needed to be transformed to Cartesian positions/velocities of the master and slave endpoints ($X_m, \dot{X}_m, X_s, \dot{X}_s$). Subsequently the PERR controller calculated the required control forces (F_m, F_s). Finally the calculated Cartesian forces needed to be transformed to motor torques (τ_m, τ_s) again. To implement these transformations, the forward kinematics and the Jacobian of the master and the slave are required.

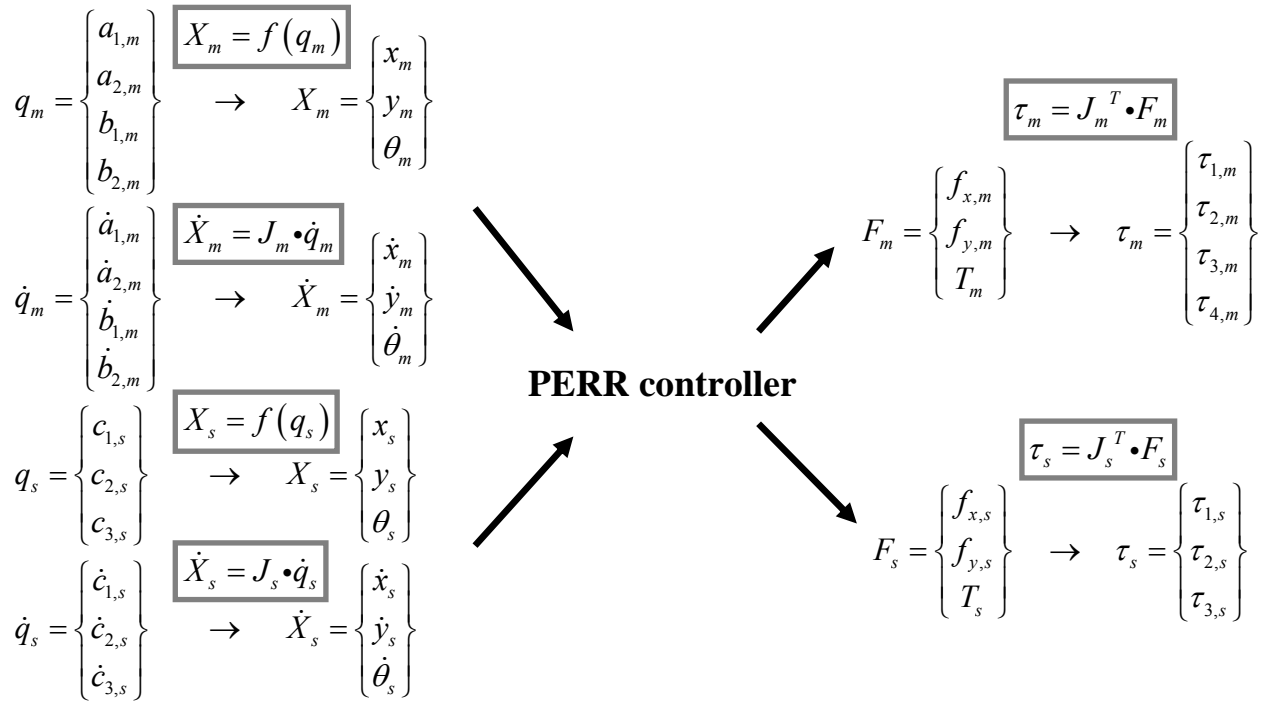


Figure 16: The PERR controller is implemented in Cartesian space. The transformation from motor angles q to Cartesian coordinates X and from forces in Cartesian coordinates F to motor torques τ , requires the forward kinematics f and the Jacobian J for the slave and the master.

Recalculation of master dynamics to improve positional accuracy.

Acknowledgement: The master kinematics and Jacobian have been derived in cooperation with J. Wildenbeest.

The master device is based on a double rhomb parallel architecture. The two parallelograms, defined as the *lower* and *upper parallelogram* (see *Figure 17*), are both actuated by two motors.

The original control model assumes the link lengths to be equal ($L1 = L2 = L3$, see *Figure 18*). However, this is not totally true, as the structure is not exactly a parallelogram (see Table 2). The result of this simplification of the system is a nonlinear error of the master end-position of maximal 9 mm in the y-direction and a maximum of 10 degrees in rotational direction (the error in the x-direction cancels out because of symmetry).

In previous research this inaccuracy of the master was not such a big issue, as the data analyses were performed at the slave side and human did not notice the error. However, in this research, shared control forces were added at the master side, requiring an accurate

master. Moreover data analyses will also be done at the master side, as the master is a data recorder during the *Direct Control* conditions. For this reason the master kinematics are recalculated for the actual link lengths (see Table 2).

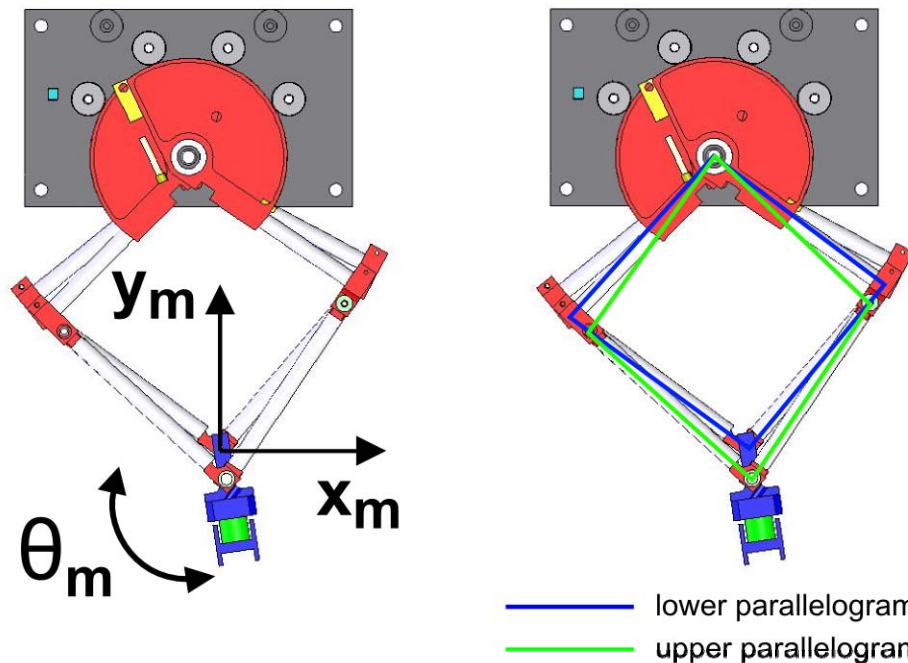


Figure 17: A schematic picture of the master device, showing the upper and lower parallelograms (right)

The definitions to calculate the forward kinematics for the lower parallelogram are shown in *Figure 18*. The angles a_1 and a_2 correspond to the motor angles of the lower parallelogram (angles b_1 and b_2 for the upper parallelogram).

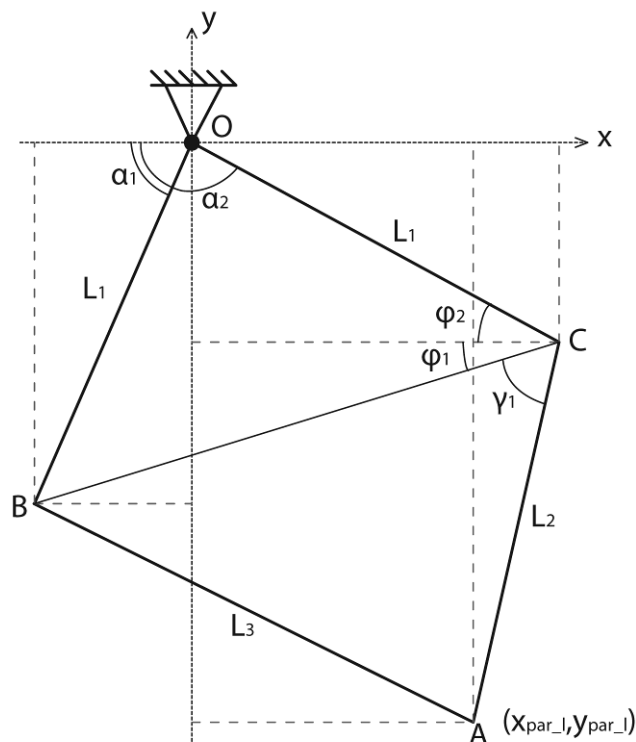


Figure 18: Definitions to calculate the forward kinematics of the lower parallelogram. The definitions for the upper parallelogram are similar, however L_2 and L_3 exchange and angles a_1, a_2 are b_1, b_2 .

Table 2: Actual lengths of parallelogram links (See *Figure 18* and *Figure 20*)

Parameter	Link length
L1	130.0 mm
L2	134.0 mm
L3	129.5 mm

The relation between the master-endpoint position and the endpoints of the lower and upper parallelograms is shown in *Figure 19*.

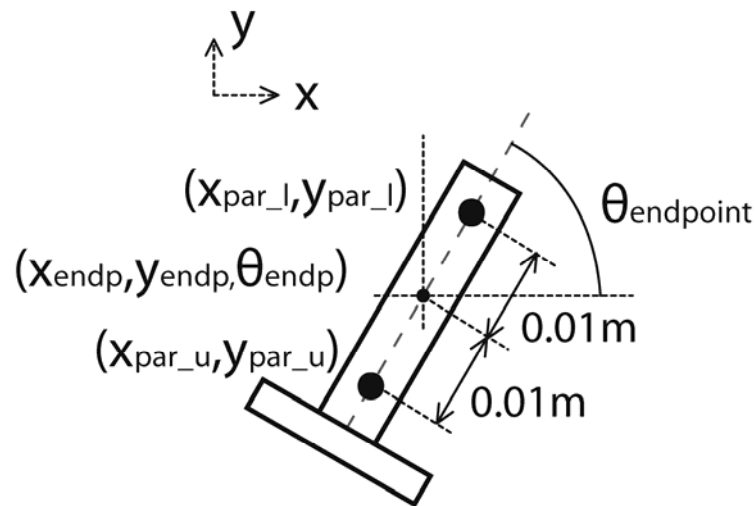


Figure 19: Relation between the master-endpoint position (*endp*) and the endpoint positions of the lower and upper parallelograms (*par_l* and *par_u*)

The matlab code below shows the calculation of the forward kinematics.

Matlab code: Forward kinematics (m-file: Jacobian1.m):

```

-----
%Master dynamics
%Henri Boessenkool, 28-5-2010
close all, clear all, clc

syms a1 a2 b1 b2

% Units in meters results in big errors!! so use cm and convert later!!
% L1 = 0.13;           %[m] length base arms
% L2 = 0.1295;        %[m] length arm 2
% L3 = 0.134;         %[m] length arm 3

L1 = 13;              %[cm] length base arms
L2 = 12.95;           %[cm] length arm 2
L3 = 13.4;            %[cm] length arm 3

%Parallelogram below
x_B_b = -cos(a1) * L1 ;
x_C_b = -cos(a2) * L1 ;
y_B_b = -sin(a1) * L1 ;
y_C_b = -sin(a2) * L1 ;
angle_t2_b = (pi-a2);

```

```

angle_t1_b = (pi-a2+a1)/2 - angle_t2_b;

BC_b = (x_C_b - x_B_b) / cos(angle_t1_b);
angle_g_b = acos((L3^2 - BC_b^2 - L2^2) / (-2* BC_b * L2));

x_b = x_C_b - cos(angle_g_b + angle_t1_b)*L2
y_b = y_C_b - sin(angle_g_b + angle_t1_b)*L2

%Upper parallelogram (L2 and L3 are switched)
x_B_u = -cos(b1) * L1 ;
x_C_u = -cos(b2) * L1 ;
y_B_u = -sin(b1) * L1 ;
y_C_u = -sin(b2) * L1 ;
angle_t2_u = (pi-b2);
angle_t1_u = (pi-b2+b1)/2 - angle_t2_u;

BC_u = (x_C_u - x_B_u) / cos(angle_t1_u);
angle_g_u = acos((L2^2 - BC_u^2 - L3^2) / (-2* BC_u * L3));

x_u = x_C_u - cos(angle_g_u + angle_t1_u)*L3;
y_u = y_C_u - sin(angle_g_u + angle_t1_u)*L3;

%Endpoint
x = ( x_b + (x_u - x_b)/2 )
y = ( y_b + (y_u - y_b)/2 )
s = sqrt((x_u - x_b)^2+(y_u - y_b)^2);
theta = ( acos((-x_u + x_b)/s) )


```

Calculation of the master Jacobian ($J_m = \left(\frac{\partial X_m}{\partial q_m} \right)$) was not valid as the system is redundant and $q_1..q_4$ are not independent. Therefore the master Jacobian was recalculated based on the principle of the Moore-Penrose pseudoinverse [Penrose,1955]. The Moore-Penrose theorem offers a least-square solution for the force redundancy problem. Hence a more optimal distribution of motor torques is attained. The Moore-Penrose pseudo inverse is calculated from the inverse kinematics.

Figure 20 shows the definitions to calculate the inverse kinematics. The matlab code below shows the calculation of the master Jacobian.

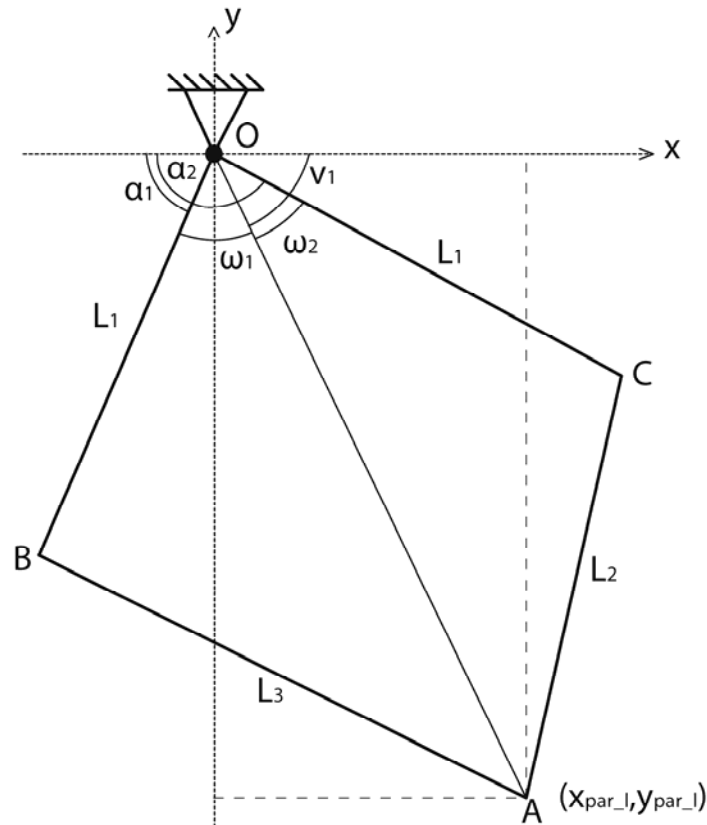


Figure 20: Definitions to calculate the inverse kinematics of the lower parallelogram. The definitions for the upper parallelogram are similar, however L_2 and L_3 exchange and angles a_1, a_2 are b_1, b_2 .

Matlab code: Calculation of Jacobian using inverse kinematics (m-file: Jacobian1.m):

```

-----
% Calculation of Jacobian, by deriving first the inverse Jacobian
clc, clear all, close all

% Units in meters results in big errors!! so use cm and convert later!!
% L1 = 0.13;           %[m] length base arms
% L2 = 0.1295;        %[m] length arm 2
% L3 = 0.134;         %[m] length arm 3

L1 = 13;              %[cm] length base arms
L2 = 12.95;           %[cm] length arm 2
L3 = 13.4;            %[cm] length arm 3

syms x y x1 y1 x2 y2 theta

x1 = x + cos(theta)*0.01;
x2 = x - cos(theta)*0.01;
y1 = y + sin(theta)*0.01;
y2 = y - sin(theta)*0.01;

% Lower parallelogram
OA1 = sqrt(x1^2 + y1^2);
v1 = acos(x1/OA1);
w1 = acos((L3^2 - L1^2 - OA1^2) / (-2*L1*OA1));
w2 = acos((L2^2 - L1^2 - OA1^2) / (-2*L1*OA1));

```

```

a1 = pi - v1 - w1
a2 = pi - v1 + w2

% Upper parallelogram
OA2 = sqrt(x2^2 + y2^2);
v2 = acos(x2/OA2);
w3 = acos((L2^2 - L1^2 - OA2^2) / (-2*L1*OA2));
w4 = acos((L3^2 - L1^2 - OA2^2) / (-2*L1*OA2));

a3 = pi - v2 - w3
a4 = pi - v2 + w4

%Figure to check results
plot(x1,y1,'bx','markersize', 15), hold on
plot(x2,y2,'rx','markersize', 15)
plot(x,y,'kx', 'markersize', 15)

Jinv = (jacobian([a1 a2 a3 a4],[x; y; theta])) %Inverse Jacobian, (A
matrix in paper "pseudo inv Jacobian")

J = pinv(Jinv) %Pseudo inv from inverse Jacobian

-----

```

Non-homogeneous stiffness problems in workspace master.

During testing a non-homogeneous stiffness was identified in the master workspace.

Applying a combination of a x-force and a torque resulted in a very low or even negative stiffness in the x- and y-direction.

The problem appeared to be the saturation of the motor torques, resulting in a very strange behavior in the Cartesian space. By limiting the controller forces in the Cartesian space, the problem could be solved. The x- and y-forces were limited to -10/10 N and the torque was limited to -0.125/0.125Nm.

A1.4 Numerical performance metrics

The performance of a tele-manipulator can be described in variety of metrics. Christiansson's open source HapticAnalysis package provides a set of toolboxes (see <http://www.haptic-analysis.org>) which include the most commonly used metrics to assess the device performance and stability. The performance and stability of the Munin in the current status was assessed by Wildenbeest [Wildenbeest,2010], using the metrics defined in the HapticAnalysis package. A detailed description of the metrics can be found in [Christianson,2007a].

The input data for the calculation of the performance metrics:

```

%Impedances of master and slave: x- and y-directions
Mm = 0.23; %[kg] x-y
bm = 4.5;  %[Ns/m]
Ms = 0.28; %[kg] x-y
bs = 6;    %[Ns/m]
Zm = Mm*s + bm;
Zs = Ms*s + bs;
Kp = 400 +. 02*s; %Controller gains (PD gain)

```

The performance metrics for the x- and y-direction are shown in Table 3.

Table 3: Performance metrics x- and y-direction

Performance metric	Value
m-to-s velocity tracking	2.4714
s-to-m velocity tracking	2.3889
s-to-m force tracking	2.0707
m-to-s force tracking	2.3889
m-to-s velocity bandwidth	42.4567
s-to-m velocity bandwidth	Inf
s-to-m force bandwidth	42.4567
m-to-s force bandwidth	Inf
scaling product	3.3557
free air m	0.1355
free air b	11.2962
free air k	-0.0269
stiff contact m	0.2300
stiff contact b	4.5200
stiff contact k	399.7956
transparency	67.5770
Zwidth	30.5110

Remarkable is the free air mass of 0.1355kg. The master is already heavier, and since the used PERR controller is not able to compensate for masses, this has to be a wrong number.

The calculation of the free air mass is shown below:

The reflected impedance to operator is:

$$Z_{to} = \left. \frac{F_h}{V_h} \right|_{F_e^{*}=0} = \frac{h_{11} + (h_{11} \cdot h_{22} - h_{12} \cdot h_{21}) \cdot Z_e}{1 + h_{22} h Z}$$

$$\text{in free air movement: } Z_e \approx 0 \Rightarrow Z_{to,free} = \frac{F_h}{V_h} = h_{11} = \frac{(sZ_m(s) + K_p)Z_s(s) + K_p Z_m(s)}{sZ_s(s) + K_p}$$

This reflected inertia was approximated by a second order system.

$$\text{Approximation: } Z_{to,free}(s) = \frac{F_h(s)}{V_h(s)} \approx \hat{m}_{free} \cdot s + \hat{b}_{free} + \frac{\hat{k}_{free}}{s}, \text{ whereas in normal free area motion } \hat{k}_{free} \approx 0.$$

It appeared that a fault in the optimization during the mbk-fit of the free air impedance resulted in a wrong 'm' value. The free air mass is now approximated by the sum of the master and the slave masses: $m = 0.23 + 0.28 = 0.51$ [kg]

A2 – Analysis force-torque sensor for experimental setup

A2.1 – Requirements force sensor

Requirements for the force sensor were:

- 3 dof measurement (planar), two translational forces and one torque.
- Nominal measurement range: +/- 15N, +/- 1.5Nm*
- Max. load (overload): +/- 75N, +/-7.5 Nm (factor 5) *
- Dimensions:
 - max. diameter: 25mm (preferably < 20 mm)
 - max. height: 20 mm (preferably < 15 mm)
- Interface:
 - analog output
- Weight:
 - lightweight (<30 gram)

*Values for current sensor location: See paragraph A2.2 for the calculations.

A2.2 – Load estimations force sensor

Which force sensor is suitable for this test setup? Which forces/torques need to be measured? To find the required measurement range of the force sensor, a simple force analyses of the task is done.

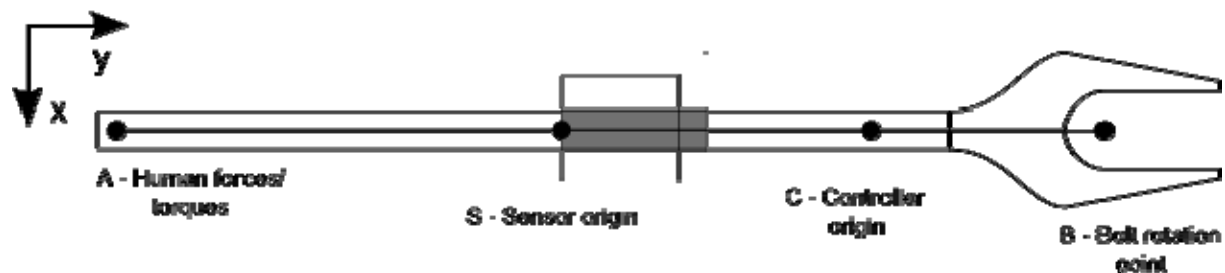


Figure 21: A schematic picture of the used bolt-spanner.

Human forces in the y-direction result in pure forces at the sensor origin. During normal manipulation, the forces exerted by the human are expected to be below 15N, resulting in a maximal sensor force of 15N (y-direction).

Forces in the x-direction and torques in the plane do have a more complex coupling. Therefore a division is made in (1) static forces – tele-operated manipulation, (2) static forces – direct manipulation, and (3) dynamic manipulation.

1. Tele-operated manipulation – Static forces

In tele-operated manipulation, the forces at the master side consist of dynamical forces (acceleration/damping master device) and forces generated by the controller.

The controller output forces of the master are limited (in software):

- Max output force x-axis (global axis): 10 N
- Max output force y-axis (global axis): 10 N
- Max output torque z-axis (global axis): 0.125 Nm

Resulting in a maximal absolute output force of $\sqrt{10^2 + 10^2} = 14.14\text{N}$, and a maximal output torque of 125 Nmm at the controller origin.

When only looking to static situations, we can distinguish three basic load cases (see figure below).

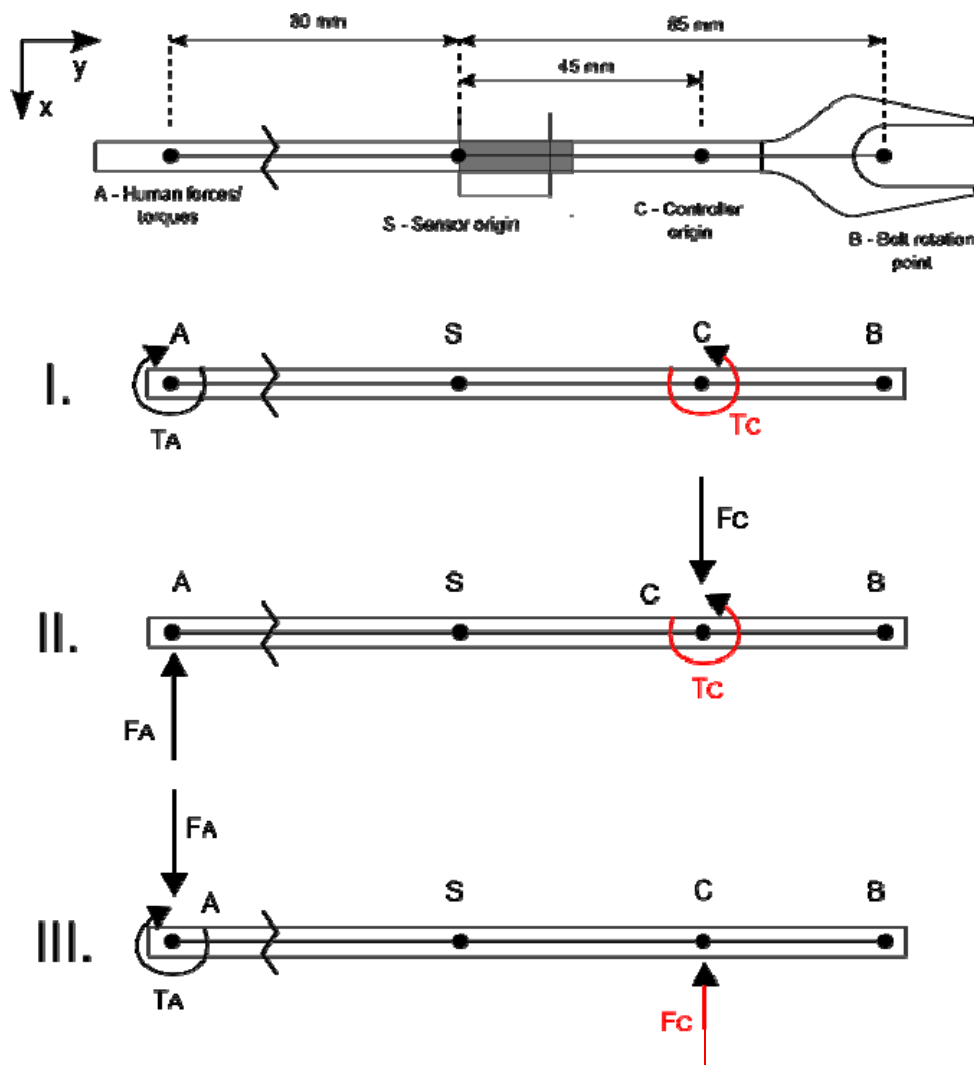


Figure 22: Three basic force situations teleoperated manipulation: (I) Maximal torque controller; pure reaction torque human, (II) Maximal torque bolthead; pure reaction force human, (III) Maximal force at bolthead; Reaction force/torque human.

Calculation of the maximal forces applied to the sensor:

Situation 1: Maximal controller torque ($T_c = 125 \text{ Nmm}$) – operator reacts with a pure torque ($T_a = 125 \text{ Nmm}$).

Maximal torque at sensor: $T_s = T_c = T_a = 125 \text{ Nmm}$

Maximal force at sensor: $F_s = 0 \text{ N}$

Situation 2: Maximal controller torque ($T_c = 125 \text{ Nmm}$) – operator reacts with a pure force (F_a)

$$F_A = \frac{T_C}{s_{AC}} = \frac{125}{125} = 1.0 \text{ N}$$

Maximal torque at sensor: $T_s = \frac{T_C}{s_{AC}} \cdot s_{AS} = \frac{125}{125} \cdot 80 = 80 \text{ Nmm}$

Maximal force at sensor: $F_s = 1.0 \text{ N}$

Situation 3: Maximal controller force (absolute force; $F_c = 14,4 \text{ N}$) – operator reacts with a counteracting force (F_a) and torque (T_a).

$$T_A = F_C \cdot s_{AC} = 14.4 \cdot 125 = 1800 \text{ Nmm} = 1.8 \text{ Nm}$$

$$F_A = F_C = 14.4 \text{ N}$$

Maximal torque at sensor: $T_s = \frac{T_C}{s_{AC}} \cdot s_{CS} = \frac{1800}{125} \cdot 45 \approx 650 \text{ Nmm}$

Maximal force at sensor: $F_s = F_a = F_c = 14.4 \text{ N}$

Conclusion:

Maximal force/torque at the force sensor for the static case occurs for the combined load cases (I) and (III):

Maximal torque at sensor: $T_s = 650 + 125 = 770 \text{ Nmm}$

Maximal force at sensor: $F_s = 14.4 \text{ N}$

2. Direct manipulation –Static forces

In direct manipulation, the forces at the master side consist of dynamical forces (acceleration/damping master device), contact forces and potentially forces generated by the controller.

The maximal forces induced by the contact are estimated:

- Max $T_b = 200 \text{ Nmm}$ (friction bolt head)
- Max $F_b = \max F_{\text{human}} = 10 \text{ N}$ (maximal expected input force from human)

When only looking at contact forces in static situations, we can distinguish three basic load cases (see figure below).

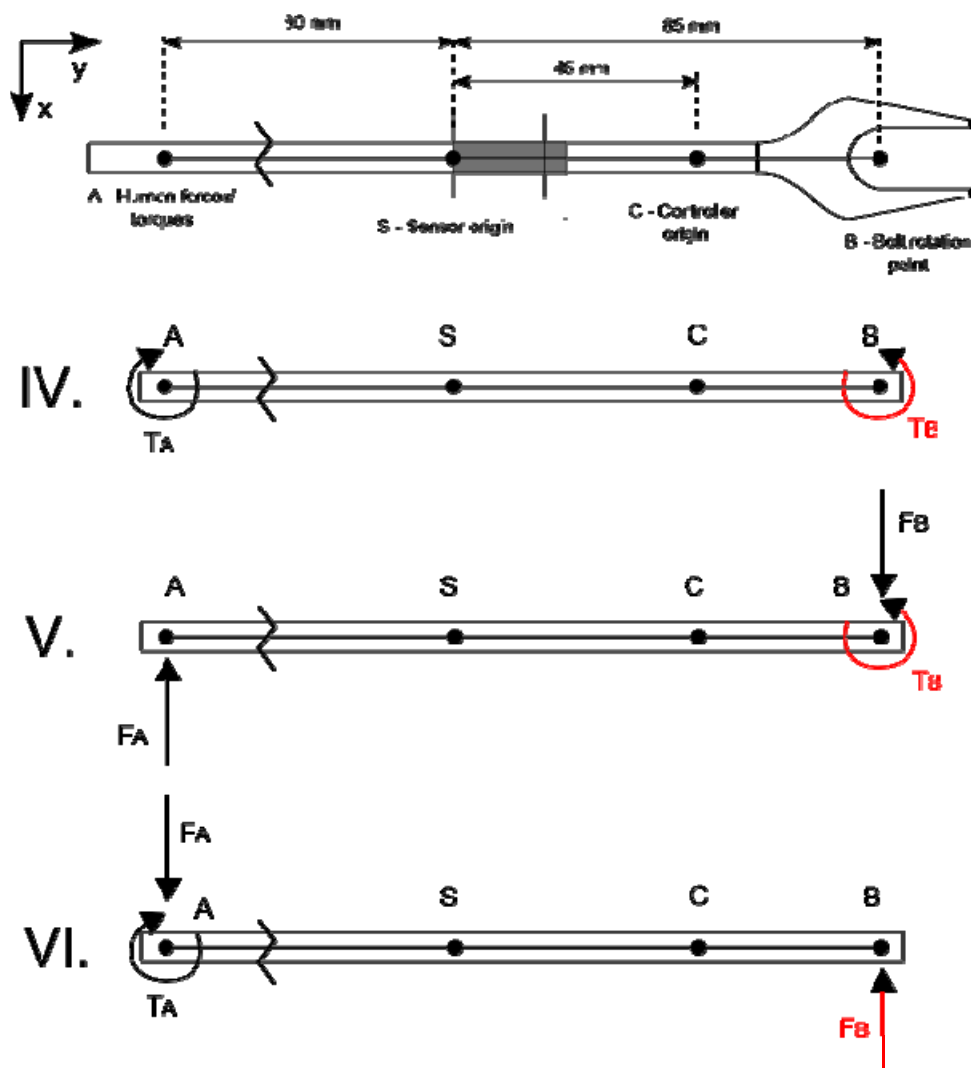


Figure 23: Three basic force situations direct control: (IV) Maximal torque bolthead; pure reaction torque human, (V) Maximal torque bolthead; pure reaction force human, (VI) Maximal force at bolthead; Reaction force/torque human.

Calculation of the maximal forces applied to the sensor:

Situation 4: Maximal bolt torque ($T_b = 200 \text{ Nmm}$) – operator reacts with a pure torque ($T_a = 200 \text{ Nmm}$).

Maximal torque at sensor: $T_s = T_b = T_a = 200 \text{ Nmm}$

Maximal force at sensor: $F_s = 0 \text{ N}$

Situation 5: Maximal bolt torque ($T_b = 200 \text{ Nmm}$) – operator reacts with a pure force (F_a)

$$F_A = \frac{T_C}{s_{AC}} = \frac{200}{165} = 1.21 \text{ N}$$

Maximal torque at sensor: $T_s = \frac{T_b}{s_{AB}} \cdot s_{AC} = \frac{200}{165} \cdot 125 \approx 152 \text{ Nmm}$

Maximal force at sensor: $F_s = 1.21 \text{ N}$

Situation 6: Maximal bolt force (absolute force; $F_b = 10 \text{ N}$) – operator reacts with a counteracting force (F_a) and torque (T_a).

$$T_A = F_C \cdot s_{AB} = 10 \cdot 165 = 1650 \text{ Nmm} = 1.65 \text{ Nm}$$

$$F_A = F_C = 10 \text{ N}$$

Maximal torque at sensor: $T_s = \frac{T_C}{s_{AB}} \cdot s_{SB} = \frac{1650}{165} \cdot 85 \approx 850 \text{ Nmm}$

Maximal force at sensor: $F_s = F_a = F_b = 10.0 \text{ N}$

Conclusion:

Maximal force/torque at the force sensor for the static case occurs for the combined load cases (IV) and (VI):

Maximal torque at sensor: $T_s = 850 + 200 = 1050 \text{ Nmm} = 1.05 \text{ Nm}$

Maximal force at sensor: $F_s = 10.0 \text{ N}$

3. Dynamic forces

Besides the static forces in the x-direction and the static torques, also dynamical forces (acceleration and damping forces (master device + reflected inertia/damping slave device)) do act on the force sensor. Especially acceleration in the x-direction results in high torques at the sensor origin (*Figure 22*; case 3). Extrapolation of test results with the current force sensor showed the following maximal dynamic forces at the force sensor origin:

Maximal torque at sensor: 450 Nmm

Maximal force at sensor (in x-direction): 10N

Final conclusion

The maximal sensor load is the summed sensor load of the static and dynamic force cases (worst case scenario).

Maximal sensor loads:

- y –direction: 15 N
- x – direction: 14.4 N
- Torque: 1050 Nmm + 450 Nmm = 1500 Nmm (combined static loads (direct control) and dynamic load)

A2.3 – Possible sensor options:

Potential suppliers:

-ATI (<http://www.ati-ia.com/products/ft/sensors.aspx>)

-Schunk (<http://www.schunk-modular-robotics.com/left-navigation/service-robotics/components/sensors/force-torque-sensors.html>)

-Kistler (http://www.kistler.com/nl_nl-nl/83_GeneralForce/Force-Measurement.html)

-JR3 (<http://www.jr3.com/sensors-e-series.html>)

ATI

See table below for product range of ‘Six-Axis Force/Torque Sensors’:

Model	Max Fx,Fy*	Max Tx,Ty*	Weight**	Diameter**	Height**
Nano17 Titanium	±32 N	±200 N-mm	0.00907 kg	17 mm	14 mm
Nano17	±50 N	±500 N-mm	0.00907 kg	17 mm	14 mm
Nano17 IP65/IP68	±50 N	±500 N-mm	0.0408 kg	20 mm	22 mm
Nano25	±250 N	±6 N-m	0.0635 kg	25 mm	22 mm
Nano25 IP65/IP68	±250 N	±6 N-m	0.136 kg	28 mm	27 mm
Nano43	±36 N	±500 N-mm	0.0408 kg	43 mm	11 mm
Mini40	±80 N	±4 N-m	0.0499 kg	40 mm	12 mm
Mini45	±580 N	±20 N-m	0.0907 kg	45 mm	16 mm

* Maximum sensing range along the axis

** Specifications include standard interface plates

*** Ingress Protection (IP) Ratings:

- IP60 - Ingress Protection Rating "60" designates protection against dust
- IP65 - Ingress Protection Rating "65" designates protection against water spray
- IP68 - Ingress Protection Rating "68" designates submergibility in fresh water, in this case, to a depth of 10 meters

Schunk

See table below for product range of ‘Six-Axis Force/Torque Sensors’ (almost similar to ATI-sensors):

Brief overview of FT

Designation		Nano	Nano	Nano	Mini	Mini	Gamma	Delta	Theta	Omega	Omega	Omega	Omega
		17	25	43	40	45				160	190	250	331
Max. F_{xy}	[\pm N]	50	250	36	80	580	130	660	2500	2500	7200	16000	40000
Max. M_{xy}	[\pm Nm]	0.5	6	0.5	4	20	10	60	400	400	1400	2000	6000
Weight	[kg]	0.01	0.07	0.04	0.05	0.09	0.25	0.91	4.99	2.72	6.35	30.0	43.0
Diameter	[mm]	17	25	43	40	45	75.4	94.5	155	156	190	254	254
Height	[mm]	14.5	21.6	11.5	12.3	15.7	33.3	33.3	61.1	55.9	55.9	95	107

JR3

Dimensions of the smallest available sensor: 50mm x 32mm (diameter x height).

Sensors size does not meet the requirements.

Kistler

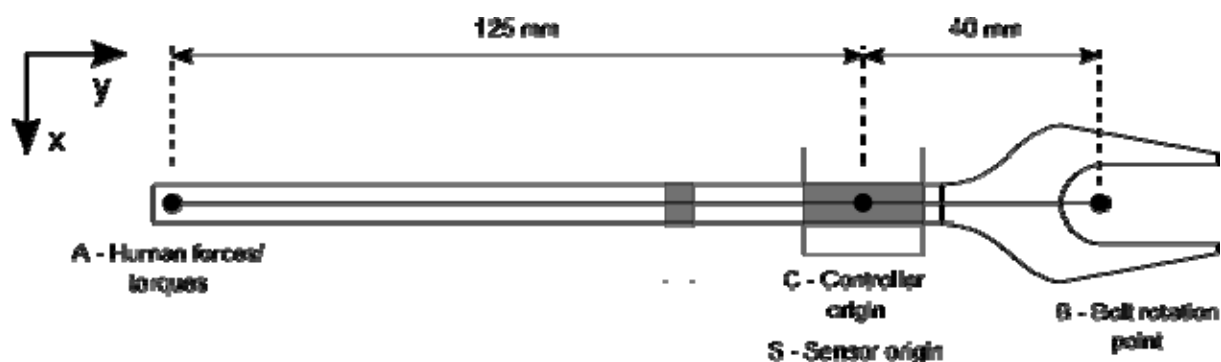
No 6 dof sensors.

A2.4 - Evaluation

Considering measurement range, dimensions and weight, there is not a perfect option:

- Nano 17 (SI-50-0.5), measurement range for torques does not meet the requirements (0.5 Nm instead of 1.5 Nm). Size and weight meet requirements.
- Nano 25 (SI-125-3) Measurement range does meet the requirements, but dimensions and weight do not meet the requirements.

An alternative approach is to change the position of the force sensor in a way it will not be exposed to the high torques. A possible position is at the controller origin; x-forces at that point (acceleration in x-direction / controller forces) will not result in torques.



With the same load examples, the sensor load will stay below the 450 Nmm (<0.5Nm)
In this case the Nano 17 (SI-50-0.5) is the best solution.

This sensor position is also from the perspective of the results analyses preferable.

Specifications Nano 17



Metric Calibrations (SI)

Calibration	F_x, F_y	F_z	T_x, T_y	T_z	F_x, F_y	F_z	T_x, T_y	T_z
SI-12-0.12	12 N	17 N	120 N-mm	120 N-mm	1/320 N	1/320 N	1/64 N-mm	1/64 N-mm
SI-25-0.25	25 N	35 N	250 N-mm	250 N-mm	1/160 N	1/160 N	1/32 N-mm	1/32 N-mm
SI-50-0.5	50 N	70 N	500 N-mm	500 N-mm	1/80 N	1/80 N	1/16 N-mm	1/16 N-mm
	SENSING RANGES				RESOLUTION			

*The resolution is typical for most applications and can be improved with filtering.

**Resolutions quoted are the effective resolution after dropping four counts of noise.

***Applied loads must be within range in each of the six axes for the F/T sensor to measure correctly.

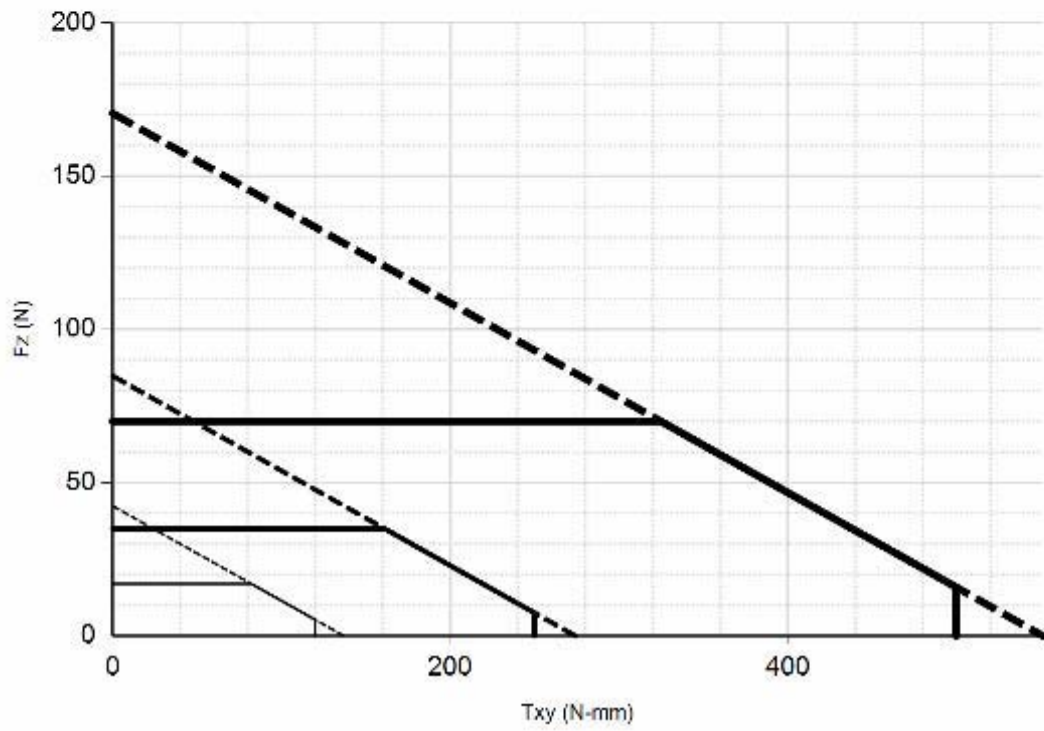
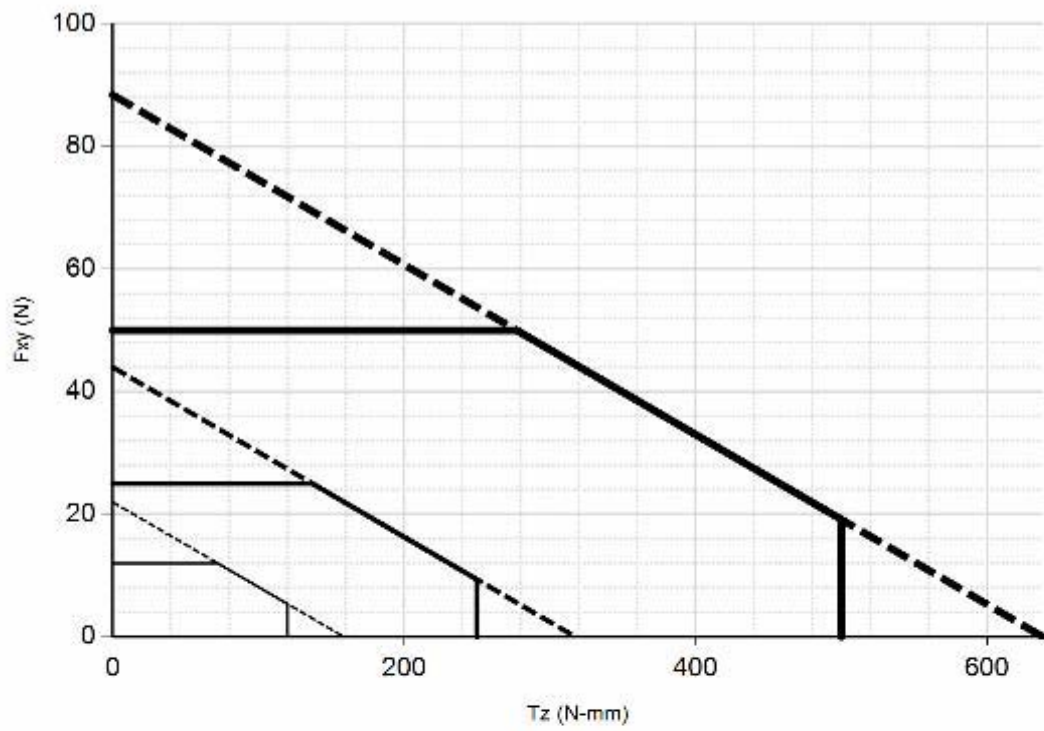
ATI's F/T calibrations are traceable to the National Institute of Standards and Technology (NIST). ATI certifies sensors are calibrated in accordance with applicable ATI procedures. These procedures are compliant with the ISO 9001 standard to ensure that products are within ATI specifications.

Contact your sales representative for accuracy information.

Nano17 Physical Properties

Single-Axis Overload	
F_{xy}	± 250 N
F_z	± 480 N
T_{xy}	± 1.6 Nm
T_z	± 1.8 Nm
Stiffness (Calculated)	
X-axis & Y-axis forces (K_x, K_y)	8.2×10^6 N/m
Z-axis force (K_z)	1.1×10^7 N/m
X-axis & Y-axis torque (K_{tx}, K_{ty})	2.4×10^2 Nm/rad
Z-axis torque (K_{tz})	3.8×10^2 Nm/rad
Resonant Frequency (Measured)	
F_x, F_y, T_z	7200 Hz
F_z, T_x, T_y	7200 Hz
Physical Specifications	
Weight*	0.00907 kg
Diameter*	17 mm
Height*	15 mm

Nano17 Complex load graphs



— SI-12-0.12
— SI-25-0.25
— SI-50-0.5

Order info

Components:

- Sensor: Nano 17 (SI-50-0.5)
- Integrated interface board and power supply
- Cable between sensor and the power supply box (standard length, 1.8m, R = radial cable outlet)
- Cable between power supply and DAQ card (standard length: 2m, U = open wires)
- No DAQ card needed (NO)

Order number (Schunk): FTD-Nano17(SI-50-0.5)-R-2U-NO

A3 – Task environment

The used task environment is designed by Wildenbeest [Wildenbeest, 2010] and consists of a M6 bolt constructed on an aluminum plate. The construction is adjustable in height, so it can be placed at the slave and at the master side. The torque required to rotate the bolt is created artificially by a friction force introduced by a spring. The tightening torques to overcome the static and dynamic friction are estimated at respectively 35.7 (2.0) Nmm and 31.6 (6.0) Nmm.



Figure 24: Task environment for a bolt and spanner task; a preloaded M6 bolt (designed by Wildenbeest, [Wildenbeest,2010]).

Angle sensor

To be able to guide the operator to the right bolt orientation during the shared control conditions, a potentiometer is added to measure the bolt angle.



Figure 25: The bolt angle is measured using a potentiometer.

Requirements angle-sensor:

- Resolution:
 - Measure the rotation corresponding to 1 mm deviation 10cm from the rotation centre:
$$\tan \alpha_{res} = \frac{0.001}{0.1} \rightarrow \alpha_{res} \approx 0.57^\circ$$
- Range:
 - min. 120°

A suitable potentiometer of 10kΩ was used (Sakae CP22E, 10kΩ ±3%, L. ±0.5%). The potentiometer was connected to an analog input (14 bit, +/- 0-10V) of the interface board (Quanser Q8 High performance control board), which was then connected to the real time controller pc.

An available 12V power supply and a serial resistor (R1) were used to reach a measurement signal of 0-10V:

$$I_{tot} = \frac{U_{AB}}{R_{pot}} = \frac{10}{10.000} = 1 \cdot 10^{-3} \text{ A}$$

$$R_{tot} = R_A + R_{pot} = \frac{U}{I_{tot}} = \frac{12}{1 \cdot 10^{-3}} = 12.000 \Omega \rightarrow R_A = R_{tot} - R_{pot} = 12.000 - 10.000 = 2000 \Omega$$

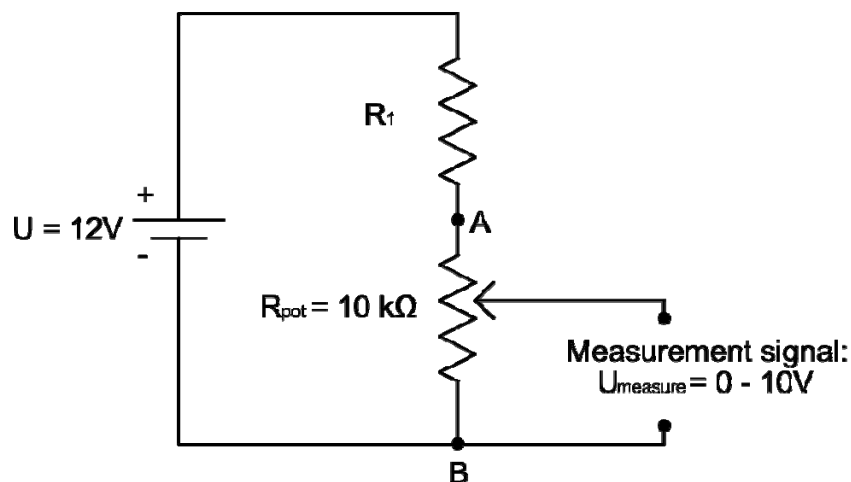


Figure 26: Electric scheme of angle sensor.

Training leds

The task environment was equipped with leds at points 1, 2 and 3, that lightened when a reference point was reached (only during training), see Figure 27.

Three green leds (2,5V, 20mA) were used. The leds were connected to three digital outputs (+/-5V) of the interface board (Quanser Q8 High performance control board), which was then connected to the real time controller pc. As the digital outputs can supply a maximum current of only 10mA, three small amplifiers were build (see Figure 28).

An available 5V power supply could be used: $R_1 = \frac{U_{R1}}{I} = \frac{2.5}{0.02} = 125 \Omega$, $R_2 = 1 \text{ k}\Omega$

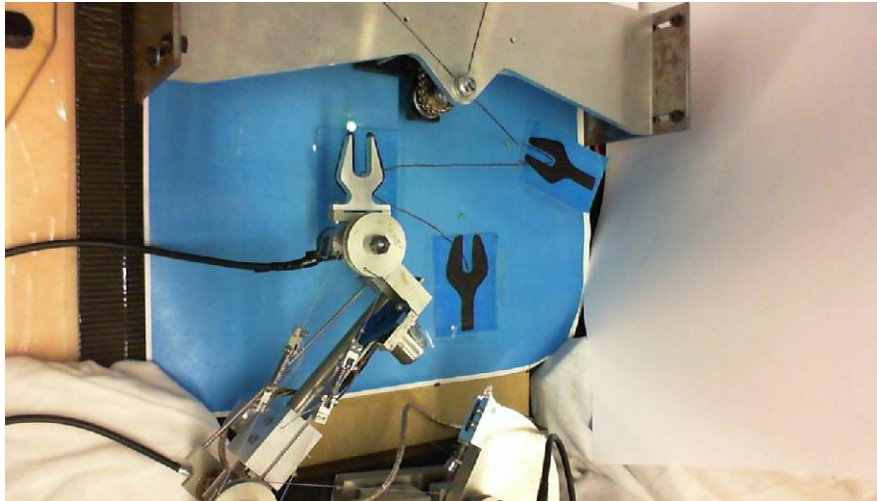


Figure 27: Camera view of the slave environment. Leds at point 1,2 and 3 show during training that the reference point is reached. In the figure point 2 is reached.

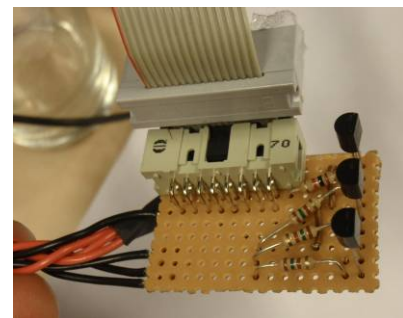
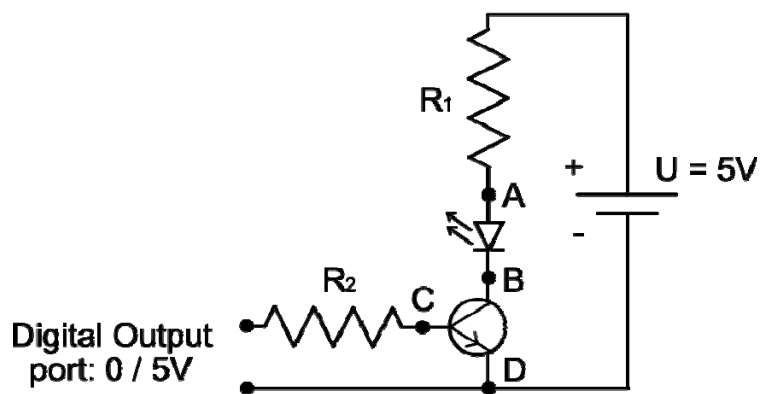


Figure 28:Electrical scheme of the led amplifier(left). Picture of constructed amplifiers(right).

A4 - The camera system

The camera system consisted of a Microsoft Lifecam Cinema HD usb camera connected to a 14 inch (laptop)screen. The camera was mounted, with an angle of 45 degrees, on a portable structure which could be placed at the slave and master side. The cameraview was displayed with a resolution of 960x544.

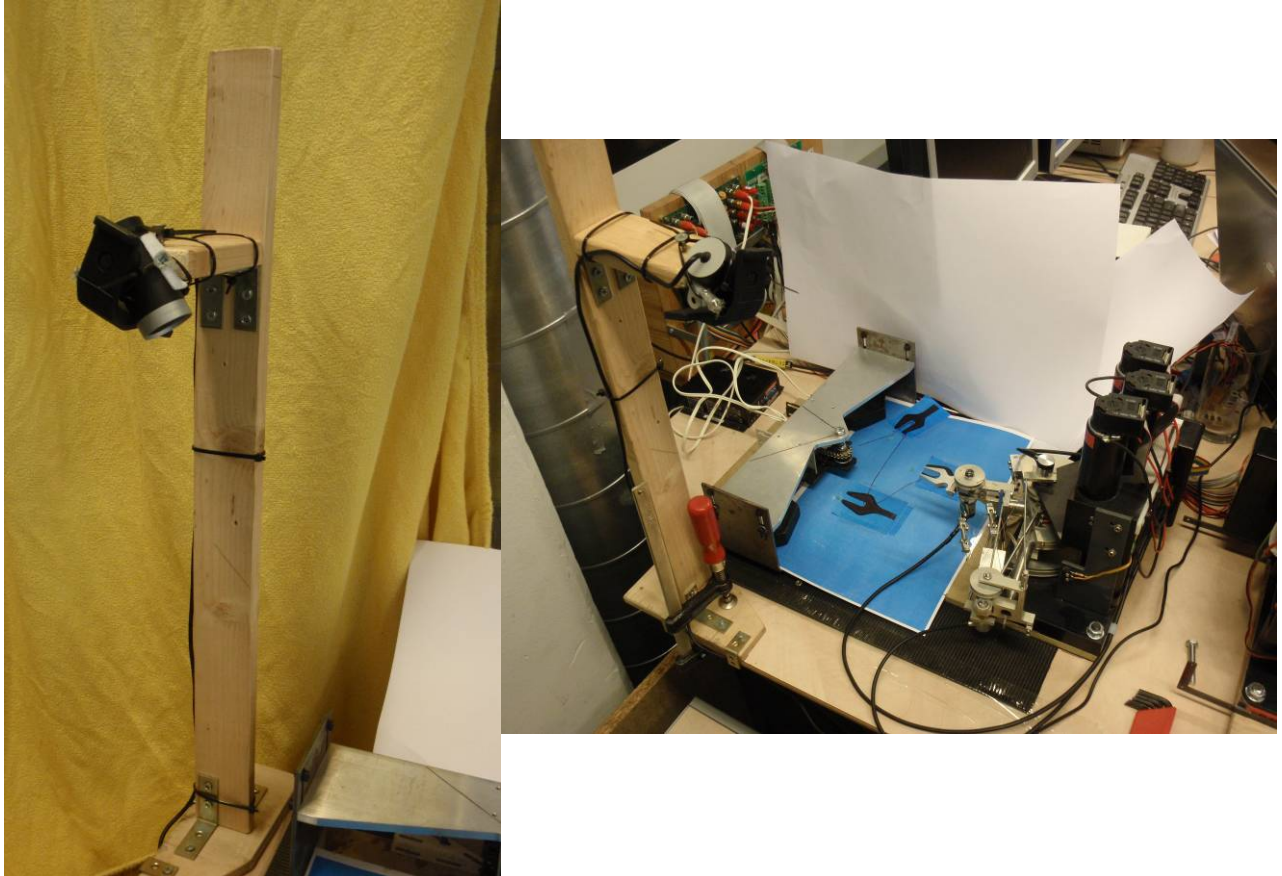


Figure 29: The 45 degrees tilted camera mounted on a portable structure (left). Camera placed at slave side (right)

A5 – Short guideline to run the setup

Adapted from Wildenbeest

The setup that drives the Munin consisted of two PCs. The first PC, the ‘target PC’, runs on a Mathworks xPC target real-time operating system and contained the interface cards connected to the telemanipulator hardware. The operating system is installed on the floppy drive. The second PC, the ‘host PC’, is a Windows XP based PC on which the models to control the manipulator were build and from which the work pc is operated.

To start, turn on both PCs. The target PC will show the xPC screen and will wait for further orders from the host PC.

- 1) On the host PC double-click on the control model you want to load. The controller used in this study is named ‘Controller_Henri_Experiment_v4.mdl’, found in the host PC directory C:\Documents and Settings\haptics\Desktop\Henri\Controller_v3.
- 2) Build the model and download to the Target PC by selecting Tools -> Real-time Workshop -> Build Model. (or press Ctrl+B). Notice that the model requires resources from the default directory (D:\haptics\planarsetup\realtime_software\basiscontroller\), and thus this directory needs to be set as the current directory.
- 3) Typing <+tg> in the Matlab command window will start the model. The model will finish running when its simulation time expires or when you type <-tg>.
- 4) Alternatively, the target PC can be controlled using the xPC Explorer on the host PC. Type <xpcexplr> in the Matlab command window to start the xPC Explorer. In the xPC Explorer, right click on the icon for the target PC (TargetPC1) displayed in the hierarchy and select ‘Connect to Target’. Pressing the play icon will now start the model, pressing the stop icon will stop the model. The xPC Explorer can also be used to change parameters of the control model. For example, the controller gains can be tuned. The settings for the different experimental conditions can loaded by changing the parameter ‘condition’ (location: ../Main program/Controller/Guiding):
 - ‘0’ = Direct Control,
 - ‘1’ = PERR controller,
 - ‘2’ = PERR controller + Shared Control,
 - ‘3’ = No Force Feedback,
 - ‘4’ = No Force Feedback + Shared Control,
 - ‘5’ = Direct control + Shared control.
- 5) Finally data can be saved by executing ‘save_OutputLog.m’.

Appendix B – Simulation of the CTS

This appendix describes the work done on modelling of the shared control during a telemanipulation task. The main objective was to gain insight in the interaction between the shared control system, the operator, the telemanipulator and the environment. However in future this models hopefully can be used to optimize shared control designs towards the human operator, due to accurate simulation of the total sequence including the operator and his neuromuscular dynamics.

The current models were only applied for Free Air Movement and Contact transition Movement. The following information should be obtained by the simulations:

- Free Air Movement:
 - What are the effects of shared control on the operator (interaction forces)
 - Order of magnitude guiding forces (depending on operator impedance/direction)
 - Effects of different shared control designs
 - Possible performance (time) improvement using shared control
- Contact Transition Movement:
 - Lower contact forces with shared control?
 - Can the operator still feel a contact sensation/impulse?

The total system of human operator, tele-manipulator and environment is referred to as Connected Telemanipulator System (CTS, shown in *Figure 30*). The model will contain the five components of the CTS and a model of the shared control system.

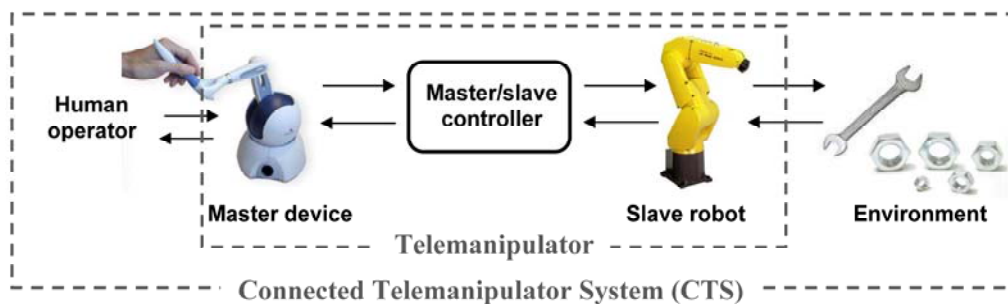


Figure 30: The five components of the Connected Telemanipulator System, adapted from [Christiansson2007]

A schematic representation of the implemented model is shown in *Figure 31*.

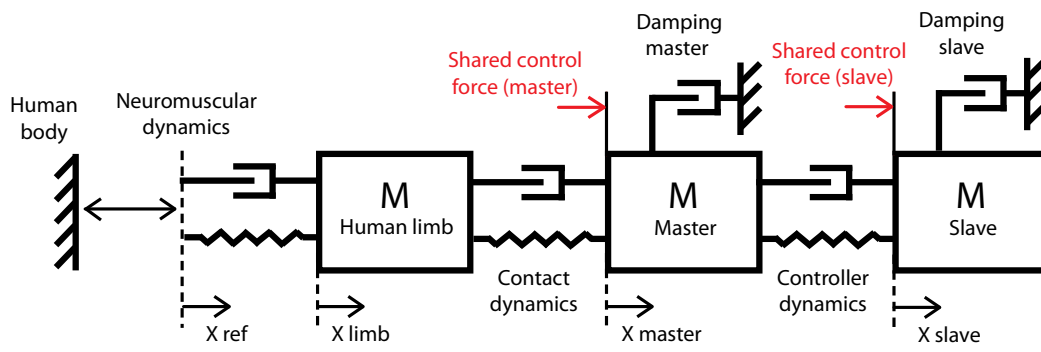


Figure 31: Schematic representation of the implemented Connected Tele-manipulator System model (situation without contact with the environment). In red the possible places to add shared control forces.

The modelling is done in Matlab Simulink and the top-level model is shown in *Figure 32*. The model was built step by step and all sub models were tested individually. At the left side human sub-model is shown (green), containing a model of the human cortex and a model of the neuromuscular system. The pink box shows the model of the contact dynamics, connecting the human to the tele-manipulator. The tele-manipulator is modelled in the yellow box and the environment and the shared control system are modelled in the grey and blue boxes.

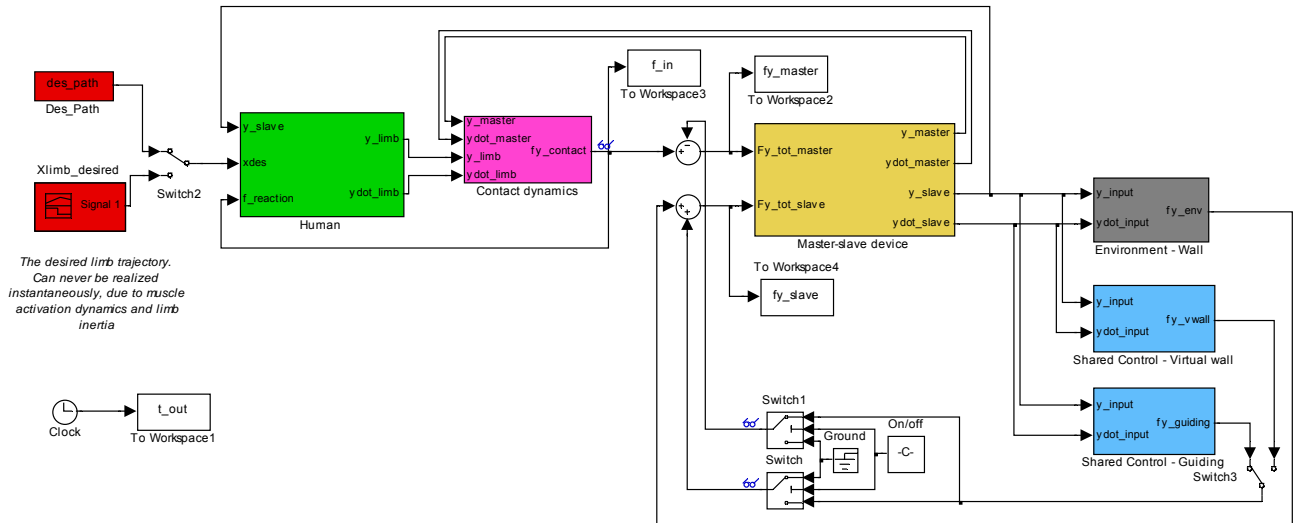


Figure 32: Top-level representation of the Connected Telemanipulator System (CTS) Matlab Simulink model. Containing sub-models for the human (green), contact dynamics (pink), tele-manipulator (yellow), environment (grey) and shared control (blue).

The different sub-models will be discussed in more detail in the next paragraphs and finally results and future work will be presented.

The Simulink models and the m-file to run them (parameters_v2.m) can be found in the folder “*\Simulations\”.

B1 – Human operator model

The human operator model consists of a human cortex model and a neuromuscular model.

B1.1 – Human cortex model

The human cortex model (see *Figure 33*) translates a desired (limb/slave) trajectory into a force send to the human limb. The desired path can never be realized instantaneously, due to muscle activation dynamics and limb inertia.

A motion can be controlled totally feed forward (blue box) or based on visual feedback of the limb/slave trajectory (pink box). Feed forward force generation requires an internal model of the limb inertia and the connected tele-manipulator.

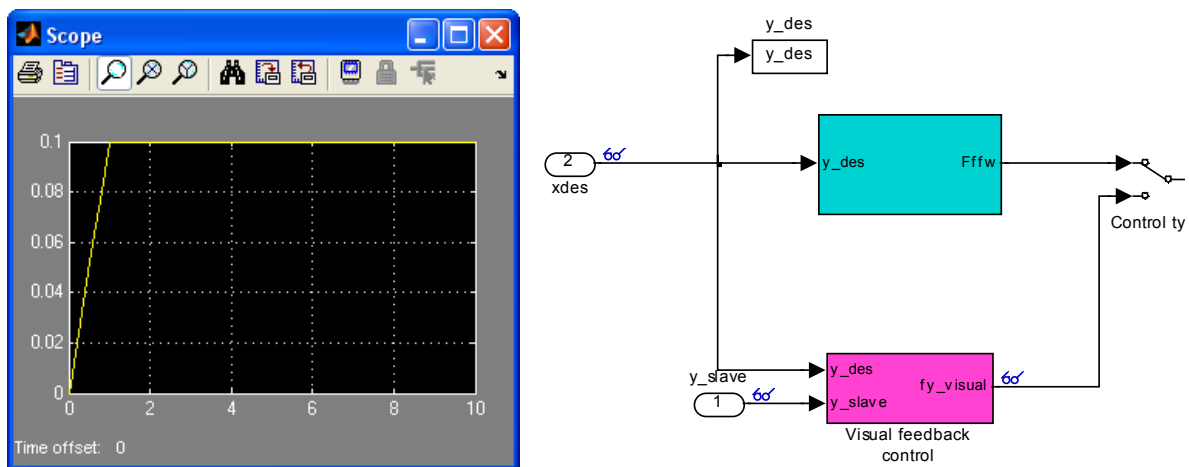


Figure 33: Example of a desired trajectory as input of the model (left), the human cortex sub-model (right)

Internal model of tele-manipulator

The human operator uses an internal model to do feed forward position control. This internal model includes knowledge of the human limb dynamics but also an estimation of external dynamics as for example a tele-manipulator. *Figure 34* shows a schematic representation of an operator interacting with a tele-manipulator in free air.

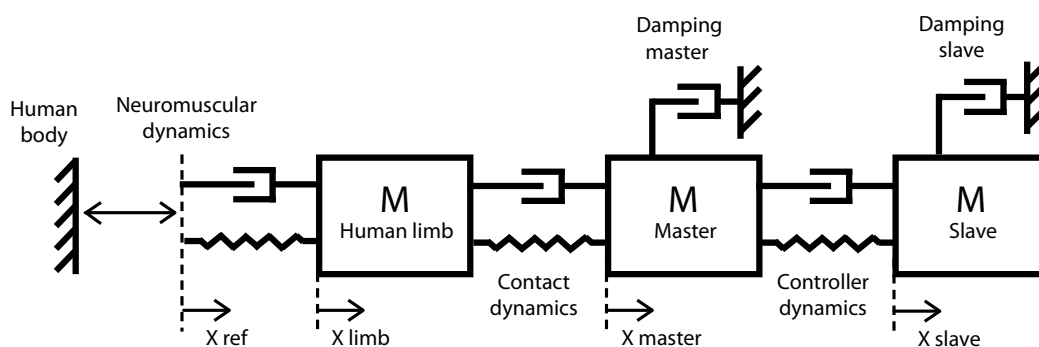
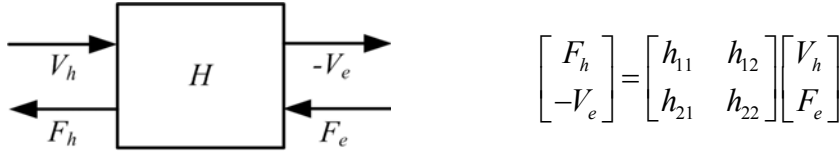


Figure 34: Schematic representation of the implemented Connected Tele-manipulator System model (situation without contact with the environment)

The reflected impedance of the teleoperator can be theoretically deduced (Christiansson 2007a, p.19-22). Therefore the Hybride Matrix Model is used:



In the case of position-position control, the H-matrix becomes:

$$H(s) = \begin{bmatrix} \frac{(sZ_m(s) + K_p)Z_s(s) + K_p Z_m(s)}{sZ_s(s) + K_p} & \frac{K_p}{sZ_s(s) + K_p} \\ -\frac{K_p}{sZ_s(s) + K_p} & \frac{s}{sZ_s(s) + K_p} \end{bmatrix}$$

For which; $Z_m(s) = m_{master} \cdot s + b_{master}$, $Z_s(s) = m_{slave} \cdot s + b_{slave}$ and $K_p =$ controller position gain.

The reflected impedance to operator becomes:

$$Z_{to} = \left. \frac{F_h}{V_h} \right|_{F_e^*=0} = \frac{h_{11} + (h_{11} \cdot h_{22} - h_{12} \cdot h_{21}) \cdot Z_e}{1 + h_{22} h Z}$$

in free air movement: $Z_e \approx 0 \Rightarrow Z_{to,free} = \frac{F_h}{V_h} = h_{11} = \frac{(sZ_m(s) + K_p)Z_s(s) + K_p Z_m(s)}{sZ_s(s) + K_p}$

This reflected inertia can be approximated by a second order system (see also *Figure 35*).

Approximation: $Z_{to,free}(s) = \frac{F_h(s)}{V_h(s)} \approx \hat{m}_{free} \cdot s + \hat{b}_{free} + \frac{\hat{k}_{free}}{s}$

whereas in normal free area motion $\hat{k}_{free} \approx 0$.

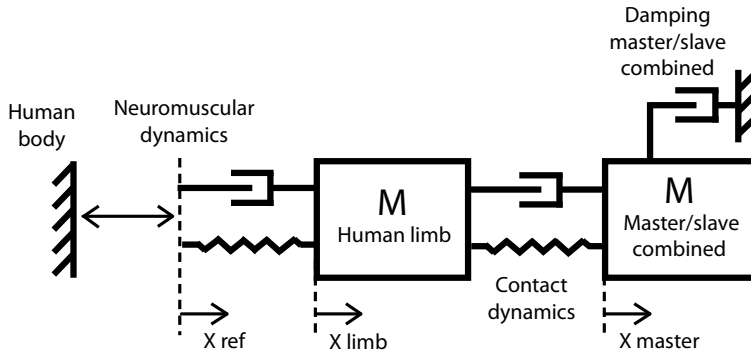


Figure 35: Schematic representation of the Connected Tele-manipulator System model, with a second order approximation of the tele-manipulator (master and slave combined) (situation without contact with the environment)

This second order approximation is probably a good choice to approximate the human internal model, since a human operator is not able to control higher order systems.

To generate the feed forward force, the operator needs a model from the master force input to the slave position output. This transfer function can be theoretically deduced similar as seen above:

$$-V_e = h_{21} \cdot V_h$$

$$Z_{to,free}(s) = \frac{F_h(s)}{V_h(s)} \Rightarrow Z_{F_h \rightarrow V_e,free}(s) = \frac{F_h(s)}{V_e(s)} = \frac{Z_{to,free}(s)}{-h_{21}} = \frac{h_{11}}{-h_{21}} = h_{11} \cdot \frac{s \cdot Z_s(s) + K_p}{K_p}$$

The transfer function $Z_{Fh \rightarrow Ve, free}(s)$ relates the slave position to the required input force at the master and can be used to estimate the feed forward force.

Visual feedback:

McRuer [McRuer,1969] developed the crossover model to represent the operator performance in auditory and visual display tracking tasks. This model contains the parameter ‘crossover frequency’, which describes up to which frequency a human operator can perform a tracking task. The crossover frequency is dependent on the task variables, but is for a human operator 0.5 ~ 0.8 Hz.

Implementation of visual feedback in the Simulink model has been done by filtering the error between the actual slave position and the aimed slave position with a second order Butterworth filter:

$$F(s) = \frac{1}{\frac{1}{\omega_c^2} s^2 + 1.4142s + 1},$$

ω_c = cut-off frequency [rad/s] = crossover frequency (-> 0.5 ~ 0.8 Hz)

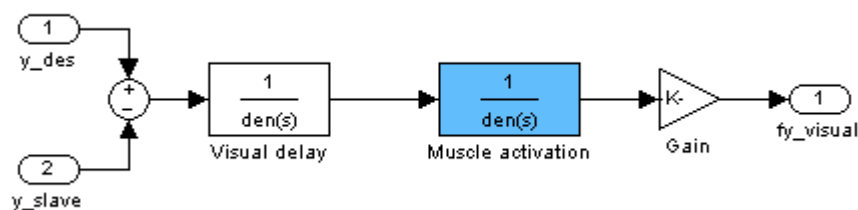


Figure 36: Implementation of visual feedback

The visual feedback gain is chosen in a way to get a critical damped system.

This implementation of visual feedback is not completely realistic, since it does not use any feed forward. It is therefore slower than real visual feedback control.

B1.2 – Human neuromuscular arm model

The human neuromuscular arm model (see Figure 37) is based on the “ControlMass.mdl” model delivered by David Abbink. The input of the model is the control force from the human cortex, the output is a realised human limb trajectory. The modelled neuromuscular dynamics are a simplified version of the dynamics described by Vlught [Vlught et al., 2006]. The model contains the human intrinsic properties (mass, stiffness and damping), but does not contain reflexive feedback (muscle spindle and GTO feedback) yet, however this could be added quite easily.

This model allows for simulation of impedance control (feedback) of the human arm around any trajectory. In other words, it is possible to simulate a motion from A to B with relaxed muscles (RT) or with co-contracted muscles (PT). Feed-forward actions are not hindered by muscle co-contraction, but external force perturbations will be attenuated by the muscle co-contractions.

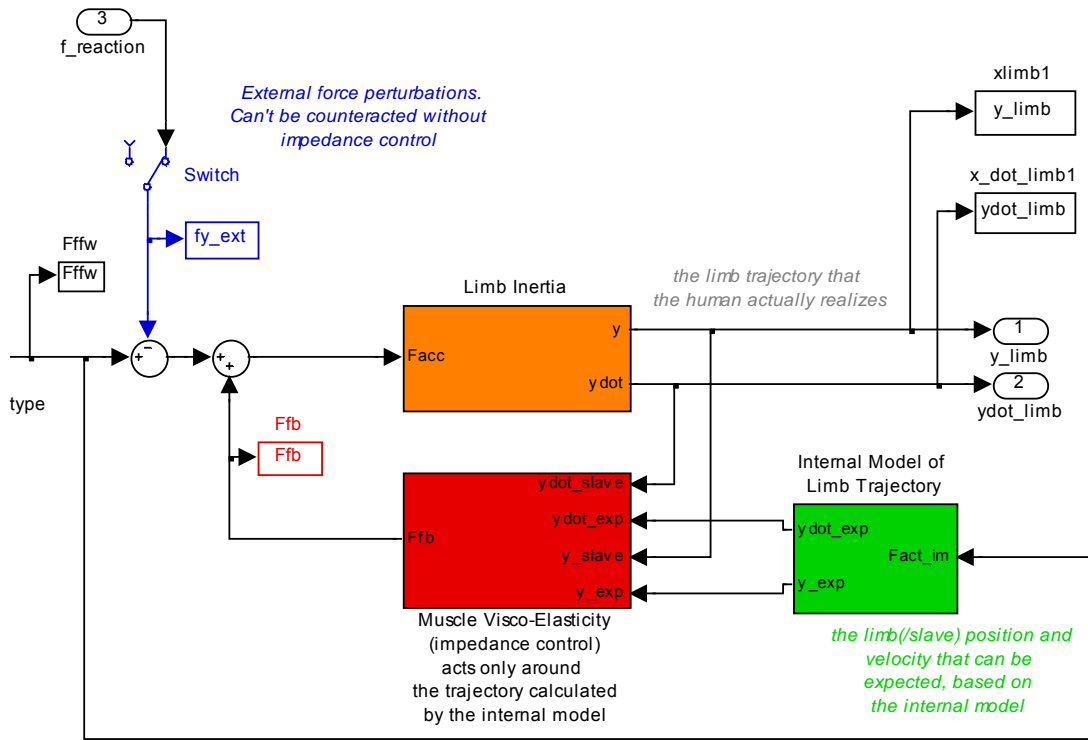


Figure 37: The human operator sub-model, containing the neuromuscular dynamics, implemented in Matlab Simulink..

B2 – Contact dynamics model

The human operator was connected to the tele-manipulator by contact dynamics (see *Figure 38*). The inputs are the limb and master positions and velocities, the output is the contact force.

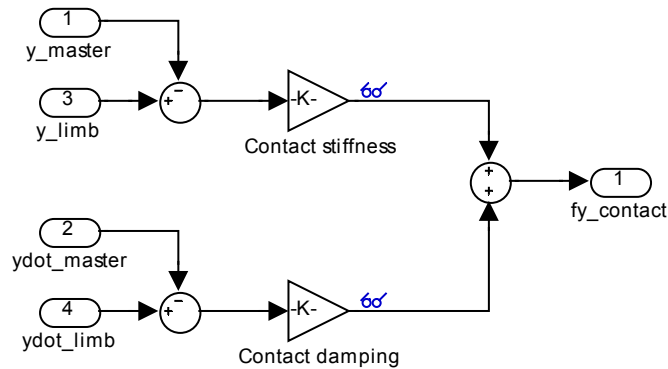


Figure 38: Implementation of the contact dynamics between the human operator and the tele-manipulator, Matlab Simulink.

B3 – Tele-manipulator model

The implementation of the tele-manipulator model is shown in *Figure 39*. The two inputs are the master and slave forces, the outputs are the master and slave positions and velocities.

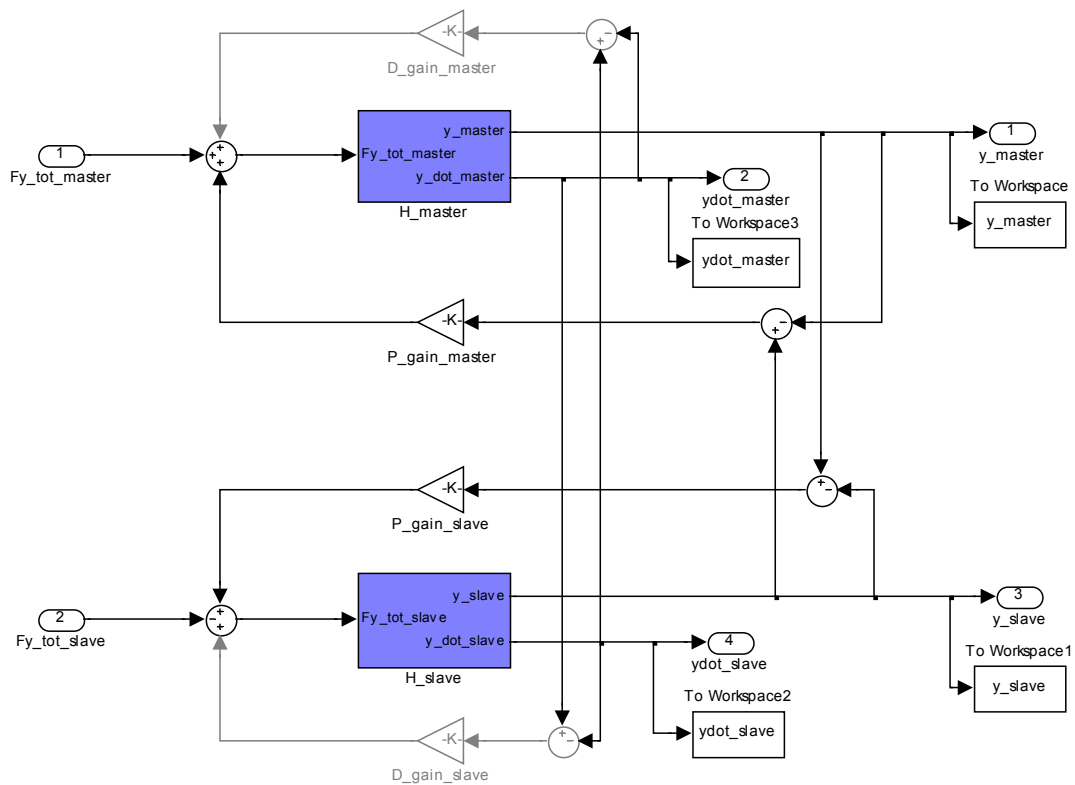


Figure 39: Implementation of the tele-manipulator (PERR controller), Matlab Simulink

B4 – Environment model

The environment is modelled for Free Air Motion (no environment) and Contact Transition Motion. The implementation of this last one is shown in *Figure 40* and *Figure 41*. The contact environment is simulated as high stiffness wall. Inputs are position and velocity of the slave, the output is the interaction force.

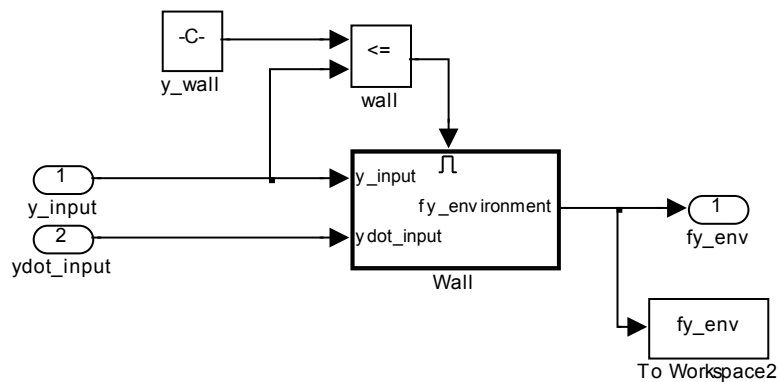


Figure 40: Implementation of a contact environment, Matlab Simulink

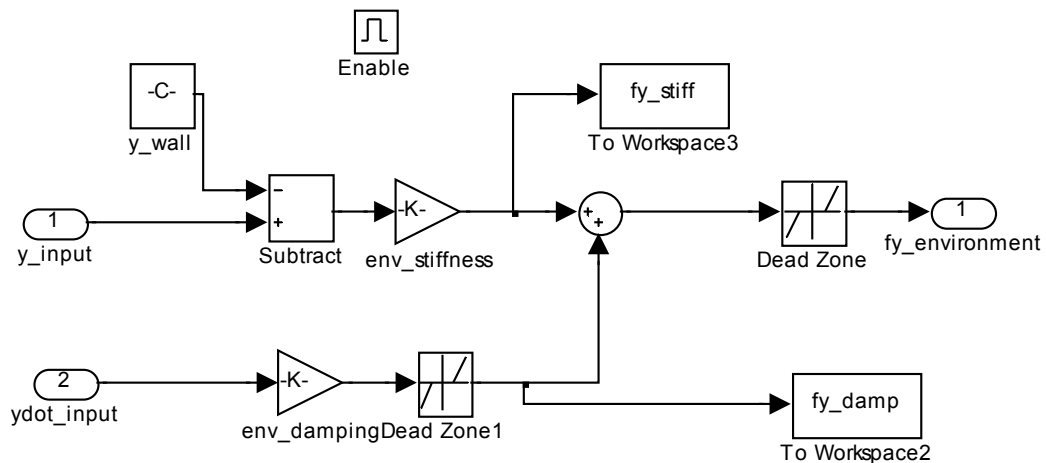


Figure 41: Implementation of a contact environment; a high stiffness wall. Matlab Simulink

B5 – Shared control model

Shared control is modelled as a virtual wall and as stiffness around a predefined path (see *Figure 42*). Inputs are the slave position and the predefined path, the output is the guiding force.

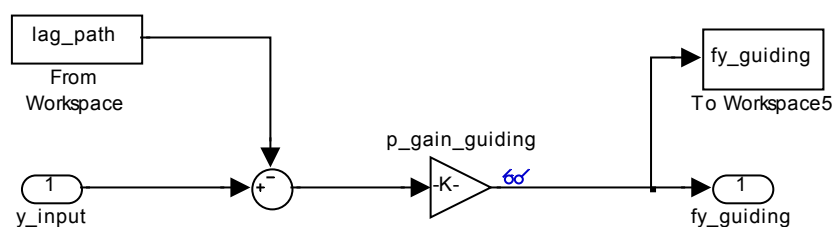


Figure 42: Implementation of shared control, Matlab Simulink

B6 – Shared control 2D, 3DOF implementation

The implantation of 2D, 3DOF shared control is done in a simplified model, not containing the human model and the tele-manipulator model. This model is used to test some shared control strategies like look ahead guiding.

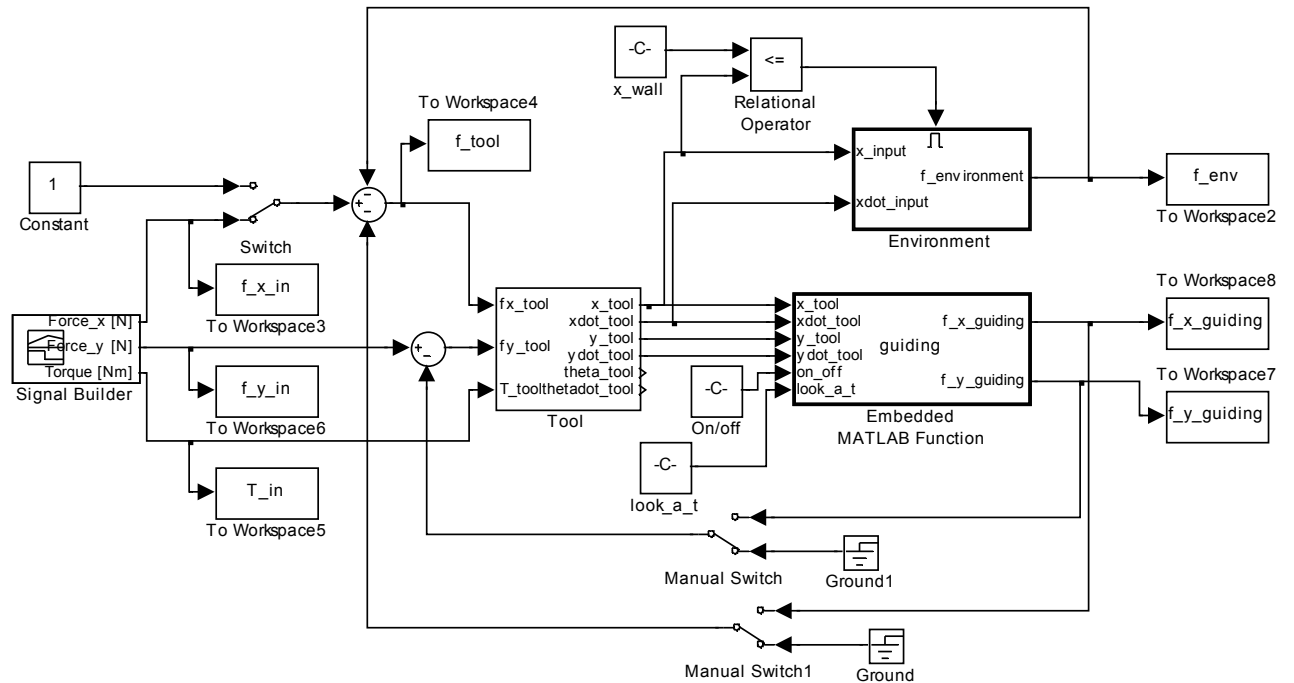


Figure 43: Implementation of tool and environment in 2D, 3DOF. Including haptic shared control based on the look ahead principle.

B7 – Results & recommendations

Figure 44 shows the simulation results for a movement from 0 to 0.1m (desired trajectory shown in black). The expected slave trajectory is not the same as the real slave trajectory, because a simplified second order model is used for the prediction.

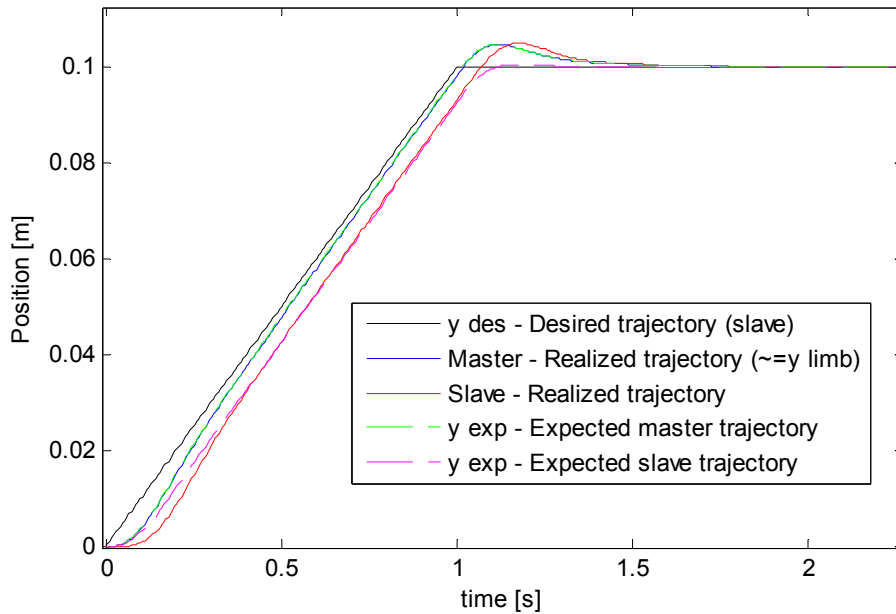


Figure 44: Simulation results (no shared control)

Figure 45 shows the simulation results for an intended movement from 0 to 0.1m. Shared control prevents the motion by a virtual wall at 0.09m.

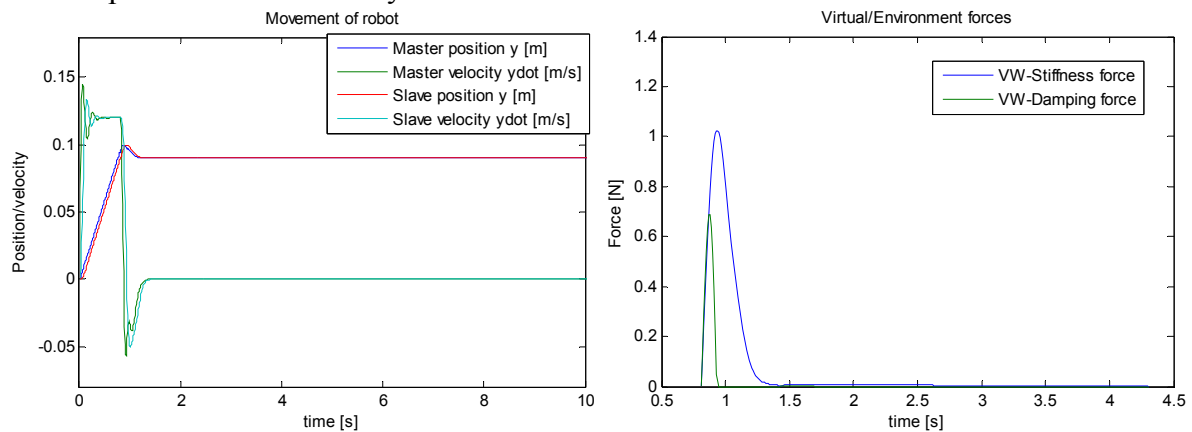


Figure 45: The master and slave trajectories for the input trajectory shown in Figure 33. The input trajectory planned to move to $y=0.1$, however the shared control prevented that with a virtual wall at $y=0.09$ (left). The shared control forces (right).

Figure 46 shows the simulation results for the 2D, 3DOF shared control implementation. The look ahead guiding was tested in this simulation. The figure shows that the shared control stiffness is not high enough to force the tool on the ideal path.

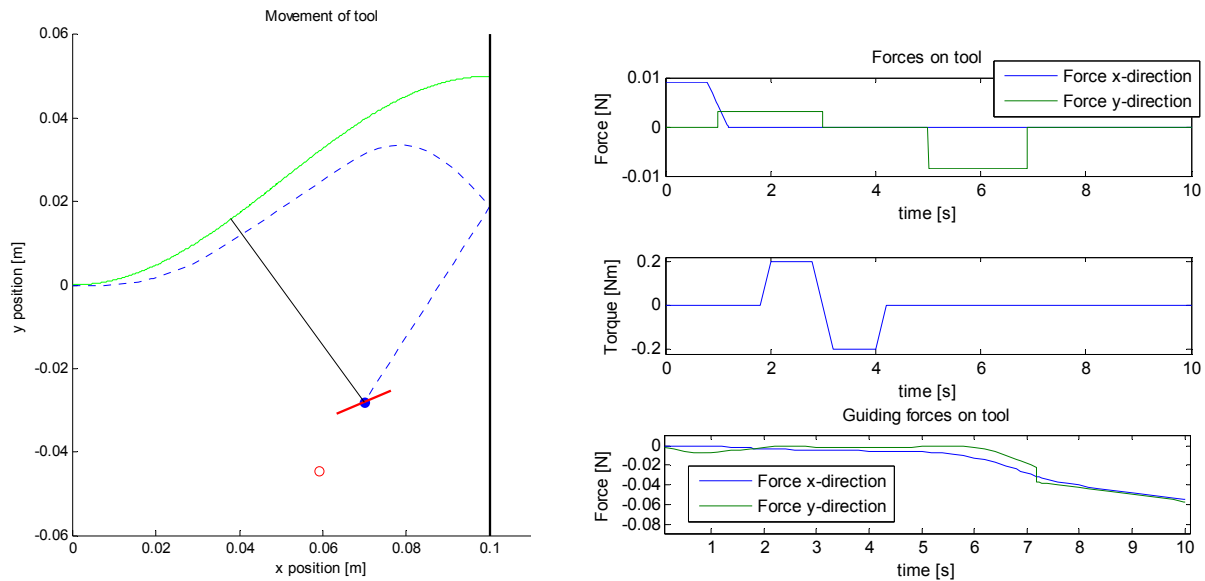


Figure 46: Simulation result (2D,3DOF), with implemented haptic shared control based on a look ahead error. Red encircled the look ahead position, the green line shows the ideal shared control path.

The results show that the models do function and can already be used for analyses of interaction forces between the human, tele-manipulator, environment and shared control. However, to be useful for further research some issues should be solved:

- Refine human cortex model:
 - Internal model: the current implementation of the internal model is too limited. It should be possible to somehow update the internal model.
 - Implementation of force tasks (important to be able to give away to shared control)
 - Improve visual feedback.
- Implement environments for the Constrained Position and Constrained Force tasks.
- Expand the complete model to 2D, 3DOF.

The simulations can be run by executing “parameters_v2.m”, which can be found in the folder “*\Simulations\”. This file contains the parameter definitions and runs the models.

Appendix C – Shared control designs & implementation

C1 – Design of haptic shared control

By means of a literature research an overview and classification of research in the shared control area was created [Boessenkool,2009]. The main application of the shared control philosophy can be found in operational assistance, and it is applied in different fields (e.g. telemanipulation/ cooperative robots/ vehicle control and training). Examples are the virtual fixtures proposed by Rosenberg [Rosenberg,1993], which work as a virtual ruler assisting a tele-manipulated peg-in-hole task. Another example is the continuous haptic guiding during car following [Abbink,2008] and curve negotiation [M.Mulder,2008] proposed by Abbink and Mulder.

The haptic shared control solutions look very promising for telemanipulation, although most research in this field is still limited to 1 or 2 degrees of freedom and/or focused to motions in free air. Continuous guiding is promising, but still not often applied.

This research proposes a continuous haptic shared control for tele-manipulation based on the principle used by Abbink and Mulder [Abbink2010]. The haptic shared controller is an intelligent system which calculates the ideal control input based on sensor information (e.g. about the slave robot, and the environment it interacts with). This ideal control input is presented as a force on the master device, so the operator continuously feels the optimal control input. The system will guide the operator to reach the optimal input, but the operator can always resist the assisting forces if he does not agree with the system. A general high-level scheme of the proposed shared control is illustrated in *Figure 47*.

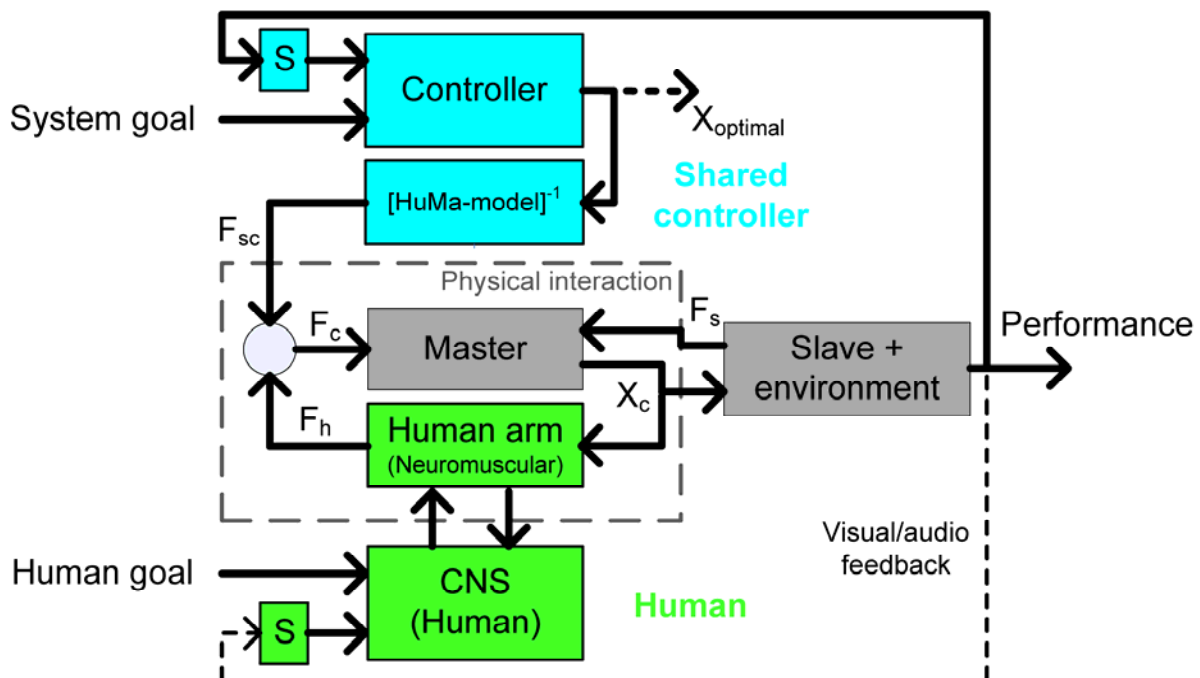


Figure 47: A schematic high-level representation of (continuous) shared control. The guiding system receives feedback by sensors (S) and uses a control model to continuously calculate the optimal system input $X_{optimal}$. An inverse human/master-model is used to derive the required input forces F_{sc} at the master side. The control input X_c may now be simultaneously influenced by both the human (below) and the shared controller (above) [adapted from Abbink [Abbink2010]].

This principle of shared control (*Figure 47*) can be implemented in many different ways and at different levels of complexity. This research aims to give a proof of principle for shared control in tele-operation for all four fundamental motion types (defined by Wildenbeest [Wildenbeest2010]). To design such a shared control system, a number of sub-designs is made (partial based on the existing literature), focused on the four fundamental motion types. These sub-designs are also shown in Table 4:

1. **Free Air Movement.** Sub-designs position guiding:

- Unconstrained movement: no guiding
- Protective layer: only guiding close to forbidden regions The guiding force: $F_{g-pos} = -E_1 \cdot k_1$, with E_1 the distance moved into the layer and k_1 a stiffness of 120 [N/m].
- Tunnel: guiding by a tunnel The guiding force: $F_{g-pos} = -E_1 \cdot k_1$, with E_1 the distance moved into the tunnel wall and k_1 a stiffness of 120 [N/m].
- Ideal path: guiding by an ideal path. The guiding force: $F_{g-pos} = -E_1 \cdot k_1$, with E_1 the path error and k_1 a stiffness of 120 [N/m].
- Look ahead guiding using an ideal path. The guiding force: $F_{g-pos} = -E_2 \cdot k_2$, with E_2 the look ahead path error and k_2 a stiffness of 120 [N/m]. The look ahead path error is defined as the path error at an estimated position in future based on the velocity vector and a look-ahead time of 0.1 s.

All with the option guiding/no guiding along the path (a constant (low) force in the direction of the path).

The same designs are used for rotation guiding, the rotational controller stiffness was [0.5Nm/rad].

2. **Contact Transition.** Sub-designs:

- Damping close to contact (prevents hard collisions)
- Position/Orientation guiding (stiffness: 120 [N/m] and [0.5Nm/rad]).
- Haptic feature (vibration) to increase contact sensation (prevents that the human misses the contact transition)

3. **Constrained Position Movement.** Sub-designs:

- Placement of compliance/rotation center at the tool tip/bolt origin
- Guide alignment (stiffness: 120 [N/m] and [0.5Nm/rad]).

4. **Constrained Force Movement.** Sub-designs:

- Position guiding perpendicular to force direction (stiffness: 120 [N/m])
- Placement of rotation centre at the bolt origin (NoFF condition).

Some notes for the designed shared control possibilities:

- *Figure 47* shows a goal input for both human and shared controller. In an ideal situation, the shared controller should be able to figure out the human goal (intention and strategy) and adapt itself to that. However, in this research the controller determines the goal (e.g. the ideal boundary/tunnel/path), and shows this visual to the human. This *ideal* path is chosen and is not optimized to human motions.
- Another simplification of the shared controller with respect to *Figure 47* is the assumption of constant dynamics of the combined human arm and master. This simplifies the inverse *Human-Master-model*, which is used for the calculation of shared control forces, to a constant gain. In reality, the human adjusts his arm

admittance depending on the task and the situation. When the human executes a position task or when he is sure of his motion (feedforward), the human arm admittance is lower, than for example during a force task. Examples are a high stiffness of the arms when drilling a hole in a wall using a drilling machine, or a low stiffness of the arm when holding a glass of water and preventing the water from going over during disturbances. The tested shared control does not compensate for the changes in human arm admittance, as the shared control gain is a hand-tuned constant.

In further research, the shared control could be optimized towards the human by including the human arm admittance in the shared controller. Neuromuscular analysis as used in [Abbink,2006] could be very useful for this. An option could be to let the shared control shift between presets of human arm admittances depending on the motion type. Or maybe even a real time estimation of the human arm admittance, based on e.g. grip force, could be used (current research in the automotive field (Abbink) investigates the relationship between grip strength and human arm admittance for a steering task.).

All these sub-designs were implemented in the controller of the test setup and were hand-tuned (e.g. stiffness, look ahead time). An appropriate shared control design was selected/combined on the basis of a small pilot experiment; two test subjects selected the most intuitive shared control designs.

The selected shared control candidate, which is described in more detail below, is not necessarily the optimal shared control. As the goal of this research is not *designing an optimal shared control*, but more a *prove-of-principle* of shared control, this chosen shared control system is suitable.

The selected shared controller consists of the following parts:

1. **Free Air Movement.**

The position guiding force is based on the look ahead path error:

$$F_{g-pos} = -E_2 \cdot k_2, \text{ with } E_2 \text{ the look ahead path error and } k_2 \text{ a stiffness of } 120 \text{ [N/m]}.$$

The look ahead path error is defined as the path error at an estimated position in future based on the velocity vector and a look-ahead time of 0.1 s. The ideal path is defined to be a smooth path between the target points (see *Figure 48*).

There will not be guiding forces along the path.

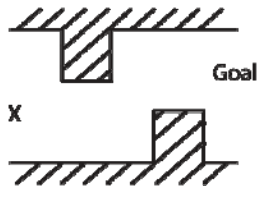

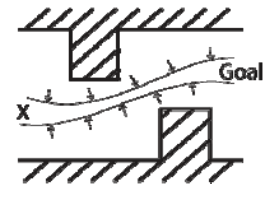
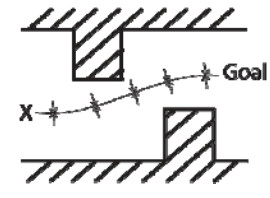
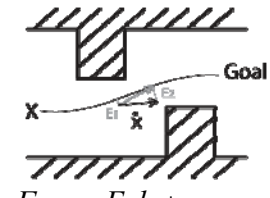
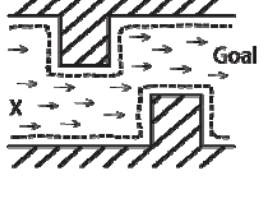

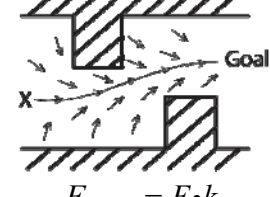
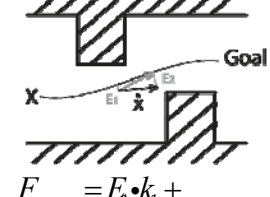


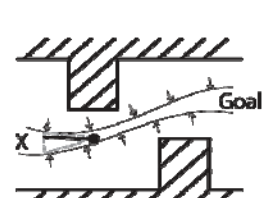
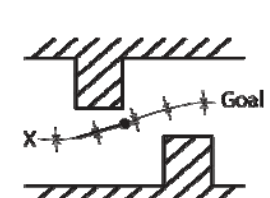
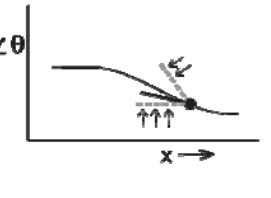
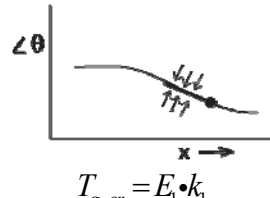
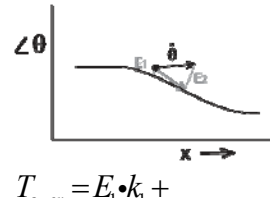
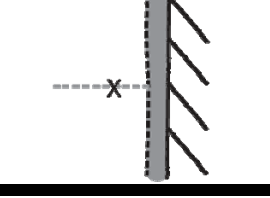



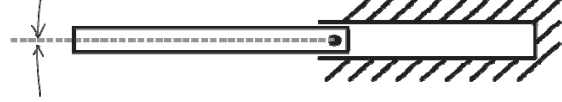
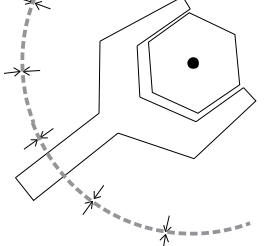
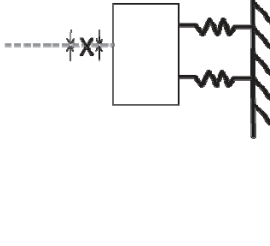
The guiding of the tool orientation was linear increased to a stiffness of 0.5 [Nm/rad] within a distance of 0.04m of the target points 1,2 and 3.

2. **Contact Transition.** Within a distance of 0.05m of the bolt, the tool orientation guiding was linear increased to a stiffness of 0.5 [Nm/rad]. The position was guided with a stiffness of 120[N/m]. An artificial damping prevented hard collisions.

3. **Constrained Position Movement.** The spanner was guided to the right orientation with a stiffness of 0.5[Nm/rad]. Furthermore a snap-feature was introduced close to the bolt.

4. **Constrained Force Movement.** The presented guiding force is only perpendicular to the force movement. The snap-feature is active to ensure that the spanner stays on the bolt head. In the NoFF condition, the shared controller introduced a virtual bolt position with a stiffness of 120[N/m].

Table 4: Overview of SC designs (inspired by literature), subdivided for the four fundamental motion types.

		Overview of possible shared control guiding-designs				
Free air motion	No guiding forces along path	Unconstrained 	Protective layer/ FRVF (repulsive) 	Virtual tunnel/ funnel (repulsive) 	Continuous (1D) static (attractive) 	Continuous (2D -> 1D) dynamic (attractive)  $F_{g-pos} = E_1 \cdot k_1 + E_2 \cdot k_2(\dot{x}) + F_{damp, > V_{max}}$
	Also guiding forces along path		Protective layer/ FRVF (repulsive) 	Virtual tunnel/ funnel (repulsive) 	Continuous (2D) static (attractive)  $F_{g-pos} = E \cdot k$	Continuous (2D -> 2D) dynamic (attractive)  $F_{g-pos} = E_1 \cdot k_1 + E_2 \cdot k_2(\dot{x}) + F_{damp, > V_{max}}$
Free air motion	Angle guided by pos. constraint	Unconstrained 	Protective layer/ FRVF (repulsive) 	Virtual tunnel/ funnel (repulsive) 	Continuous (1D) static (attractive)  $F_{g-or} = E_1 \cdot k_1$	
	Separate angle path		Protective layer/ FRVF (repulsive), Virtual tunnel/ funnel (repulsive) 	Continuous (1D) static (attractive)  $T_{g-or} = E_1 \cdot k_1$	Continuous (2D -> 1D) dynamic (attractive)  $T_{g-or} = E_1 \cdot k_1 + E_2 \cdot k_2(\dot{\theta}) + F_{damp, > \dot{\theta}_{max}}$	
Contact	Damping close to contact surface 	Haptic feature (e.g. virtual vibration) to increase contact sensation 	Guiding of positions / orientation 			
Position constrained	Placement of compliance/rotation centre, kinematic (repulsive) 	Guiding alignment forces (attractive) 				
Force constrained	Rotation centre, position guiding perpendicular to force direction 	Position guiding perpendicular to force direction 				

C2 – Implementation of shared control

The implementation of the designed and selected shared control system will be discussed in more detail in this paragraph (the full matlab code can be found at the USB-stick delivered at the BioMechanical Engineering depository). This implementation is done in Matlab Simulink, as the controller of the used telemanipulator is based on a Simulink model. The shared control algorithm was programmed in an embedded m-file. The calculated shared control forces were be added add the master side, see *Figure 14* and *Figure 15*.

Free air movement

The look ahead guiding in the x- and y-position was calculated by first calculating the ‘look ahead position’ (x_{lag} / y_{lag}), based on the current position, velocity vector and the look ahead time (t_{lag}):

```
% Calculation of x_lag and y_lag (x_m_real and x_m_real = real master position)
x_lag = x_real + (vx_real * t_lag);
y_lag = y_real + (vy_real * t_lag);
```

The minimal distance of this ‘look ahead position’ to the ideal path was calculated:

```
% Each timestep the minimal distance to the ideal path is calculated.
distVector = sqrt((x_lag-x_path(path_part)).^2 +
    (y_lag-y_path(path_part)).^2); %distance to ideal path
[minDist, ind] = min(distVector);
```

The ideal path is described by 330 points, therefore an interpolation function was used to make the result more smooth (otherwise the resolution could be felt).

The shared control force was calculated by multiplying this look ahead path error with a gain of 120 [N/m]. An example of the calculated forces can be seen in *Figure 48*

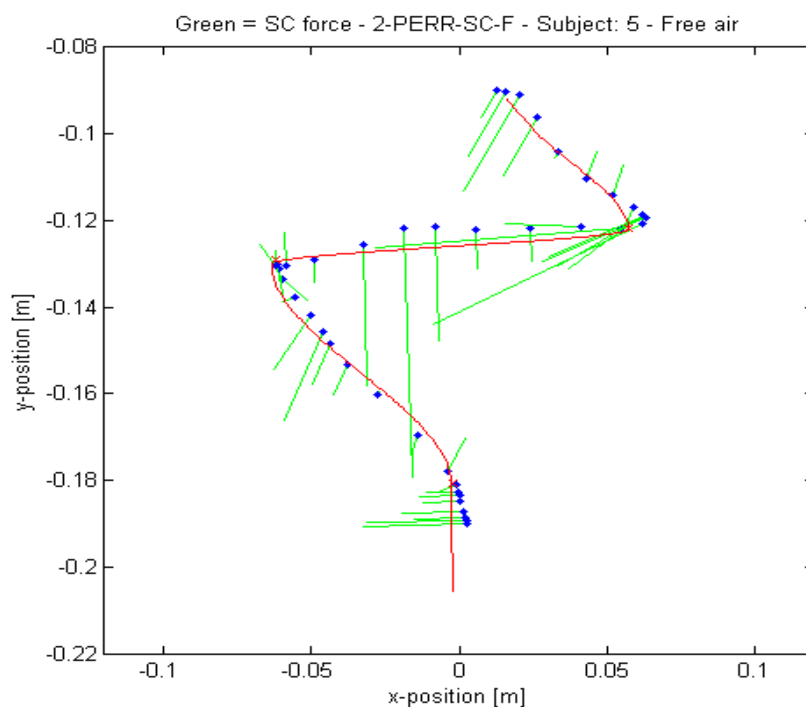


Figure 48: The shared control forces (green) shown during the task (until contact with the bolt). The red line shows the ideal path proposed by the shared controller. Scale of the forces in the graph: 20 [N/m]

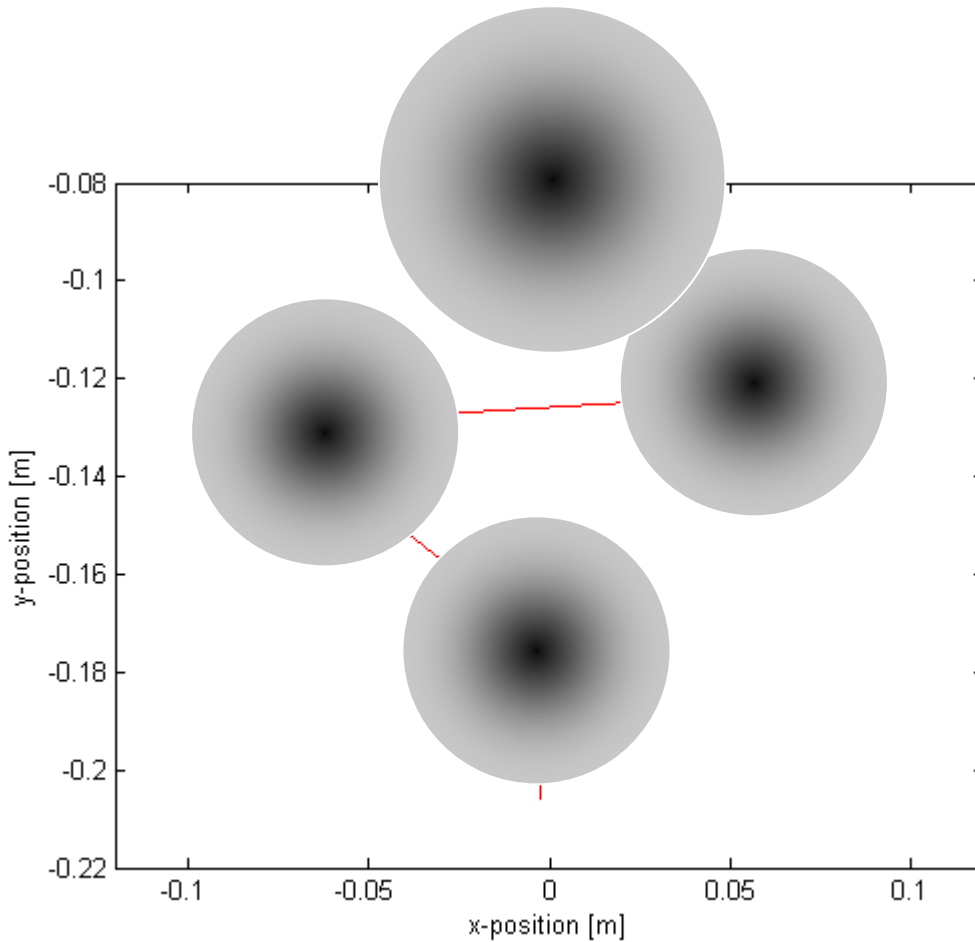


Figure 49: The guiding of the tool orientation was linear increased within a distance of 0.04m of the target points 1, 2 and 3 and within a distance of 0.05m of the bolt (see black spots). The red line shows the ideal path proposed by the shared controller. The maximal rotational guiding stiffness is [0.5Nm/rad].

The guiding of the tool orientation was linear increased to a stiffness of 0.5 [Nm/rad] within a distance of 0.04m of the target points 1,2 and 3 (see Figure 49).

Contact Transition. Within a distance of 0.05m and 0.04m of the bolt, the tool orientation guiding was linear increased to a stiffness of 0.5 [Nm/rad]. The position was guided with a stiffness of 120[N/m]. An artificial damping prevented hard collisions.

```
%A linear increasing damping force within a radius of 0.01m from the bolt
if distb < radia(6)           %distance to bolt head
    fx_damp = cos(bolt_angle) * ((radia(6)-dist4)/radia(6)) * -xdot;
    fy_damp = sin(bolt_angle) * ((radia(6)-dist4)/radia(6)) * -ydot;
```

Constrained Position Movement. The spanner was guided to the right orientation with a stiffness of 0.5[Nm/rad]. Furthermore a snap-feature was introduced close to the bolt.

```
%A constant snap force within a radius of 0.01m from the bolt
if distb < radia(6)           %distance to bolt head
    fx_snap_ff = cos(bolt_angle);
    fy_snap_ff = sin(bolt_angle);
```

Constrained Force Movement. The presented guiding force is only perpendicular to the force movement. The snap-feature is active to ensure that the spanner stays on the bolt head. In the NoFF condition, the shared controller introduced a virtual bolt position with a stiffness of 120[N/m].

Appendix D – Shared control experiment

Appendix D describes several aspects of the executed shared control experiment in more detail. Appendix D1 contains the subject tasks instruction and describes the subdivision of the task into subtasks. The evaluation metrics and subjective measures are described in appendix D2. Appendix D3 shows an overview of the data management. Finally, appendix D4 shows an extensive overview of the experimental results.

D1 – Experiment task

D1.1 – Task instruction test subjects

Before the start of the experiment, the following task instruction was handed out to the test subjects (in Dutch or English).

Task instruction [Dutch]:

Shared control experiment – Taak instructie

Tijdens dit experiment zal worden gevraagd om +/- 60 keer met behulp van een tele-operator een bout aan te draaien. De taak is als volgt gedefinieerd; begin op het startpunt, beweeg naar de drie aangegeven posities (positie en orientatie!) en volg daarbij het aangegeven pad, glij over de boutkop en draai de bout aan als aangegeven. De taak zal met 6 verschillende condities worden uitgevoerd, voor elke conditie wordt de taak 8 keer herhaald.

Twee van de condities hebben te maken met de manier waarop de taak wordt uitgevoerd: Je kunt er voor kiezen om een taak heel snel uit te voeren, of juist heel nauwkeurig. Tijdens de experimenten zal steeds expliciet aangegeven worden of de taak snel (zo snel mogelijk) of juist nauwkeurig (zo nauwkeurig mogelijk) moet worden uitgevoerd.

Voorafgaand aan een set experimenten is er steeds gelegenheid om met de taak te oefenen. Tijdens deze oefening kun je verschillende strategieën proberen/testen. Tijdens de echte experimenten is het belangrijk om binnen een set testen niet meer van strategie te wisselen.

Probeer tijdens het experiment een comfortabele houding te vinden recht voor de tele-manipulator. De houding van het lichaam heeft invloed op het experiment, daarom is het belangrijk om je lichaamshouding tijdens het experiment zoveel mogelijk constant te houden.

Na elke twee sets van experimenten zal gevraagd worden een enquête in te vullen. Een aantal vragen hebben te maken met het bepalen van de ‘workload’. Hiervoor is nodig een aantal begripdefinities te kennen, deze kun je vinden in ‘Appendix A’. (Verdere uitleg hierover volgt...)

Het experiment zal ongeveer 1,5 uur in beslag nemen. Aan het einde van het experiment kan worden uitgelegd waar het onderzoek op gericht is.

Task instruction [Dutch]:

Shared control experiment – Task instruction

During this experiment you will be asked to perform a ‘bolt fastening task’ using a tele-operator. The task is defined as follows; start at the starting point, reach the 3 marked positions (position and orientation!) following the stated path, slide over the bolt head and rotate the bolt as indicated.

The task will be executed with 6 different conditions, each repeated 8 times (in total +/- 60 trials).

Two conditions have to do with the way of task execution: You can choose to optimize task performance for speed, or to optimize task performance for accuracy. During the experiments it will be explicitly stated whether the task has to be executed fast (perform the task as fast as possible) or accurate (perform the task as accurate as possible).

Preceding a set of experiments there will be the possibility to have some exercise and to train the task. During this short training-time it’s useful to test some different strategies. During the real experiments it is important to have one strategy (and not to change your strategy).

Try to sit in a natural and comfortable position in front of the tele-manipulator. Your posture influences the experiment, so it’s important to hold it constant during the experiments.

After each two sets of experiments you will be asked to answer a questionnaire. Some of the questions have to do with the determination of the ‘workload’. For this it is necessary to know some definitions, which you can read in ‘Appendix A’. (More explanation will follow...)

The experiment will take around 1,5 hour. The focus of the research could be explained at the end of the experiment.

Task instruction appendix A:

RATING SCALE DEFINITIONS		
Title	Endpoints	Descriptions
MENTAL DEMAND	<i>Low/High</i>	How much mental and perceptual activity was required (e.g., thinking, deciding, calculating, remembering, looking, searching, etc.)? Was the task easy or demanding, simple or complex, exacting or forgiving?
PHYSICAL DEMAND	<i>Low/High</i>	How much physical activity was required (e.g., pushing, pulling, turning, controlling, activating, etc.)? Was the task easy or demanding, slow or brisk, slack or strenuous, restful or laborious?
TEMPORAL DEMAND	<i>Low/High</i>	How much time pressure did you feel due to the rate or pace at which the tasks or task elements occurred? Was the pace slow and leisurely or rapid and frantic?
EFFORT	<i>Low/High</i>	How hard did you have to work (mentally and physically) to accomplish your level of performance?
PERFORMANCE	<i>Good/Poor</i>	How successful do you think you were in accomplishing the goals of the task set by the experimenter (or yourself)? How satisfied were you with your performance in accomplishing these goals?
FRUSTRATION LEVEL	<i>Low/High</i>	How insecure, discouraged, irritated, stressed and annoyed versus secure, gratified, content, relaxed and complacent did you feel during the task?

D1.2 – Selection of motion types

The subjects were asked to execute a bolt-and-spanner task with the following description (see also *Figure 50*); start at the lower y-limit, move to points 1, 2 and 3, move to the bolt, slide the spanner over the bolt, and rotate the bolt to the visible reference angle. The locations of these points are respectively: $(x, y, \theta) = (0\text{m}, 0\text{m}, 0^\circ)$, $(0\text{m}, 0.02\text{m}, 0^\circ)$, $(-0.06\text{m}, 0.07\text{m}, 0^\circ)$, $(0.06\text{m}, 0.08\text{m}, 65^\circ)$ and the bolt position $(x, y) = (0\text{m}, 0.12\text{m})$.

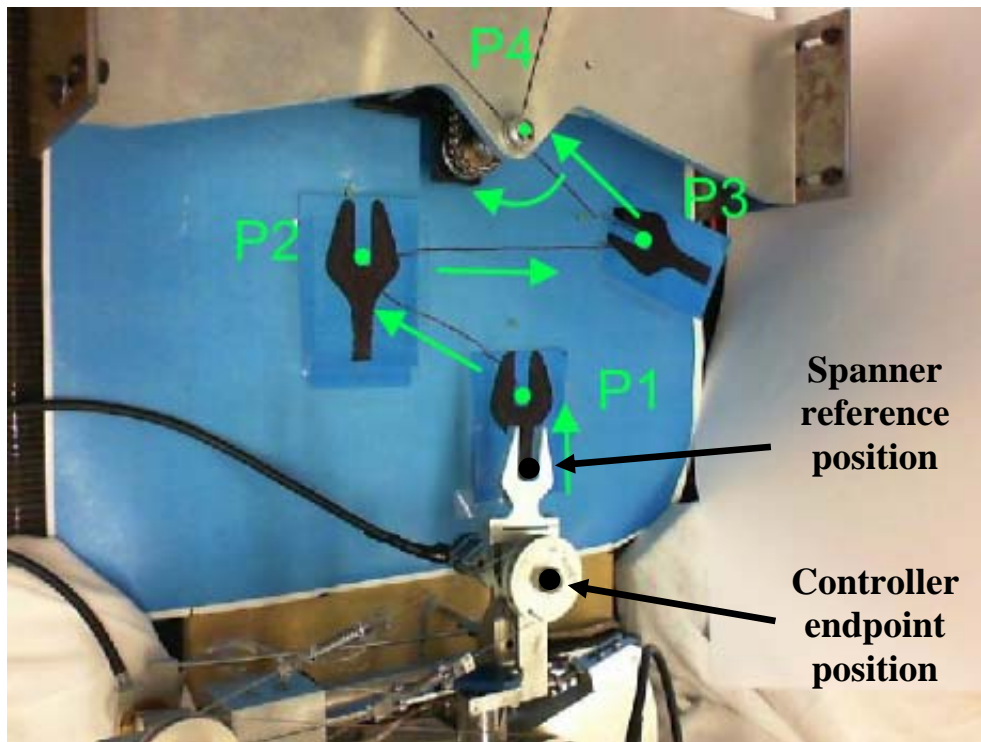


Figure 50: Camera view from the environment at the slave side. The task sequence is shown in green; move to target points P1, P2 and P3, move to the bolt (P4), slide over the bolt and rotate the bolt to the visible reference. The black dots denote the Cartesian endpoint position used in the controller and the spanner reference position.

To be able to analyse the recorded data per subtask, for each individual trial seven reference points were identified (see *Figure 51*). The relation between the subtasks and reference points and is shown in Table 5. The selection of the reference points was automated using m-file “DataProcessing2_Subtasks_Experiment.m”.

Table 5: Definition of the four fundamental subtasks based on the reference point as shown in *Figure 51*.

Subtasks	Ref. points	
Free Air Movement (FAM)	T0	Start ‘Free Air Movement’
	T1	Point 1
	T2	Point 2
	T3	Point 3 – End ‘Free Air Movement’
Contact Transition Movement (CTM)	T3	Start ‘Contact Transition Movement’
	T4	End ‘Contact Transition Movement’
Constrained Position Movement (CPM)	T4	Start ‘Constrained Position Movement’
	T5	End ‘Constrained Position Movement’
Constrained Force Movement (CFM)	T5	Start ‘Constrained Force Movement’
	T6	End ‘Constrained Force Movement’

Note that the slave trajectory shown in *Figure 51* shows the controller endpoint instead of the spanner reference point (see *Figure 50*). The controller endpoint was used to identify the reference points, since this resulted in a more simple implementation of the identification algorithm.

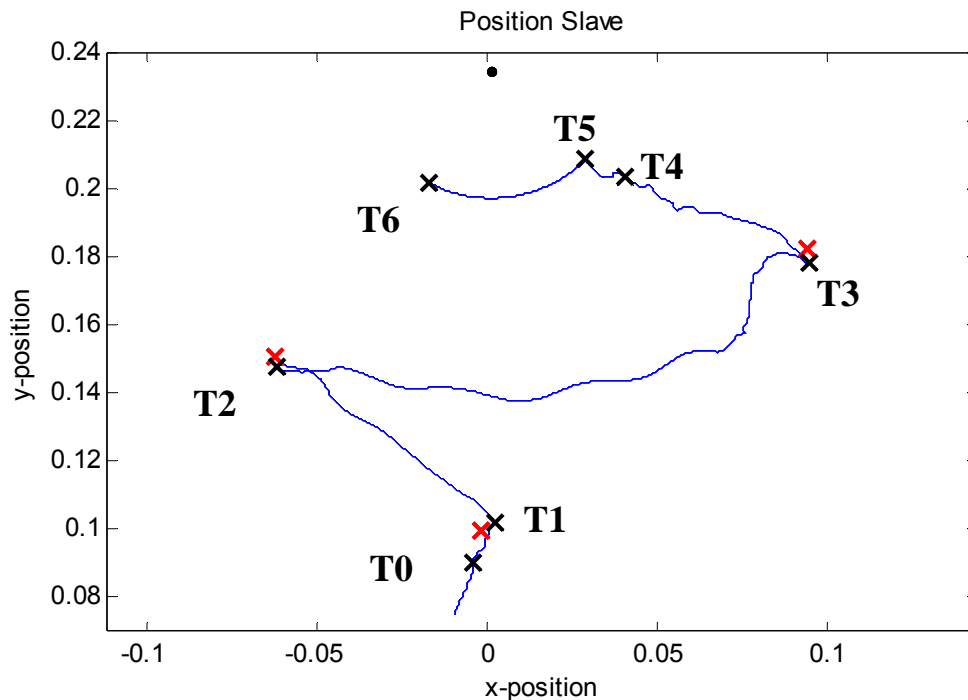


Figure 51: Selection of the seven reference points (“**T**”; black crosses) shown at the slave trajectory (controller endpoint). Red crosses denote the real positions of target points 1,2 and 3.

The following criteria were used to select the reference points. Some of them are simplified to save some space; only showing the most strict criteria. The full code can be found in m-file: `DataProcessing2_Subtasks_Experiment.m`.

Reference point T0

Go through ‘`slave_y_pos`’-vector in reverse direction; Save `index_T0` when the y-position becomes smaller than 0.09.

```
if y_val < 0.09      → index_t0
```

Reference point T1

Go through ‘`slave_y_pos`’-vector in reverse direction; Save `index_T1` when the absolute position and rotation velocity becomes lower than 0.005 [m/s] resp. 0.005 [rad/s], within a radius of 0.02m from point 1.

```
if (dist1 < 0.02)
    if ((abs_velo_s(i) < 0.005) && (abs(rot_velo_s(i)) < 0.005))
        → index_t1
```

Otherwise, save `index_T1` for the closest distance to point 1, within a radius of 0.02m from point 1.

```
if (dist1 < 0.02)
    smallest dist1      → index_t1
```

Reference point T2

Go through 'slave_y_pos'-vector in reverse direction; Save index_T2 when the absolute position and rotation velocity becomes lower than 0.005 [m/s] resp. 0.005 [rad/s], within a radius of 0.02m from point 2.

```
if (dist2 < 0.02)
    if ((abs_velo_s(i) < 0.005) && (abs(rot_velo_s(i)) < 0.005))
        → index_2
```

Otherwise, save index_T2 for the closest distance to point 2, within a radius of 0.02m from point 2.

```
if (dist2 < 0.02)
    smallest dist2      → index_t2
```

Reference point T3

Go through 'slave_y_pos'-vector in reverse direction; Save index_T3 when the absolute position and rotation velocity becomes lower than 0.005 [m/s] resp. 0.005 [rad/s], within a radius of 0.02m from point 3.

```
if (dist3 < 0.02)
    if ((abs_velo_s(i) < 0.005) && (abs(rot_velo_s(i)) < 0.005))
        → index_3
```

Otherwise, save index_T3 for the closest distance to point 3, within a radius of 0.02m from point 3.

```
if (dist3 < 0.02)
    smallest dist3      → index_t3
```

Reference point T4

Go through 'slave_y_pos'-vector in reverse direction; Save index_T4 when the distance to the bolt becomes larger than 0.05 [m].

```
if (distb > 0.050)      → index_4
```

Reference point T5

Go through 'slave_y_pos'-vector in reverse direction; Save index_T5 when the position or rotation velocity become again larger than 0.003 [m/s] and 0.01 [rad/s], for a distance to the bolt smaller than 0.043 [m].

```
if ( (abs_velo_s(i) > 0.003) || (abs(rot_velo_s(i)) > 0.01 ) ) &&
    (distb < 0.043)
    → index_5
```

Reference point T6

Go through 'slave_y_pos'-vector in reverse direction; Save index_T6 when the bolt angle starts to deviate from the final bolt angle.

```
if (( bolt_angle(i) > (angle_mean + 0.003) ) ||
    ( bolt_angle(i) < (angle_mean - 0.003) ))
    → index_6
```

In case the algorithm was not able to find a point meeting the requirements, the reference point was selected manually.

D2 – Description of evaluation metrics

The performance of a Connected Telemanipulation System can be quantified by a broad variety of metrics. Task performance metrics like time-to-complete, accuracy and exerted contact forces are commonly used. As we are interested in the effect of shared control and want to understand how human operators respond to these guiding forces, also a number of control effort and mental load metrics is included.

The analyzed metrics can be divided into three categories:

- Task performance (TP) metrics:
 - tcc = Time to complete
 - err_{int} = Integrated path error (accuracy)
 - $e_{p3,rot}$ = Error in rotation at point 3 (accuracy)
 - $F_{e,max}$ = Maximal force exerted on environment
 - $F_{e,av}$ = Average force exerted on environment
 - Fault rate (number of trials containing a fault in the task execution. Type 1: Normal fault (slide beside bolt/ leave bolt unintended). Type 2: Counteraction with shared control (take the wrong path).

- Control effort (CE) metrics:
 - $F_{SC,max}$ = Maximal shared control force (compared to controller forces FF-NoSC)
 - $F_{SC,av}$ = Average shared control force (compared to controller forces FF-NoSC)
 - n_{rev} = Reversal rate

- Mental load (ML):
 - Self reported workload (NASA TLX)
 - Subjects were asked to grade their performance in accuracy and speed. In shared control conditions also the helpfulness of the guiding had to be graded.

In fact the Control Effort metrics ‘physical workload’ (W_{phys}), ‘maximal operator force’ ($F_{op,max}$) and ‘average operator force’ ($F_{op,av}$) should also be analyzed. These metrics give valuable information about how human deal with the shared control forces. Unfortunately a suitable force sensor was not available. Therefore, we were not able to measure the human input forces.

Not all metrics were available or relevant for all motion types. Table 6 shows an overview of the analyzed metrics per motion type.

Table 6: Analyzed metrics, divided into Task Performance metrics (TP), Control Effort metrics (CE) and Mental load metrics (ML).

Metric no.	Metric description	Abbrev.	Total task	FAM	CM	CPM	CFM
TP1	Time to complete	tcc	x	x	x	x	x
TP2	Integrated path error	err_{int}		x			
TP3	Error in orientation at point 3	$e_{p3,rot}$		x			
TP4	Maximal force exerted on environment	$F_{e,max}$			x	x	x
TP5	Average force exerted on environment	$F_{e,av}$			x	x	x

TP6	Fault rate	FR	X				
CE1	Reversal rate	n_{rev}	X	X	X	X	
CE2*	Maximal shared control force	$F_{SC, max}$	X	X	X	X	X
CE3*	Average shared control force	$F_{SC, av}$	X	X	X	X	X
ML1	NASA TLX workload	TLX	X				
ML2	Subjective: How fast?	-	X				
ML3	Subjective: How accurate?	-	X				
ML4*	Subjective: Did the guiding help?	-	X				

*Only available in SC conditions. No statistical analyses done for these metrics.

Calculation of the metrics:

TP1 - Time to complete

The time-to-complete for a (sub) task was calculated by subtracting the corresponding indices and dividing the result by 1000 (since the recorded data was sampled at 1000Hz).

For example the time-to-complete for the free air motion: $t_{tc_FA} = (T3 - T0) / 1000$

TP2 – Integrated path error

The integrated path error was calculated by first projecting the path error to the ideal path (closest datapoint). For each datapoint of the ideal path the largest corresponding error value was selected (see *Figure 53*, right). The projected error was integrated over the length of the ideal path.

The calculated integrated path error is an approximation, since it not represents the exact area between the trajectory and the ideal path, but it will be suitable for comparison of trials.

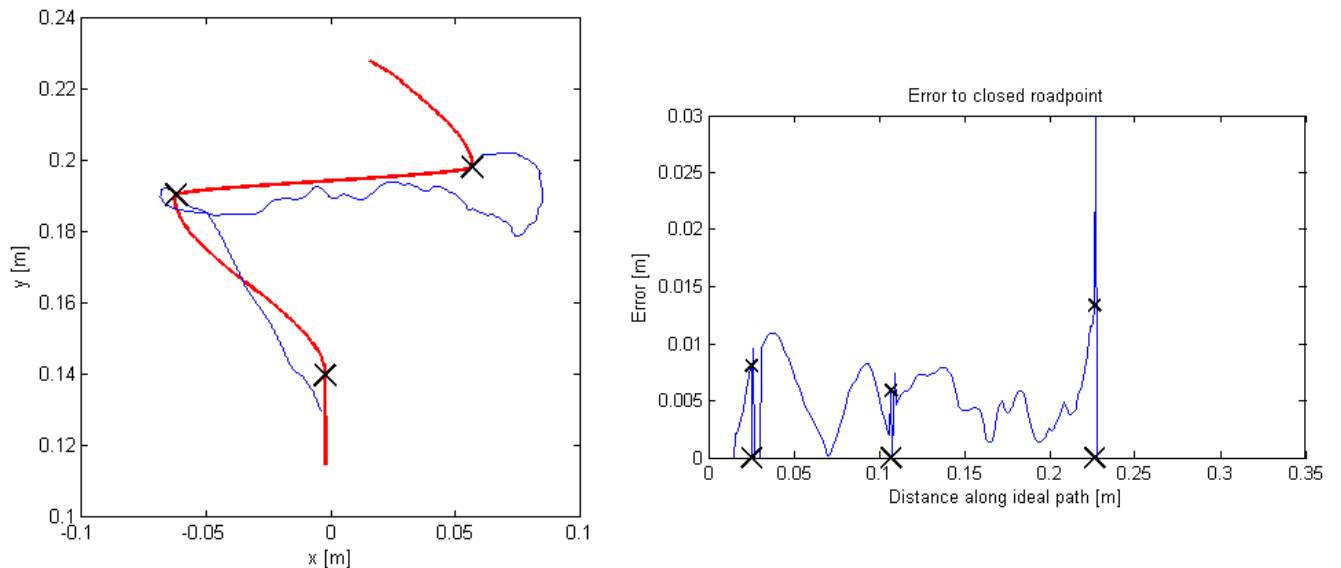


Figure 52: The integrated path error was calculated by projecting the path error to the ideal path. The area under this graph (right) was used as a measure for the path error. 'X' denotes the target points 1, 2 and 3.

TP3 - Error in orientation at point 3

The exact tool orientation at point 3 is hard to distinguish by only using the visual feedback, since the camera is mounted under an angle. The orientation error is therefore an interesting metric in order to analyse the effect of shared control.

The orientation error at point 3 was calculated by subtracting the target orientation from the actual orientation at point 3.

TP4, TP5 - Maximal and average force exerted on environment

For the tele-operated conditions the series-elastic force estimation was used to calculate the maximum and average force exerted on the environment.

TP6 - Fault rate

The fault rate was defined as the relative number of trials containing a fault in the task execution. The following faults were considered:

- Movement of the spanner beside the bolt head (overshoot)
- Leaving the bolt head during the force task.

Furthermore the number of trials containing counteracting control behaviour between human and shared control was recorded.

CE1 - Reversal rate

The reversal rate was defined as the amount of times the movement changes direction (amount of sign changes of the velocity). The reversal rate was determined separately for the x- y- and θ -direction. The paper only presents the reversal rate for the x-direction, but same trends were found in y- and rotational direction.

CE2, CE3 - Maximal and average shared control force

The controller forces were used to calculate the maximum and average shared control force.

ML1 - NASA TLX workload

Self reported workload was obtained using the standard NASA TLX questionnaires. The NASA TLX weights were obtained using the software program 'Slider', which is provided by NASA: <http://humansystems.arc.nasa.gov/groups/TLX/computer.php>. The NASA TLX ratings were obtained using hard-copy questionnaires (see questionnaires on following pages).

ML2, ML3, ML4 - Subjective: How fast/accurate? and: Did the guiding help?

The subjective measures were obtained using questionnaires (see questionnaires on following pages).

Experiment 1 – Questionnaire

Date: -11-2010

Questions before experiment:

-Subject name:

-Age:

-Left-handed or right-handed: [LEFT / RIGHT]

-Background (study):

-Hobbies (related to the task/locomotion, for example: sport/repair of bicycles/..):

.....

-Problems with locomotion/motor system (‘motoriek’): NO / YES,

Questions during experiment:

1. Conditions 1 – Fast [1_PERR – Fast]

-How **accurate** did you perform the task? [1 (totally not accurate) ---- 8 (very accurate)]

1	2	3	4	5	6	7	8

-How **fast** did you perform the task? [1 (totally not fast) ---- 8 (very fast)]

1	2	3	4	5	6	7	8

2. Conditions 2 – Fast [2_PERR_SC – Fast]

-How **accurate** did you perform the task? [1 (totally not accurate) ---- 8 (very accurate)]

1	2	3	4	5	6	7	8

-How **fast** did you perform the task? [1 (totally not fast) ---- 8 (very fast)]

1	2	3	4	5	6	7	8

-To what extent **did the guiding help** you with the task? [-4 (it was totally opposing) ---- 4 (it was very helpful)]

-4	-3	-2	-1	0	1	2	3	4
----	----	----	----	---	---	---	---	---

--	--	--	--	--	--	--	--	--	--	--	--	--	--	--	--	--	--	--	--

3. Conditions 3 – Fast [3_SlavePD – Fast]

-How **accurate** did you perform the task? [1 (totally not accurate) ---- 8 (very accurate)]

1	2	3	4	5	6	7	8

-How **fast** did you perform the task? [1 (totally not fast) ---- 8 (very fast)]

1	2	3	4	5	6	7	8

4. Conditions 4 – Fast [4_SlavePD_SC – Fast]

-How **accurate** did you perform the task? [1 (totally not accurate) ---- 8 (very accurate)]

1	2	3	4	5	6	7	8

-How **fast** did you perform the task? [1 (totally not fast) ---- 8 (very fast)]

1	2	3	4	5	6	7	8

-To what extent **did the guiding help** you with the task? [-4 (it was totally opposing) ---- 4 (it was very helpful)]

-4	-3	-2	-1	0	1	2	3	4

5. Conditions 5 – Fast [5_HandsOn – Fast]

-How **accurate** did you perform the task? [1 (totally not accurate) ---- 8 (very accurate)]

1	2	3	4	5	6	7	8

-How **fast** did you perform the task? [1 (totally not fast) ---- 8 (very fast)]

1	2	3	4	5	6	7	8

6. Conditions 6 – Fast [6_HandsOn_SC – Fast]

-How **accurate** did you perform the task? [1 (totally not accurate) ---- 8 (very accurate)]

1	2	3	4	5	6	7	8

-How **fast** did you perform the task? [1 (totally not fast) ---- 8 (very fast)]

1	2	3	4	5	6	7	8

-To what extent **did the guiding help** you with the task? [-4 (it was totally opposing) ---- 4 (it was very helpfull)]

-4	-3	-2	-1	0	1	2	3	4

Workload questionnaire (NASA TLX):

NASA Task Load Index

Hart and Staveland's NASA Task Load Index (TLX) method assesses work load on five 7-point scales. Increments of high, medium and low estimates for each point result in 21 gradations on the scales.

Name	Task	Date

Mental Demand How mentally demanding was the task?

Physical Demand How physically demanding was the task?

Temporal Demand How hurried or rushed was the pace of the task?

Performance How successful were you in accomplishing what you were asked to do?

Effort How hard did you have to work to accomplish your level of performance?

Frustration How insecure, discouraged, irritated, stressed, and annoyed were you?

D3 – Data management

Each subject performed the experimental task for 6 conditions and 8 repetitions, resulting in 48 trials per subject. During the measurements the following 46 output signals were recorded with a sample rate of 1kHz:

Raw data vector:

- 1-6: Force sensor signals ($F_x, F_y, F_z, T_x, T_y, T_z$), [N and Nmm]
- 7-9: Position master (x, y, θ), [m]
- 10-12: Velocity master (v_x, v_y, v_θ), [m/s]
- 13-16: Motor angles master ($\alpha_1, \alpha_2, \alpha_3, \alpha_4$), [rad]
- 17-19: Cartesian controller forces master (F_x, F_y, T_z), [N]
- 20-22: Position slave (x, y, θ), [m]
- 23-25: Velocity slave (v_x, v_y, v_θ), [m/s]
- 26-28: Motor angles slave ($\beta_1, \beta_2, \beta_3$), [rad]
- 29-31: Cartesian controller forces slave (F_x, F_y, T_z), [N]
- 32-38: Calculated motor torques ($T_{m1}, T_{m2}, T_{m3}, T_{m4}, T_{s1}, T_{s2}, T_{s3}$), [Nm]
- 39-41: Shared control forces (F_x, F_y, T_z), [N]
- 42-44: Measured slave forces (series-elastic) (F_x, F_y, T_z), [N]
- 45: Accelerometer signal [m/s^2]
- 46: Bolt angle [deg]

The following sequence of actions was performed to analyse the measurement data:

1. **Measurement of individual trials.** The measurement data of individual trials was saved in the directory “**\Thesis\Experiments\MeasurementData\Experiment\Rawdata\<subjectname>\<condition>\<trial number>*”.
(m-file: save_OutputLog.m).
2. **Addition questionnaire data.** The questionnaire data was added and all data was saved in the directory “**\Thesis\Experiments\MeasurementData\Experiment\Conditions\<subjectname>\<condition>\<trial number>*”.
During this step, the data from the pilot experiments was separated for the task instructions ‘accurate’ and ‘fast’ execution.
(m-file: DataProcessing1_Cond_Experiment.m).
3. **Subdivision of individual trials in subtasks.** The individual trials were subdivided in the four fundamental subtasks and the data was saved in the directory “**\Thesis\Experiments\MeasurementData\Experiment\Subtasks\<subjectname>\<condition>\<trial number>*”.
(m-file: DataProcessing2_Subtasks_Experiment.m)
4. **Calculation of evaluation metrics.** The evaluation metrics were calculated per subtask for each individual trial and were saved in the structure array “Results2”. The data was saved in the directory “**\Thesis\Experiments\MeasurementData\Experiment\AnalyzedData\ Results.mat*”.
(m-file: DataProcessing3_Metrics_Experiment.m)
5. **Plot results and perform statistical analyses.** The results were plotted per evaluation metric and the statistical analyses were performed.
(DataProcessing4a_Plot_Metrics_Experiment.m)

6. **Plot addition results.** Addition results like motion trajectories of the master and the slave were plotted using “DataProcessing4b_Plot_data.m”.

D4 – Results

This paragraph presents an overview of the main results of the shared control experiments. The results are presented for the total task (D4.1), the free air movement (D4.2), the contact movement (D4.3), the constrained position movement (D4.4) and the constrained force movement (D4.5). Furthermore the subjective measures are discussed in D4.6. Some additional results are presented in D4.7.

All presented results contain the measurement data of 9 subjects and 8 repetitions per condition.

To quantify the differences between the experimental conditions, statistical analyses of the data were done. Because of the large variance between subjects, a multi-way ANOVA is considered as most suitable for further analyses. A two-way ANOVA was used to analyze the effects of shared control separately for the three different *transparency* conditions. The two factors in this two-way ANOVA are the experimental factor *With/without Shared Control* (F2), and the *Between-subject variation* (F3). Results were tested with a significance level of $p = 0.05$. Significance levels of $p < 0.01$ were considered highly significant and levels of $0.1 < p < 0.05$ marginally significant.

Normality assumption was checked on all dependent variables ($p = 0.05$) to ensure the applicability of the statistical tests. This was done using a normal probability plot and the Lilliefors test (see *Figure 53*). The Lilliefors test tests the default null hypothesis that the sample in vector x comes from a distribution in the normal family, against the alternative that it does not come from a normal distribution.

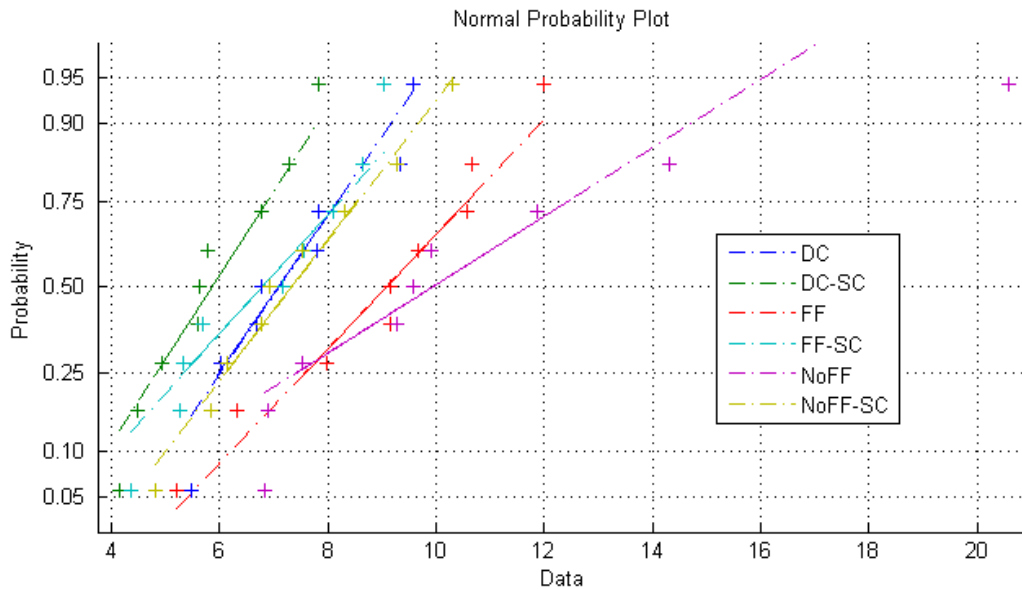


Figure 53: A normal probability plot and the Lilliefors test were used to check all dependent variables on normality. This figure shows the normal probability plots for the total time-to-complete measurement date.

D4.1 - Total task

The metric *time-to-complete* was analyzed for the total task. A univariate analysis of variance (ANOVA) was used to determine the statistical significance between the six experimental conditions (Figure 54). A difference between the six conditions was found ($p = 0.0009$, $F[4.97]$).

A two-way ANOVA was used to analyze the effects of shared control separately for the three different *transparency* conditions. The two factors in this two-way ANOVA are the experimental factor *With/without Shared Control* (F2), and the *Between-subject variation* (F3). The results are shown in Table 7. Shared control resulted in an improved time-to-complete of 19.7% ($p = 0.006$), 24.2% ($p = 0.0002$) and 31.9% ($p = 0.008$) for respectively the DC, FF and NoFF condition. The significance in the second row (F3) of table 4 shows the large variance between subjects.

Table 7: ANOVA results from the factors F2 and F3 on time-to-complete (TP1) for the total task, shown for each F1 condition. All results are significant.

Metric:	F1: Direct control (DC)		Force Feedback (FF)		No Force Feedback (NoFF)	
	<i>F2</i> <i>With/without</i> <i>SC</i>	<i>F3</i> <i>Subject</i> <i>variation</i>	<i>F2</i> <i>With/without</i> <i>SC</i>	<i>F3</i> <i>Subject</i> <i>variation</i>	<i>F2</i> <i>With/without</i> <i>SC</i>	<i>F3</i> <i>Subject</i> <i>variation</i>
TP1 (ttc)	F[14.15] p=0.006	F[4.79] p=0.02	F[42.85] p=0.0002	F[14.12] p=0.0006	F[12.57] p=0.008	F[4.33] p=0.027

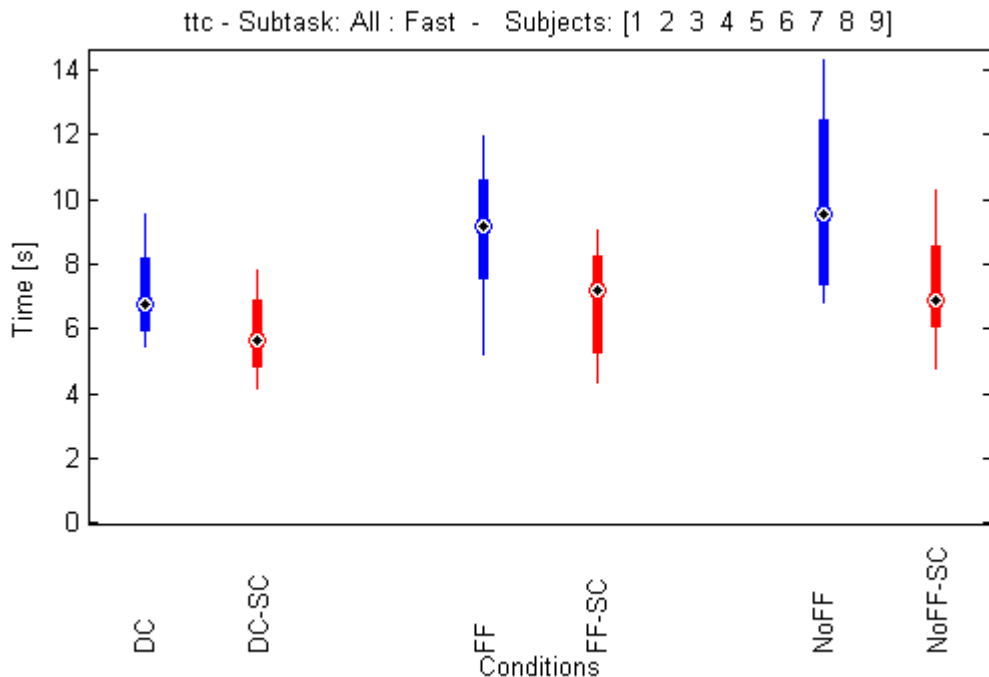


Figure 54: Time-to-complete [TP1] for the total task, shown for the six experimental conditions (No SC: blue / SC: red).

Figure 55 shows a bar graph of the time-to-complete, separated for the 4 subtasks. These different subtasks will be analysed in more detail in the next 4 paragraphs.

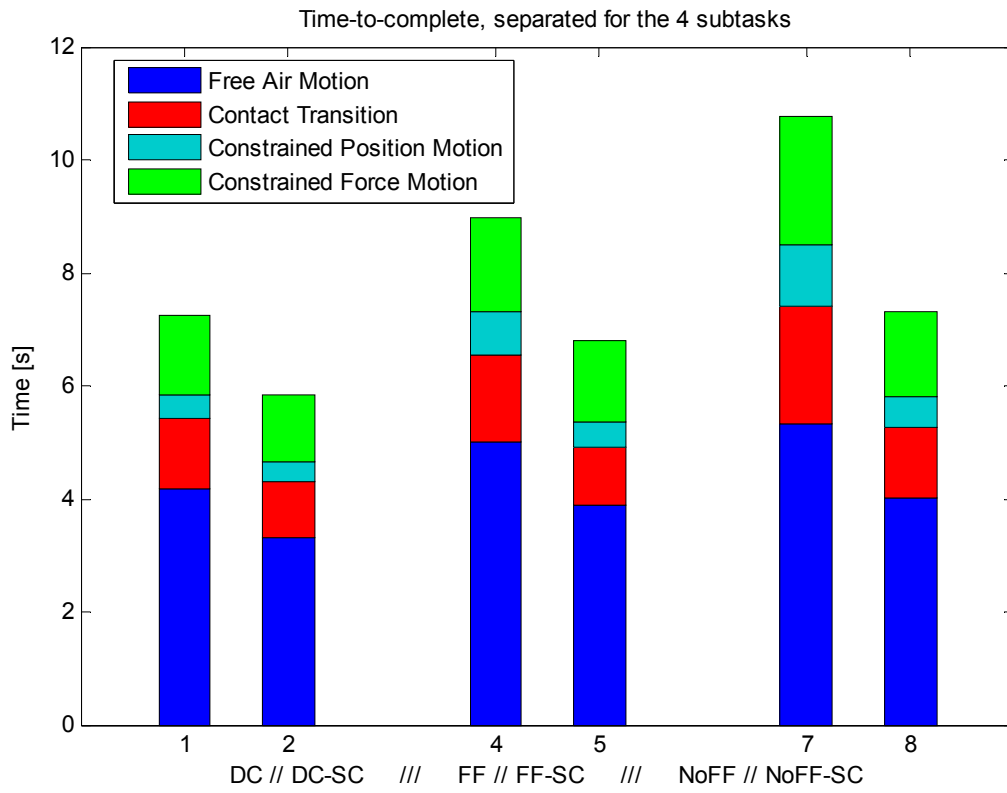


Figure 55: Bar graph of the time-to-complete [TP1] separated for the 4 subtasks, shown for the six experimental conditions

D4.2 – Free Air Movement (FAM)

A two-way ANOVA was used to analyze the effects of shared control separately for the three different *transparency* conditions. The two factors in this two-way ANOVA were the experimental factor *With/without Shared Control* (F2), and the *Between-subject variation* (F3). The results are shown in Table 8.

Table 8: ANOVA results from the factors F2 and F3 on the defined metrics for the free air motion, shown for each F1 condition. Significant results are shown **bold**.

Metric:	F1: Direct control (DC)		Force Feedback (FF)		No Force Feedback (NoFF)	
	<i>F2</i> <i>With/without</i> <i>SC</i>	<i>F3</i> <i>Subject</i> <i>variation</i>	<i>F2</i> <i>With/without</i> <i>SC</i>	<i>F3</i> <i>Subject</i> <i>variation</i>	<i>F2</i> <i>With/without</i> <i>SC</i>	<i>F3</i> <i>Subject</i> <i>variation</i>
TP1 (ttc)	F[8.07] p=0.0218	F[2.84] p=0.0808	F[31.32] p=0.0005	F[18.02] p=0.0002	F[32.97] p=0.0004	F[16.24] p=0.0003
TP2 (x_{ppd})	F[11.97] p=0.0086	F[0.55] p=0.7895	F[21.51] p=0.0017	F[1.24] p=0.3827	F[14.26] p=0.0054	F[0.64] p=0.7266
TP3 ($e_{p3,rot}$)	F[10.43] p=0.0121	F[2.54] p=0.1048	F[0.77] p=0.4071 *	F[2.91] p=0.0762*	F[9.2] p=0.0162 *	F[9.72] p=0.0021*
CE1 – x (n_{rev})	F[6.74] p=0.0318	F[1.58] p=0.2672	F[6.73] p=0.0319	F[4.79] p=0.02	F[12.45] p=0.0078	F[5.23] p=0.0154
CE1 – y (n_{rev})	F[7.27] p=0.0272	F[1.51] p=0.288	F[12.57] p=0.0076	F[4.64] p=0.022	F[13.35] p=0.0065	F[4.75] p=0.0206
CE1 – θ (n_{rev})	F[11.5] p=0.0095	F[4.27] p=0.0278	F[4.8] p=0.0597	F[7.96] p=0.0041	F[12.82] p=0.0072	F[15.15] p=0.0004

* The input vector(s) do(es) not satisfy the normal distribution criteria ($p > 0.05$).

The data of the metrics TP1..TP3 and CE1..C3 for the FAM is shown on the following pages.

As already seen for the total task, shared control leads to a reduction in time-to-complete (TP1). The path deviation (TP2) decreased with 37.3%, 54.8% and 49.6% for respectively the DC, FF and NoFF condition. The reversal rate (CE1) shows also a significant decrease for all conditions (except the θ -direction for the FF conditions, which is only marginal significant), which indicates that the task required less control effort from the human.

TP3 shows a increase of rotational error at point 3 for the DC condition, which is very strange. Also the fact that the errors are higher for DC condition when compared to the FF and NoFF conditions, was not expected. A possible cause could be the worse visibility of the orientation goals (P1,P2 and P3), as the parallel structure of the master obstructs partly the view during the task.

The F3 columns show the large variation between subjects; an example is shown for the TP1 in Figure 57.

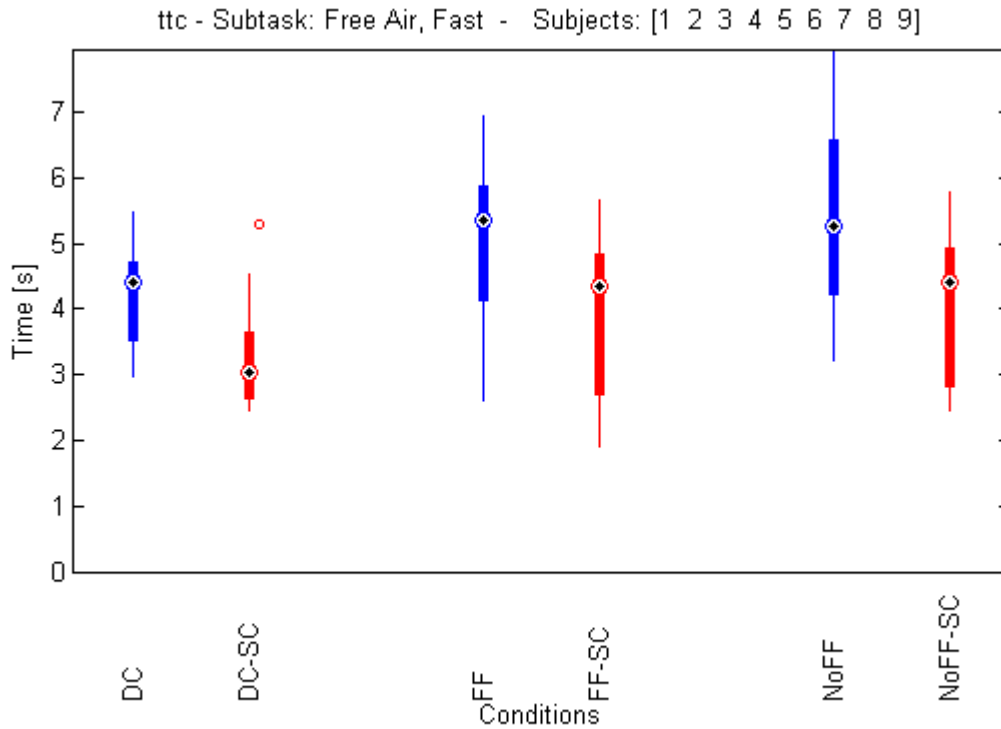


Figure 56: Time-to-complete [TP1] for the free air motion, shown for the six experimental conditions (No SC: blue / SC: red).

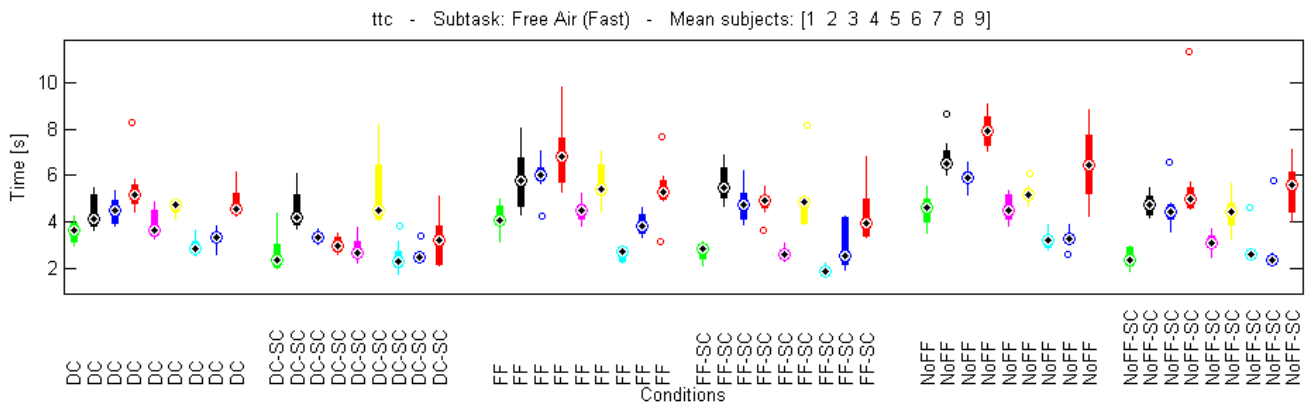


Figure 57: Time-to-complete [TP1] for the free air motion, shown for each subject for the six experimental conditions. The plot shows a large variety between the subjects, however all subjects respond positive to Shared Control for at least two FF condition; this excludes the opportunity of a group responders and a group non-responders.

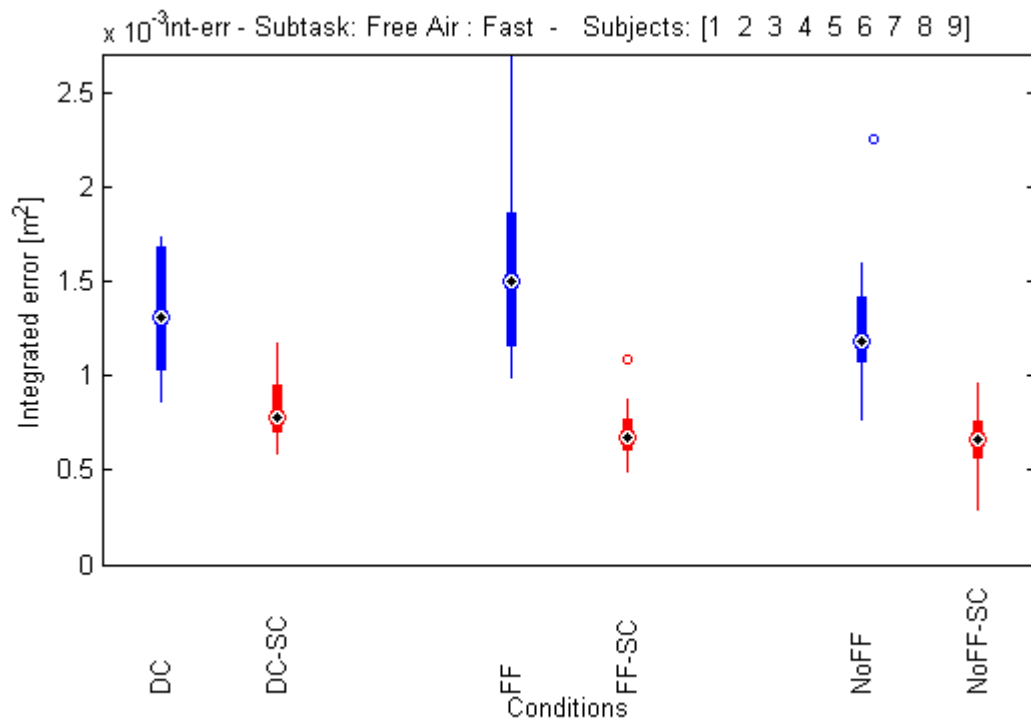


Figure 58: Nominal path deviation [TP2] for the free air motion, shown for the six experimental conditions (*No SC: blue / SC: red*).

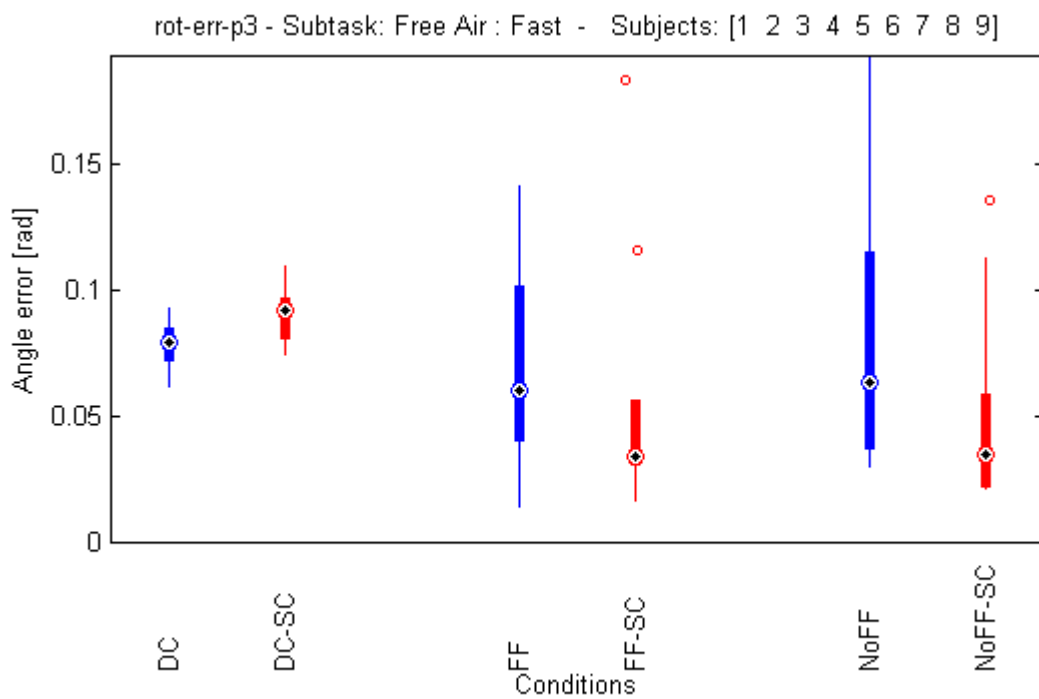


Figure 59: Orientation error at point 3 [TP3] for the free air motion, shown for the six experimental conditions (*No SC: blue / SC: red*).

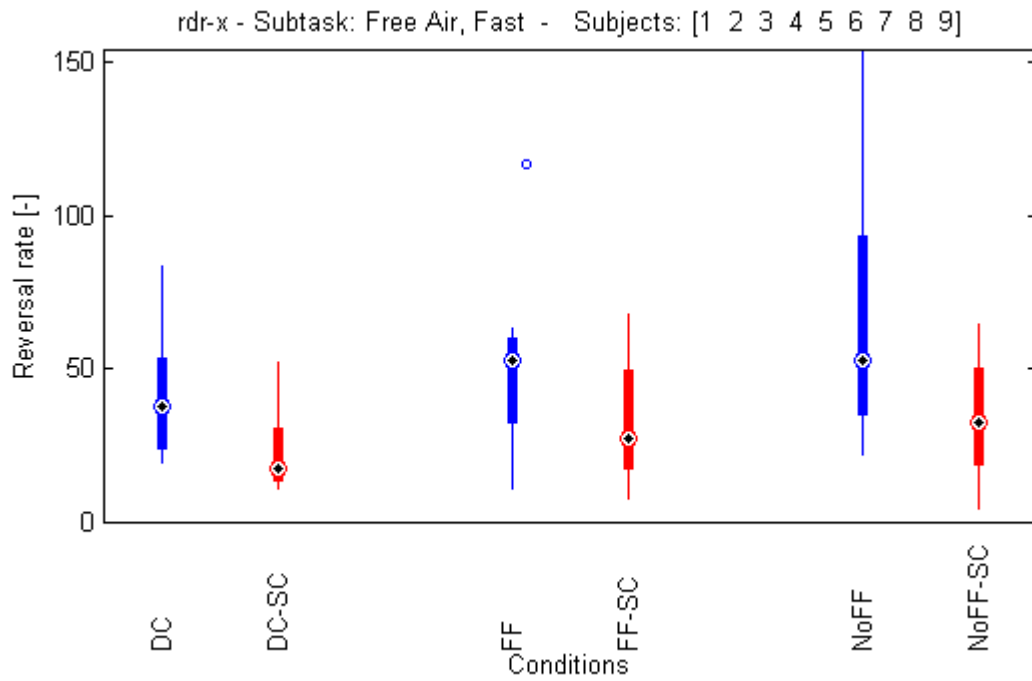


Figure 60: Reversal rate *x*-direction [CEI] for the free air motion, shown for the six experimental conditions (No SC: blue / SC: red).

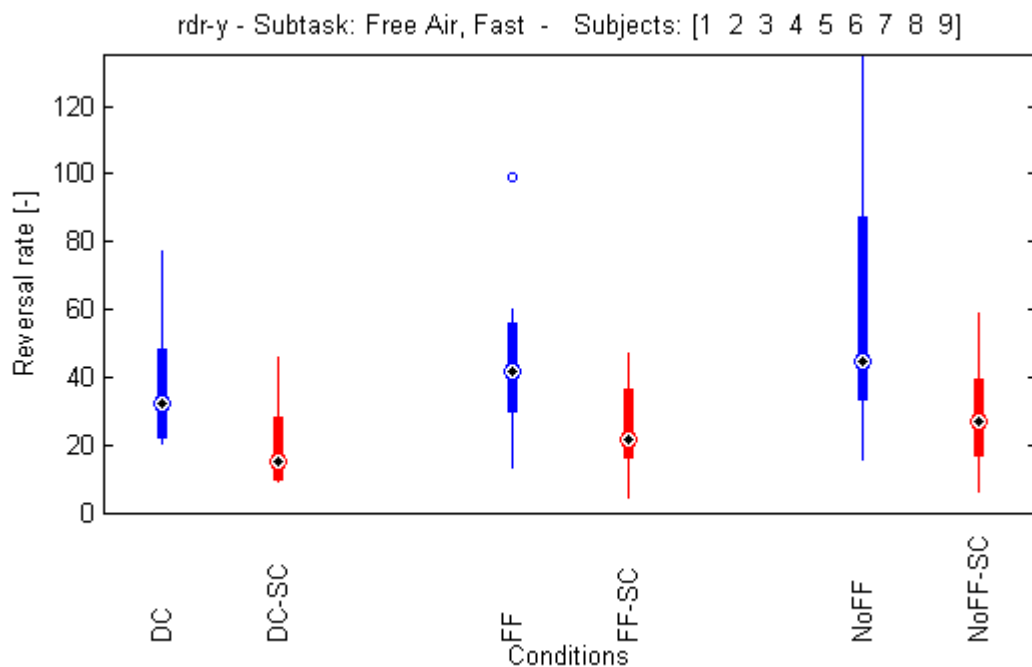


Figure 61: Reversal rate *y*-direction [CEI] for the free air motion, shown for the six experimental conditions (No SC: blue / SC: red).

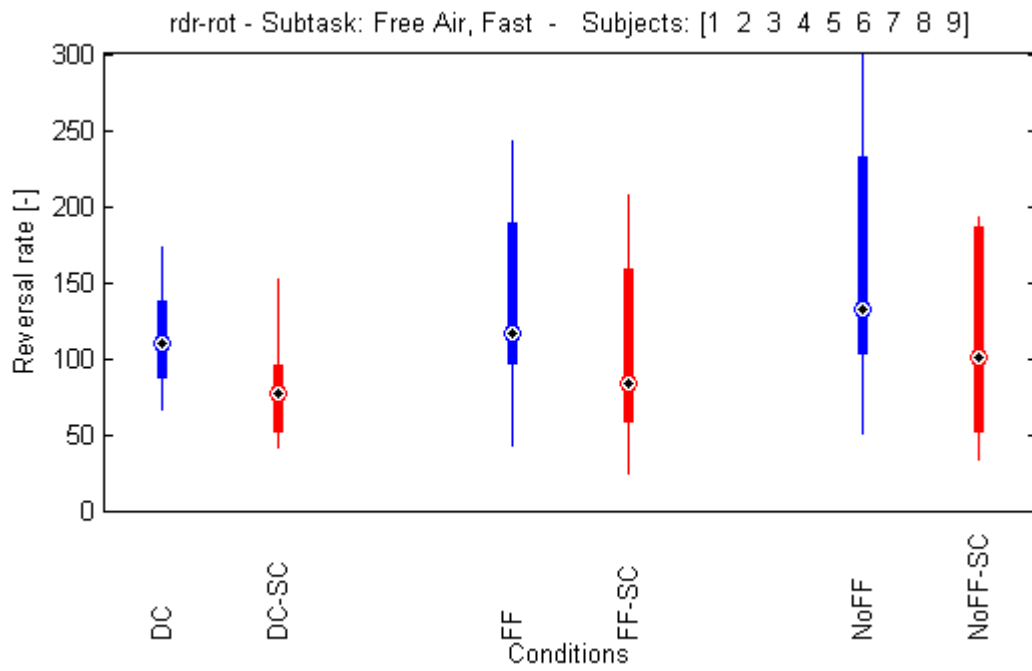


Figure 62: Reversal rate θ -direction [CE1] for the free air motion, shown for the six experimental conditions (No SC: blue / SC: red).

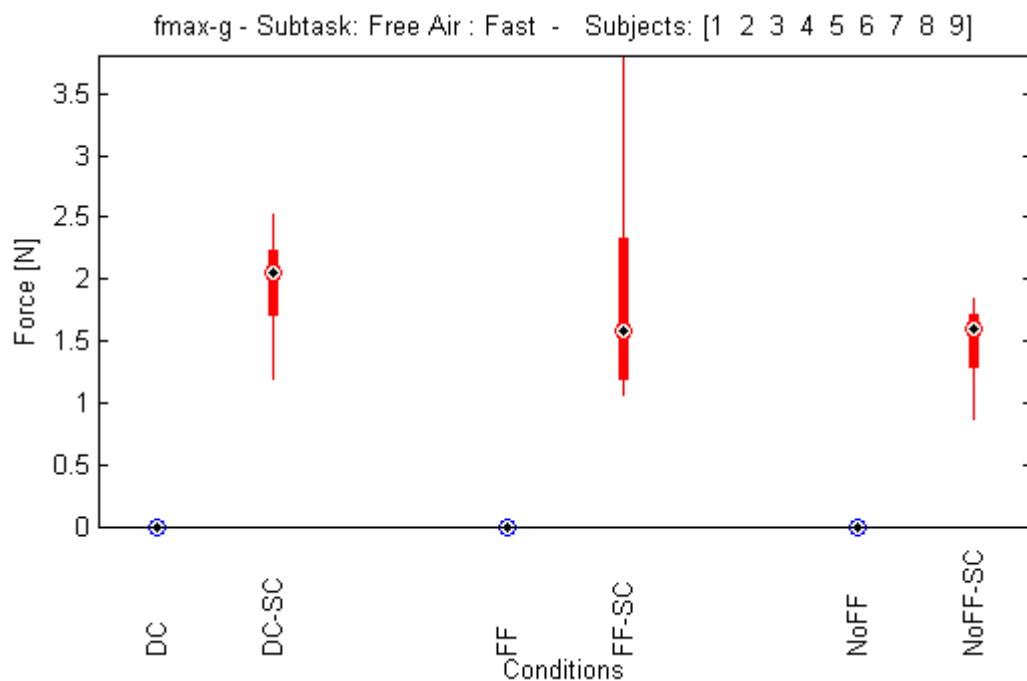


Figure 63: Maximal guiding force [CE2] for the free air motion, shown for the three shared control experimental conditions (SC: red).

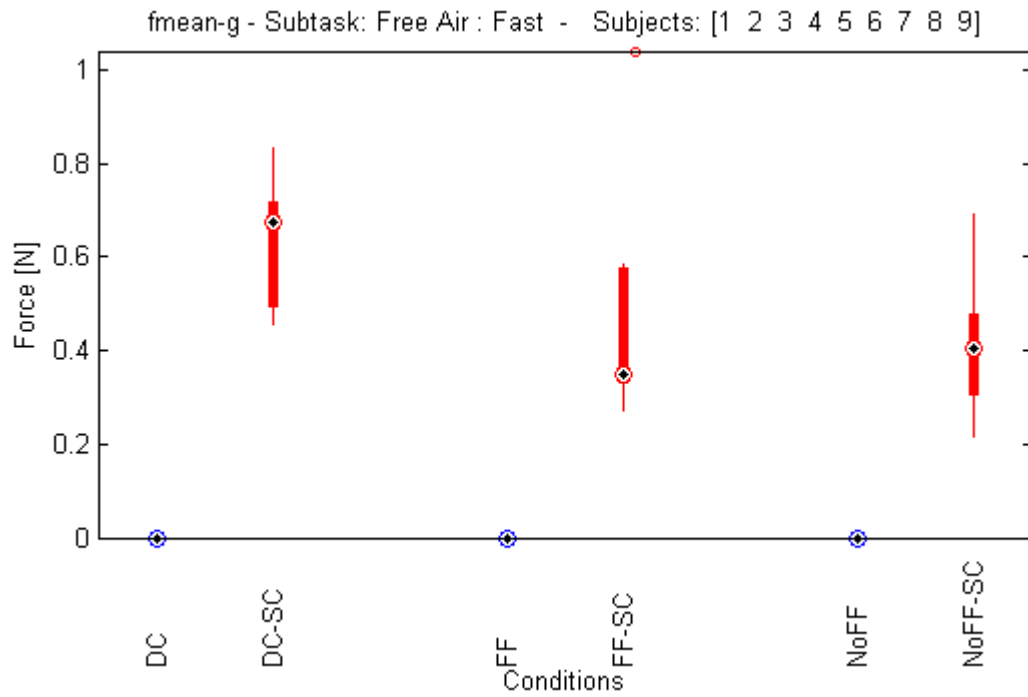


Figure 64: Average guiding force [CE3] for the free air motion, shown for the three shared control experimental conditions (SC: red).

D4.3 – Contact Transition Motion (CTM)

A two-way ANOVA was used to analyze the effects of shared control separately for the three different *transparency* conditions. The two factors in this two-way ANOVA were the experimental factor *With/without Shared Control* (F2), and the *Between-subject variation* (F3). The results are shown in Table 9.

Table 9: ANOVA results from the factors F2 and F3 on the defined metrics for the contact transition motion, shown for each F1 condition. Significant results are shown **bold**.

Metric:	Direct control (DC)		Force Feedback (FF)		No Force Feedback (NoFF)	
	<i>F2</i> <i>With/without</i> <i>SC</i>	<i>F3</i> <i>Subject</i> <i>variation</i>	<i>F2</i> <i>With/without</i> <i>SC</i>	<i>F3</i> <i>Subject</i> <i>variation</i>	<i>F2</i> <i>With/without</i> <i>SC</i>	<i>F3</i> <i>Subject</i> <i>variation</i>
TP1 (ttc)	F[6.17] p=0.0379	F[4.7] p=0.0211	F[9.54] p=0.0149	F[1.79] p=0.2144	F[2.63] p=0.1432*	F[1.52] p=0.2842*
TP4 ($F_{e,max}$)	-	-	F[2.01] p=0.1939	F[2.25] p=0.136	F[0.07] p=0.7948	F[2.62] p=0.0975
TP5 ($F_{e,av}$)	-	-	F[2.68] p=0.1402	F[2.77] p=0.0856	F[0.09] p=0.7686	F[2.27] p=0.1336
CE1 – x (n_{rev})	F[5.28] p=0.0507*	F[8.73] p=0.003*	F[6.38] p=0.0355	F[0.9] p=0.5603	F[1.48] p=0.2586*	F[1.68] p=0.2388*
CE1 – y (n_{rev})	F[1.14] p=0.3159*	F[2.33] p=0.1262*	F[7.52] p=0.0254	F[1.31] p=0.3567	F[1.06] p=0.3327*	F[2.11] p=0.1554*
CE1 – θ (n_{rev})	F[13.27] p=0.0066	F[2.7] p=0.0905	F[5.45] p=0.0478	F[1.22] p=0.3917	F[3.57] p=0.0954*	F[1.49] p=0.2933*

* The input vector(s) do(es) not satisfy the normal distribution criteria ($p > 0.05$).

The data of the metrics TP1, TP4 and TP5 and CE1 for the CTM is shown on the following pages.

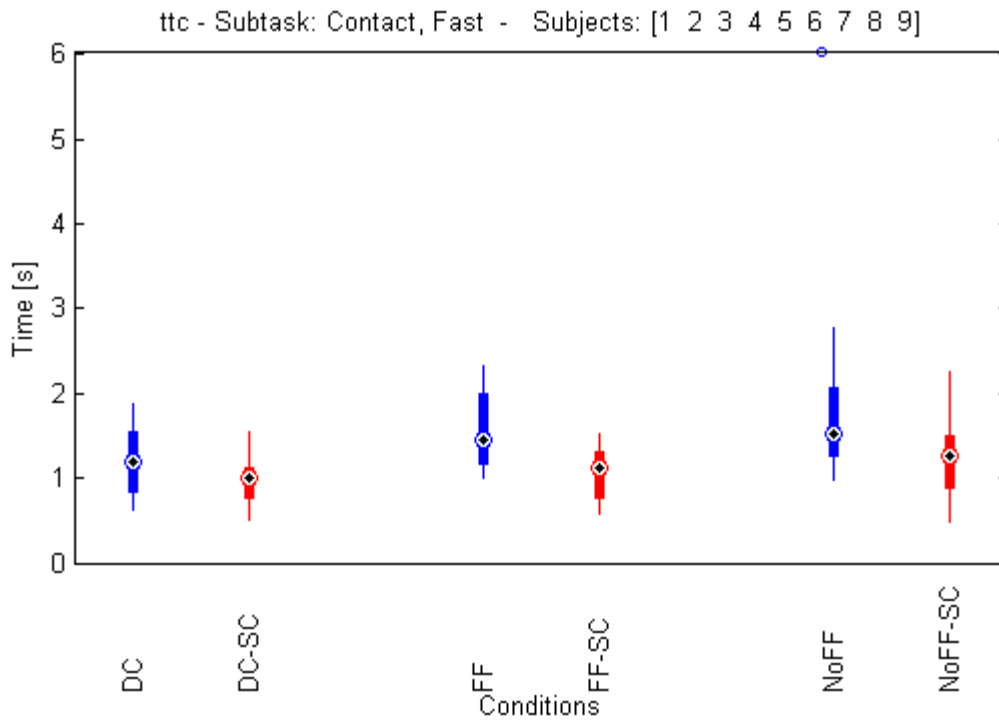


Figure 65: Time-to-complete [TP1] for the contact transition motion (CTM), shown for the six experimental conditions (No SC: blue / SC: red).

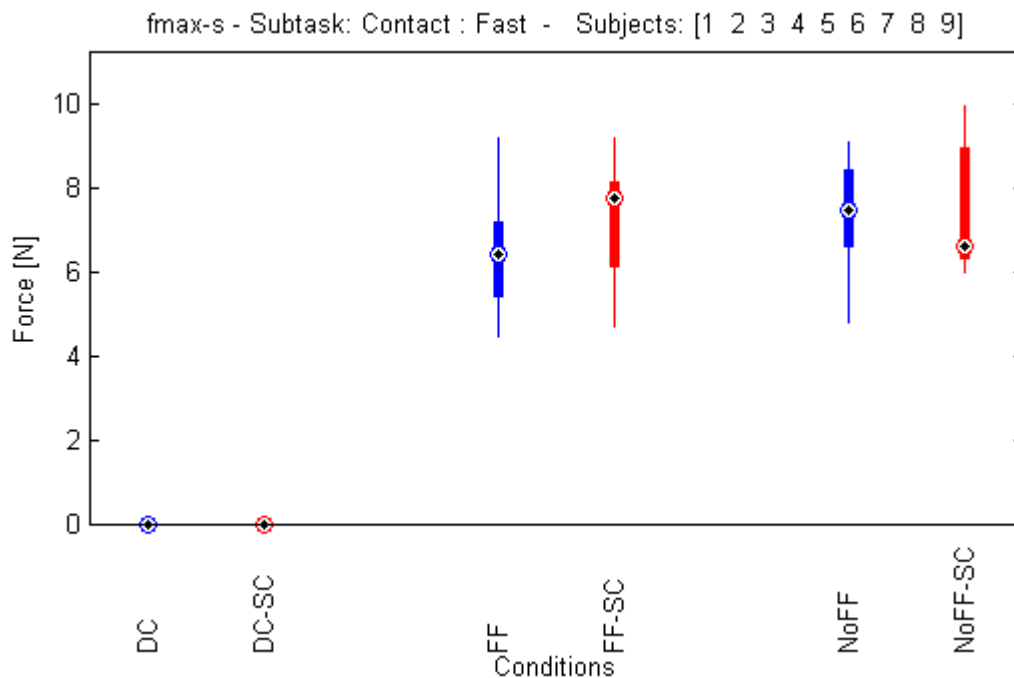


Figure 66: Maximal force exerted on environment [TP4] for the contact transition motion (CTM), shown for the four teleoperated experimental conditions (No SC: blue / SC: red).

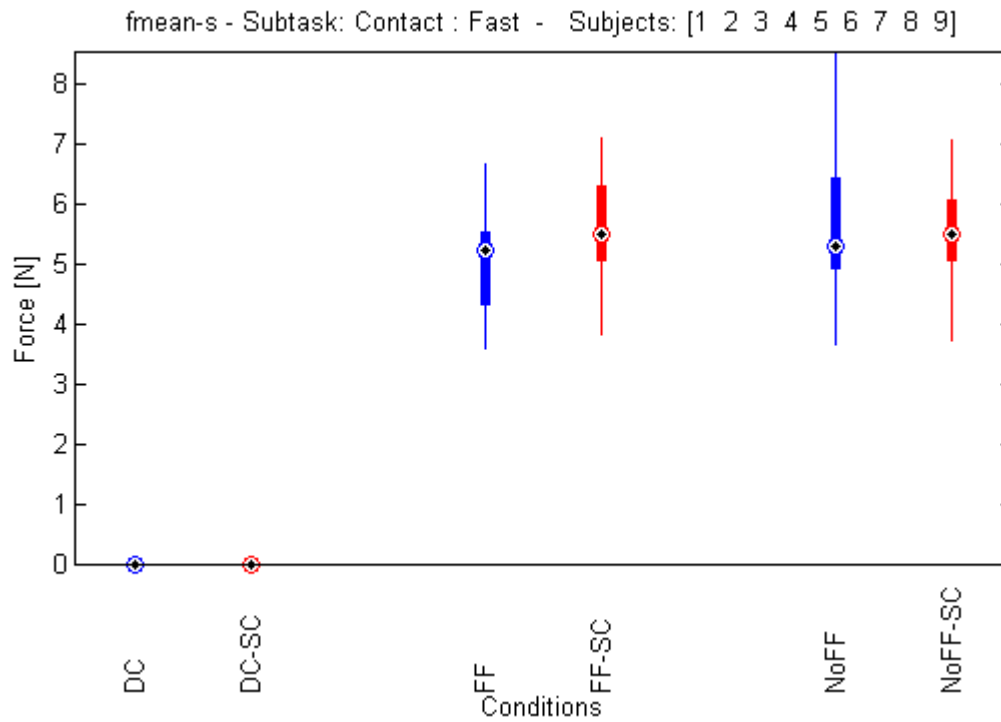


Figure 67: Average force exerted on environment [TP5] for the contact transition motion (CTM), shown for the four teleoperated experimental conditions (No SC: blue / SC: red).

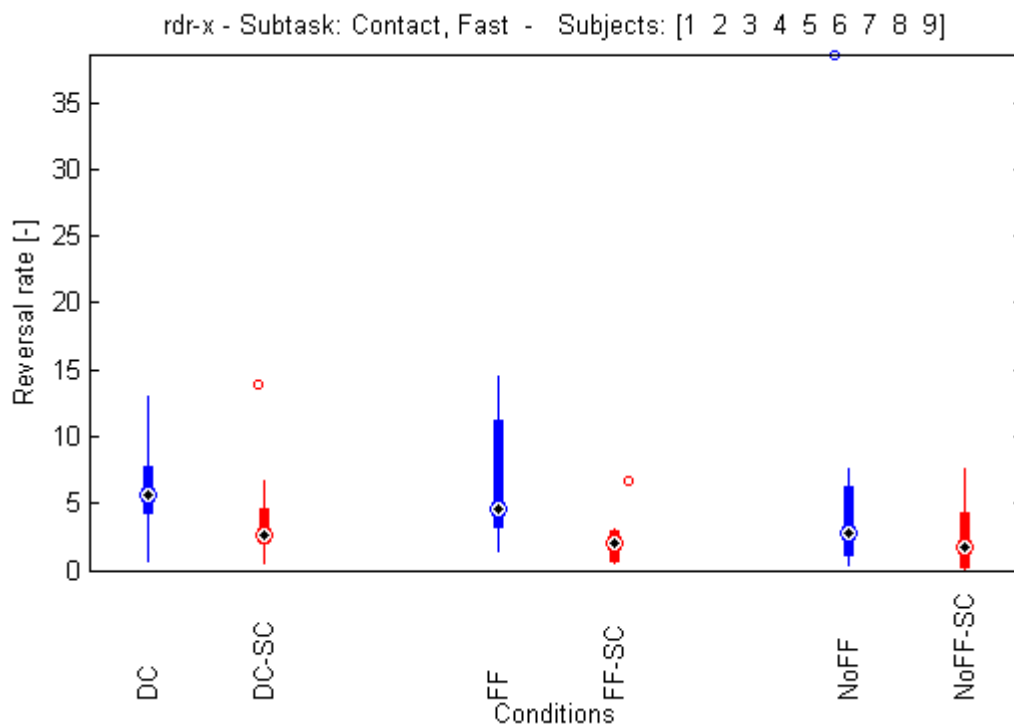


Figure 68: Reversal rate x -direction [CE1] for the contact transition motion (CTM), shown for the six experimental conditions (No SC: blue / SC: red).

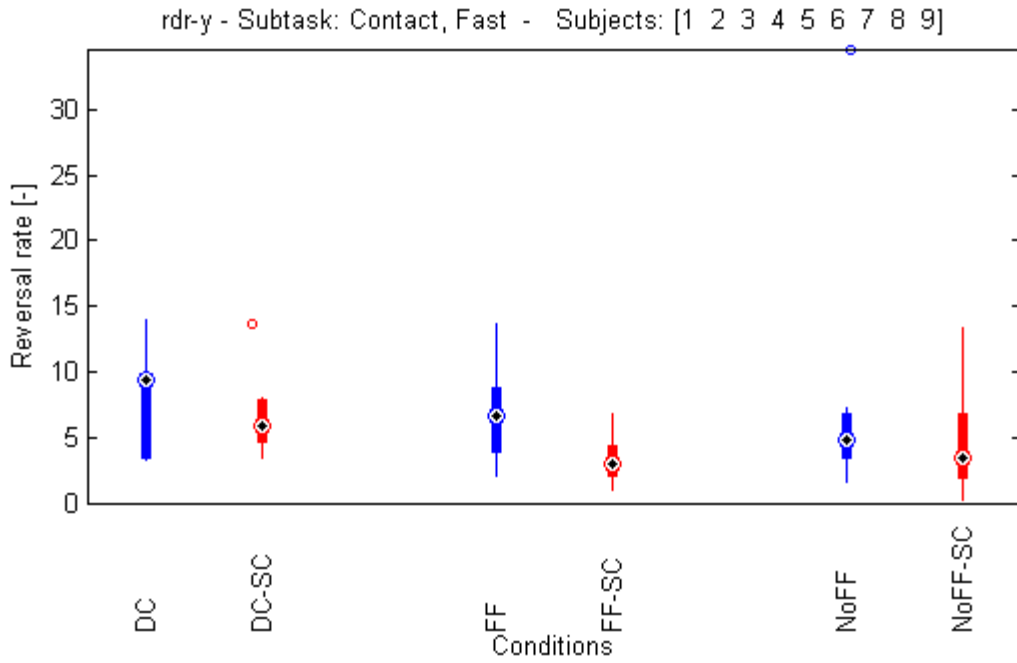


Figure 69: Reversal rate y -direction [CE1] for the contact transition motion (CTM), shown for the six experimental conditions (No SC: blue / SC: red).

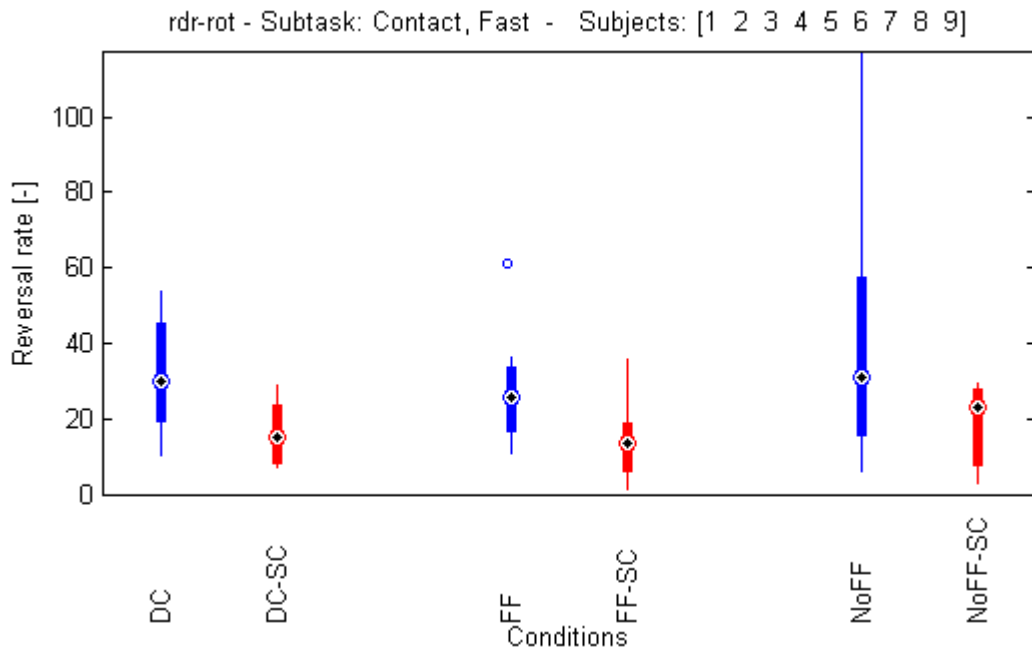


Figure 70: Reversal rate θ -direction [CE1] for the contact transition motion (CTM), shown for the six experimental conditions (No SC: blue / SC: red).

D4.4 – Constrained position Motion (CPM)

A two-way ANOVA was used to analyze the effects of shared control separately for the three different *transparency* conditions. The two factors in this two-way ANOVA were the experimental factor *With/without Shared Control* (F2), and the *Between-subject variation* (F3). The results are shown in Table 108.

Table 10: ANOVA results from the factors F2 and F3 on the defined metrics for the constrained position motion, shown for each F1 condition. Significant results are shown **bold**.

Metric:	Direct control (DC)		Force Feedback (FF)		No Force Feedback (NoFF)	
	<i>F2</i> <i>With/without</i> <i>SC</i>	<i>F3</i> <i>Subject</i> <i>variation</i>	<i>F2</i> <i>With/without</i> <i>SC</i>	<i>F3</i> <i>Subject</i> <i>variation</i>	<i>F2</i> <i>With/without</i> <i>SC</i>	<i>F3</i> <i>Subject</i> <i>variation</i>
TP1 (ttc)	F[17.99] p=0.0028	F[27.94] p<0.0001	F[6.92] p=0.0301*	F[3.22] p=0.0591*	F[7.89] p=0.0229	F[2.61] p=0.0983
TP4 ($F_{e,max}$)	-	-	F[2.31] p=0.1673	F[4.29] p=0.0274	F[1.13] p=0.3193	F[2.64] p=0.0954
TP5 ($F_{e,av}$)	-	-	F[1.68] p=0.2311	F[3.06] p=0.0672	F[0.67] p=0.4371	F[2.55] p=0.1036
CE1 – x (n_{rev})	F[1.59] p=0.2426	F[8.32] p=0.0036	F[5.47] p=0.0475*	F[3.25] p=0.0577*	F[2.09] p=0.1867*	F[1.37] p=0.3343*
CE1 – y (n_{rev})	F[0.45] p=0.5201	F[13.07] p=0.0007	F[8.02] p=0.0221	F[3.96] p=0.0344	F[1.99] p=0.1964*	F[1.21] p=0.3956*
CE1 – θ (n_{rev})	F[1.36] p=0.2763*	F[8.89] p=0.0028*	F[1.49] p=0.2574	F[1.97] p=0.178	F[4.05] p=0.0788*	F[1.72] p=0.2304*

* The input vector(s) do(es) not satisfy the normal distribution criteria ($p > 0.05$).

The data of the metrics TP1, TP4 and TP5 and CE1 for the CPM is shown on the following pages.

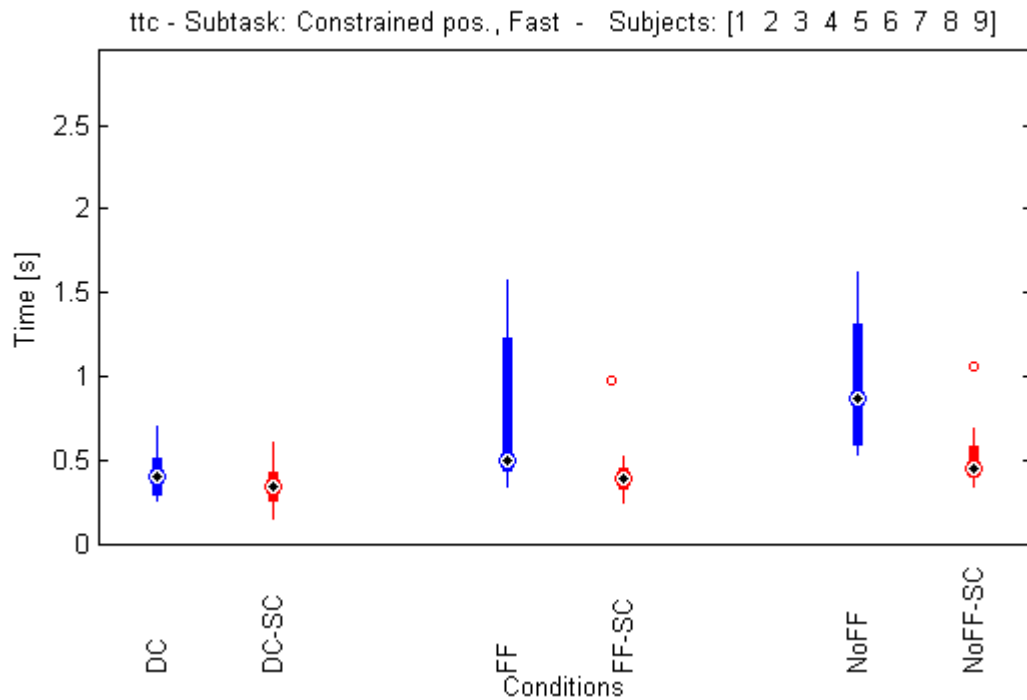


Figure 71: Time-to-complete [TP1] for the constrained position motion (CPM), shown for the six experimental conditions (No SC: blue / SC: red).

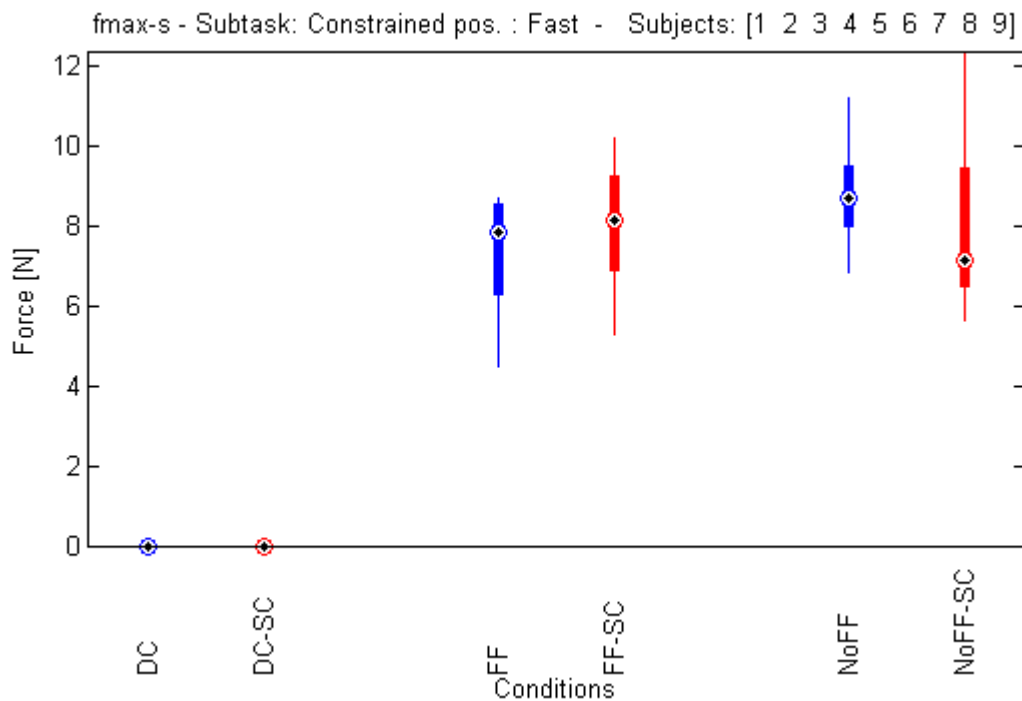


Figure 72: Maximal force exerted on environment [TP4] for the constrained position motion (CPM), shown for the four teleoperated experimental conditions (No SC: blue / SC: red).

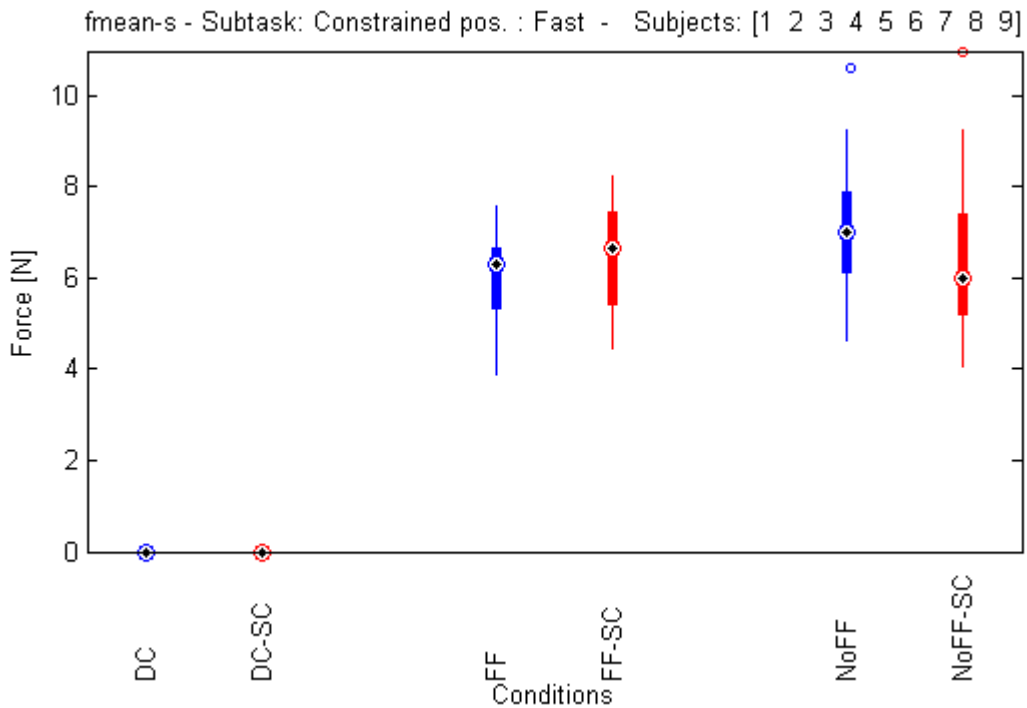


Figure 73: Average force exerted on environment [TP5] for the constrained position motion (CPM), shown for the four teleoperated experimental conditions (No SC: blue / SC: red).

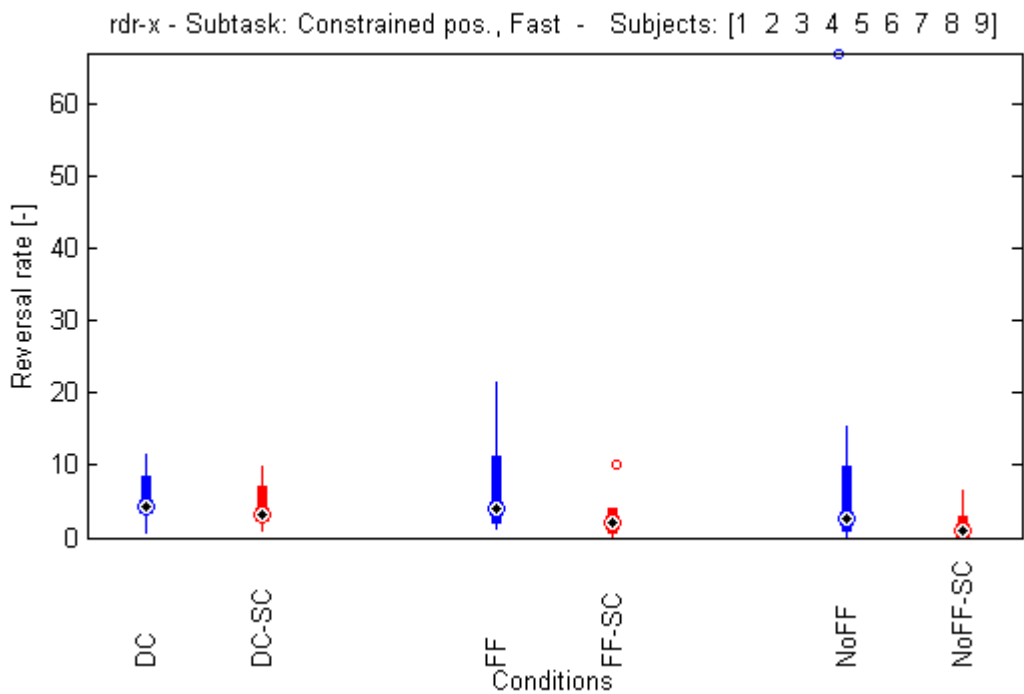


Figure 74: Reversal rate x-direction [CE1] for the constrained position motion (CPM), shown for the six experimental conditions (No SC: blue / SC: red).

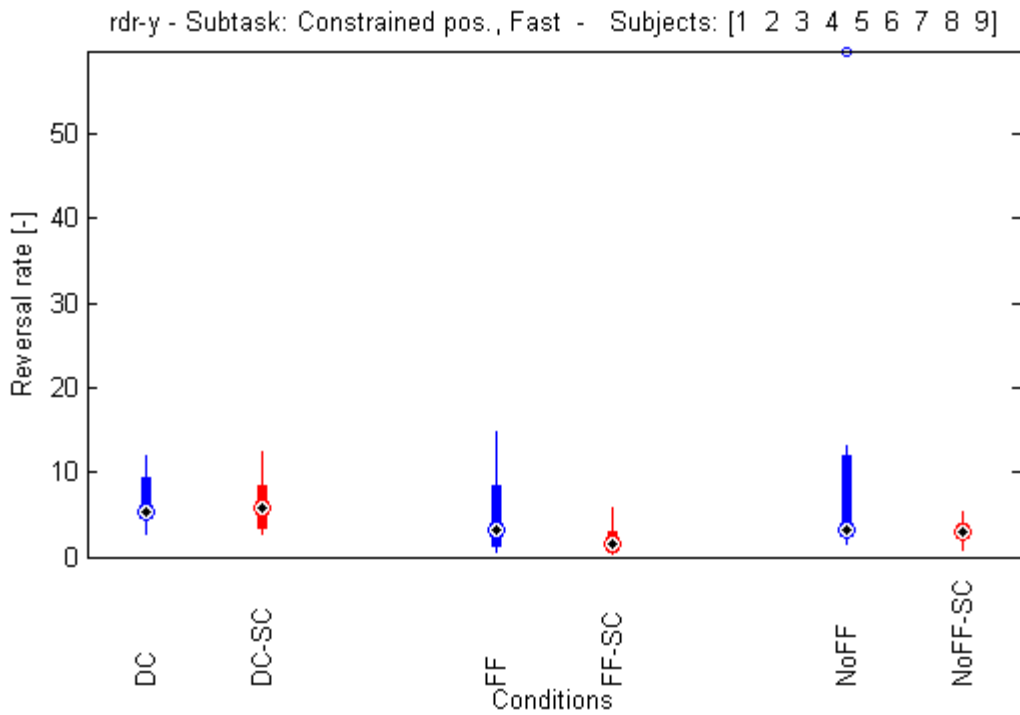


Figure 75: Reversal rate y -direction [CE1] for the constrained position motion (CPM), shown for the six experimental conditions (No SC: blue / SC: red).

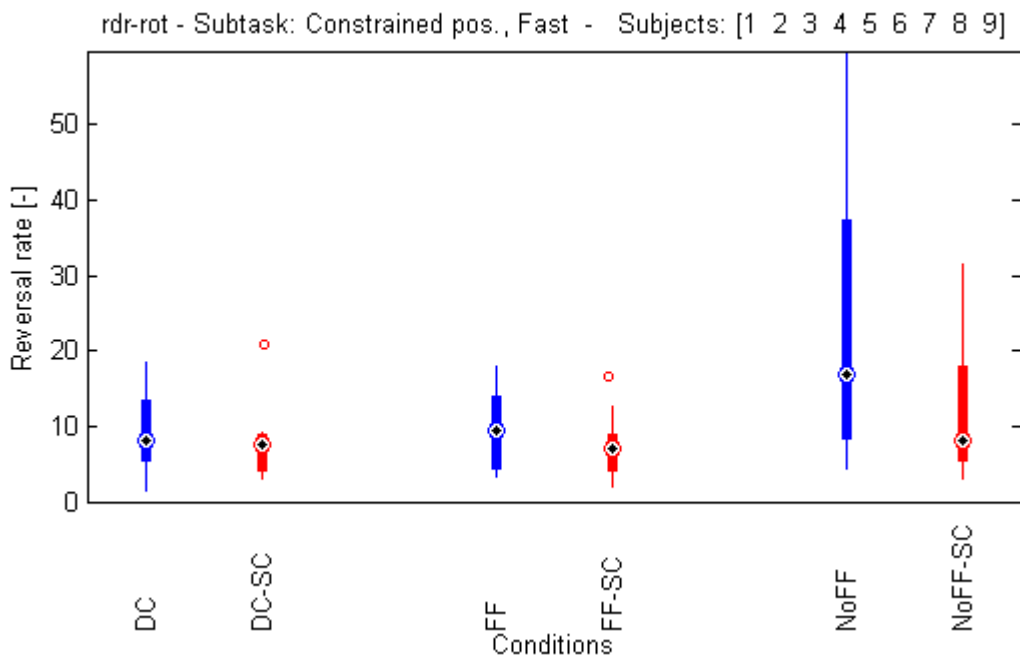


Figure 76: Reversal rate θ -direction [CE1] for the constrained position motion (CPM), shown for the six experimental conditions (No SC: blue / SC: red).

D4.5 – Constrained Force Motion (CFM)

A two-way ANOVA was used to analyze the effects of shared control separately for the three different *transparency* conditions. The two factors in this two-way ANOVA were the experimental factor *With/without Shared Control* (F2), and the *Between-subject variation* (F3). The results are shown in Table 119.

Table 11: ANOVA results from the factors F2 and F3 on the defined metrics for the constrained force motion, shown for each F1 condition. Significant results are shown **bold**.

Metric:	F1: Direct control (DC)		Force Feedback (FF)		No Force Feedback (NoFF)	
	<i>F2</i> <i>With/without</i> <i>SC</i>	<i>F3</i> <i>Subject</i> <i>variation</i>	<i>F2</i> <i>With/without</i> <i>SC</i>	<i>F3</i> <i>Subject</i> <i>variation</i>	<i>F2</i> <i>With/without</i> <i>SC</i>	<i>F3</i> <i>Subject</i> <i>variation</i>
TP1 (ttc)	F[10.29] p=0.0125	F[5.82] p=0.0111	F[2.81] p=0.1323	F[6.38] p=0.0084	F[4.68] p=0.0625*	F[1.84] p=0.2029*
TP4 ($F_{e,max}$)	-	-	F[4.99] p=0.0559	F[4.5] p=0.024	F[7.14] p=0.0282	F[3.12] p=0.0642
TP5 ($F_{e,av}$)	-	-	F[8.42] p=0.0198	F[5.23] p=0.0154	F[2.37] p=0.1622	F[1.96] p=0.1802

* The input vector(s) do(es) not satisfy the normal distribution criteria ($p > 0.05$).

The data of the metrics TP1, TP4 and TP5 for the CFM is shown on the following pages.

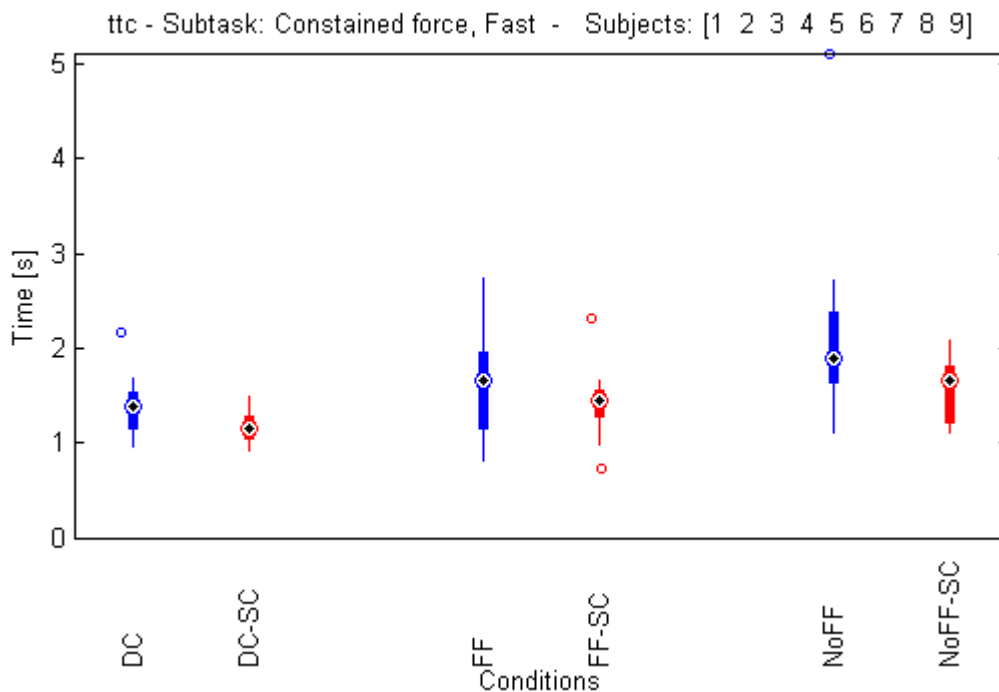


Figure 77: Time-to-complete [TP1] for the constrained force motion (CFM), shown for the six experimental conditions (No SC: blue / SC: red).

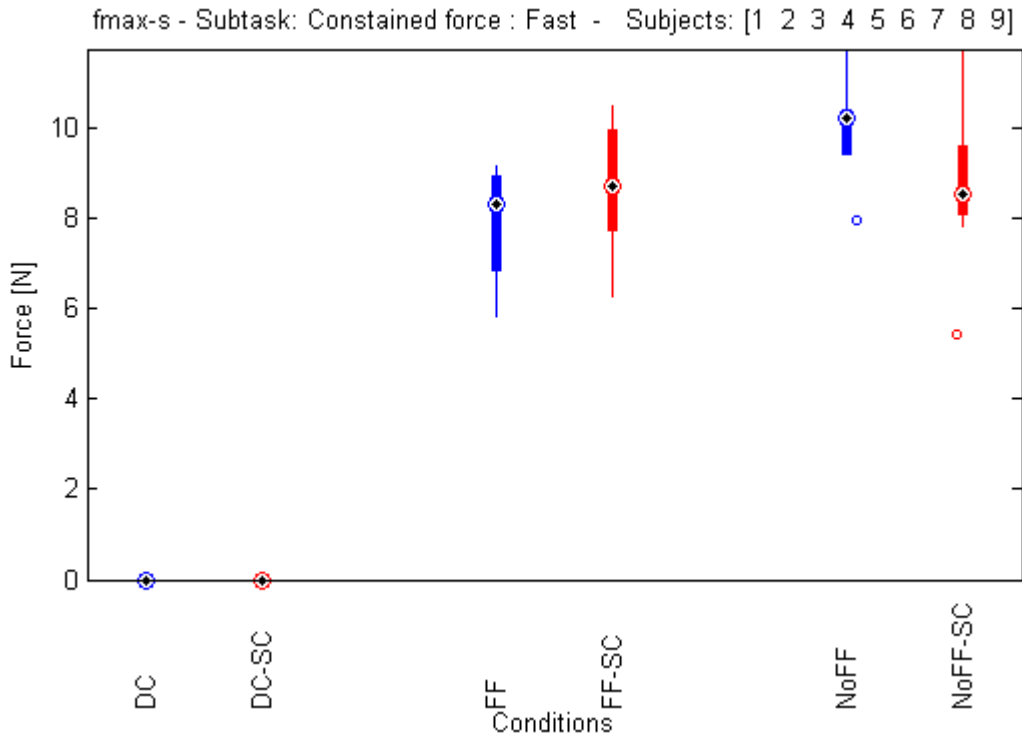


Figure 78: Maximal force exerted on environment [TP4] for the constrained force motion (CFM), shown for the four teleoperated experimental conditions (No SC: blue / SC: red).

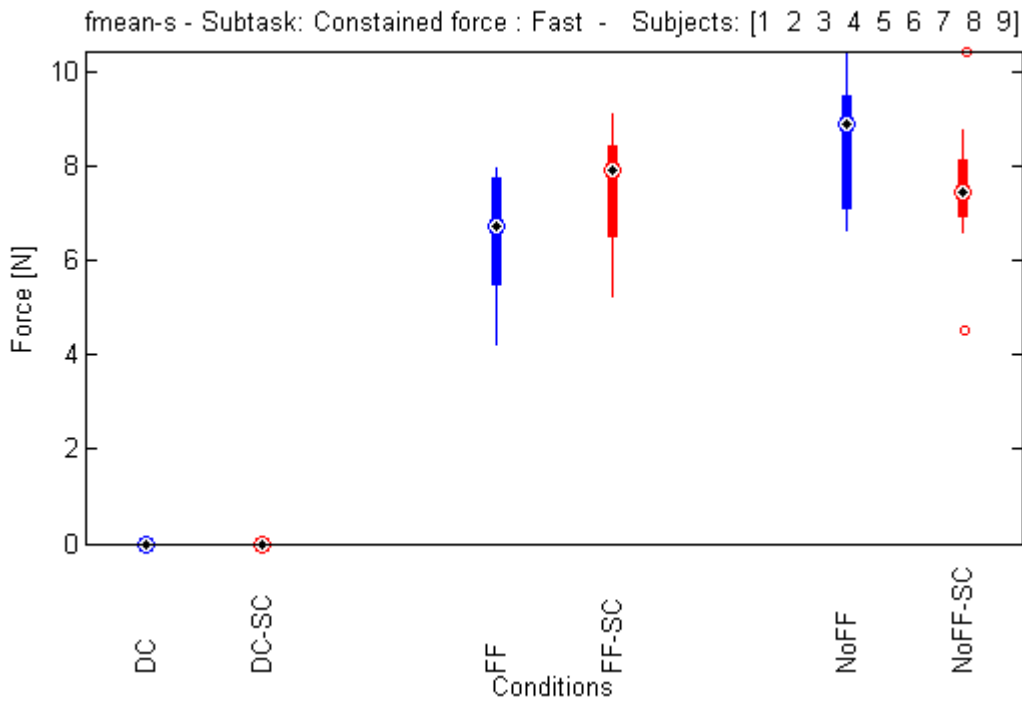


Figure 79: Average force exerted on environment [TP5] for the constrained force motion (CFM), shown for the four teleoperated experimental conditions (No SC: blue / SC: red).

D4.6 – Subjective measures

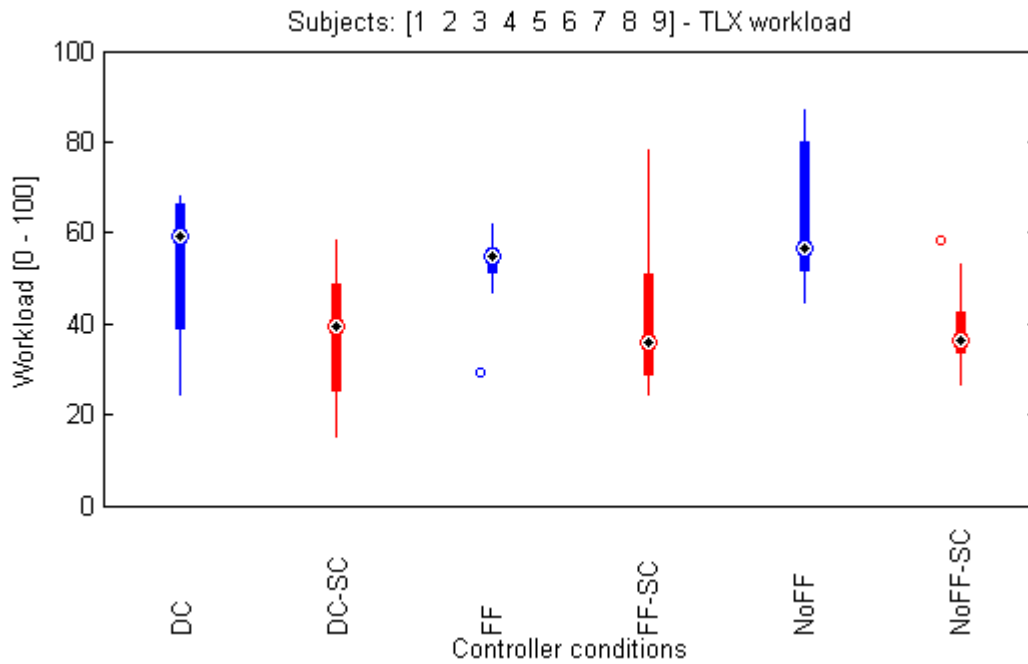


Figure 80: Self reported workload [ML1] for the total task (TT), shown for the six experimental conditions (No SC: blue / SC: red).

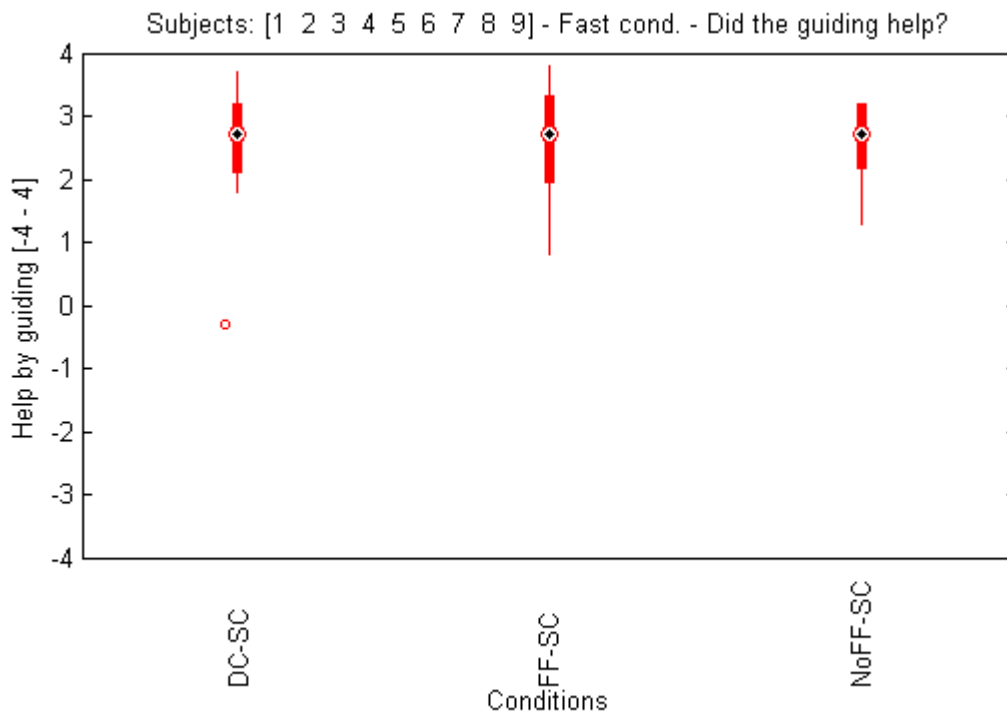


Figure 81: Subjective measure; Did the guiding help? [ML4] for the total task (TT), shown for the three shared control experimental conditions (SC: red).

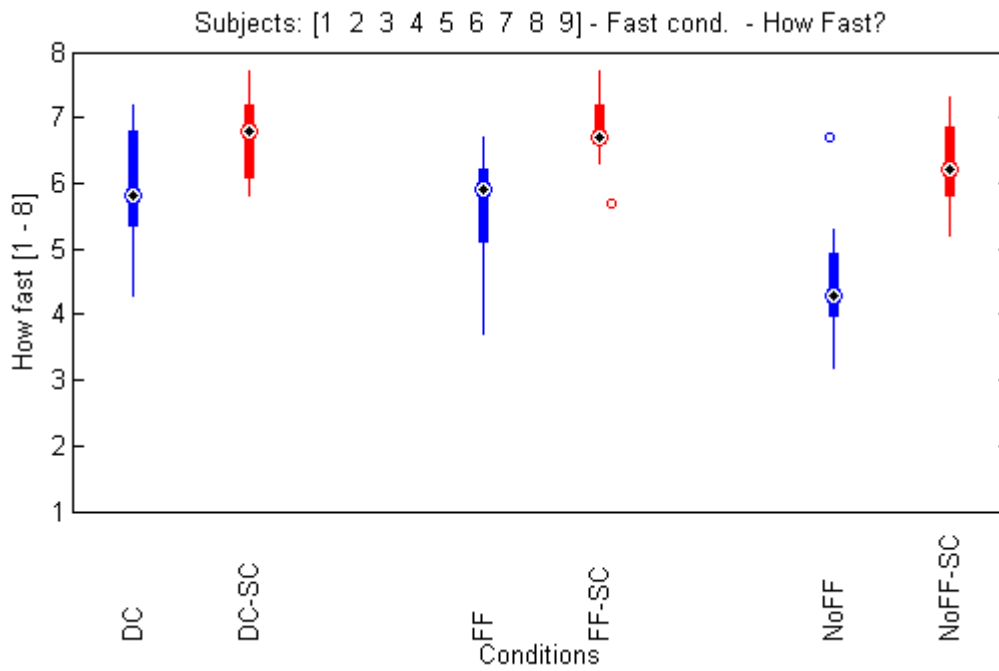


Figure 82: Subjective measure; How fast did you perform the task? [ML2] for the total task (TT), shown for the six experimental conditions (No SC: blue / SC: red).

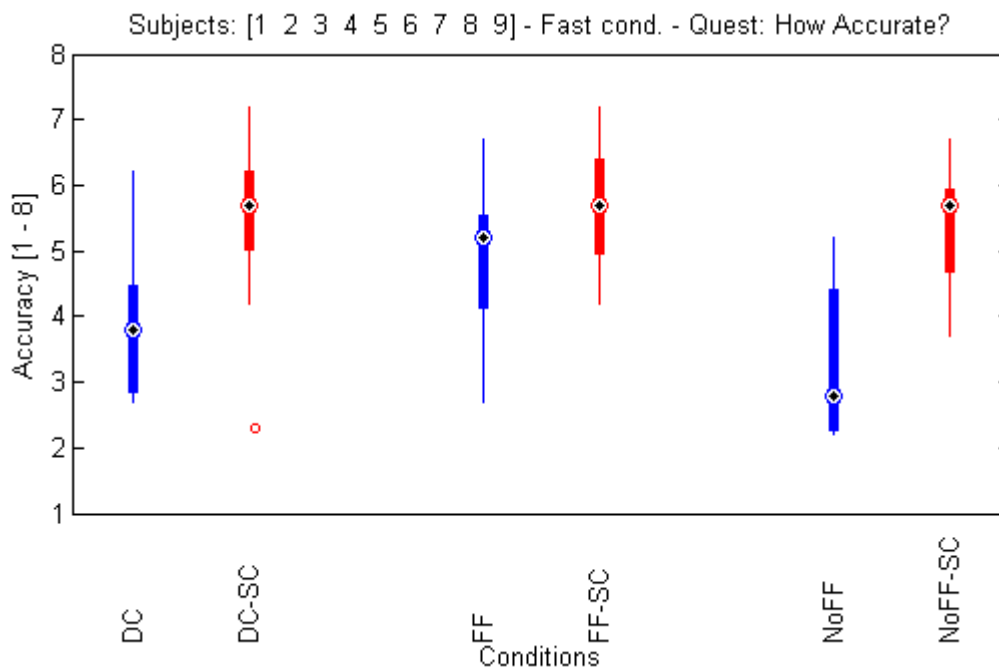


Figure 83: Subjective measure; How accurate did you perform the task? [ML3] for the total task (TT), shown for the six experimental conditions (No SC: blue / SC: red).

NASA TLX Workload subdivided into the six measures (real ratings):

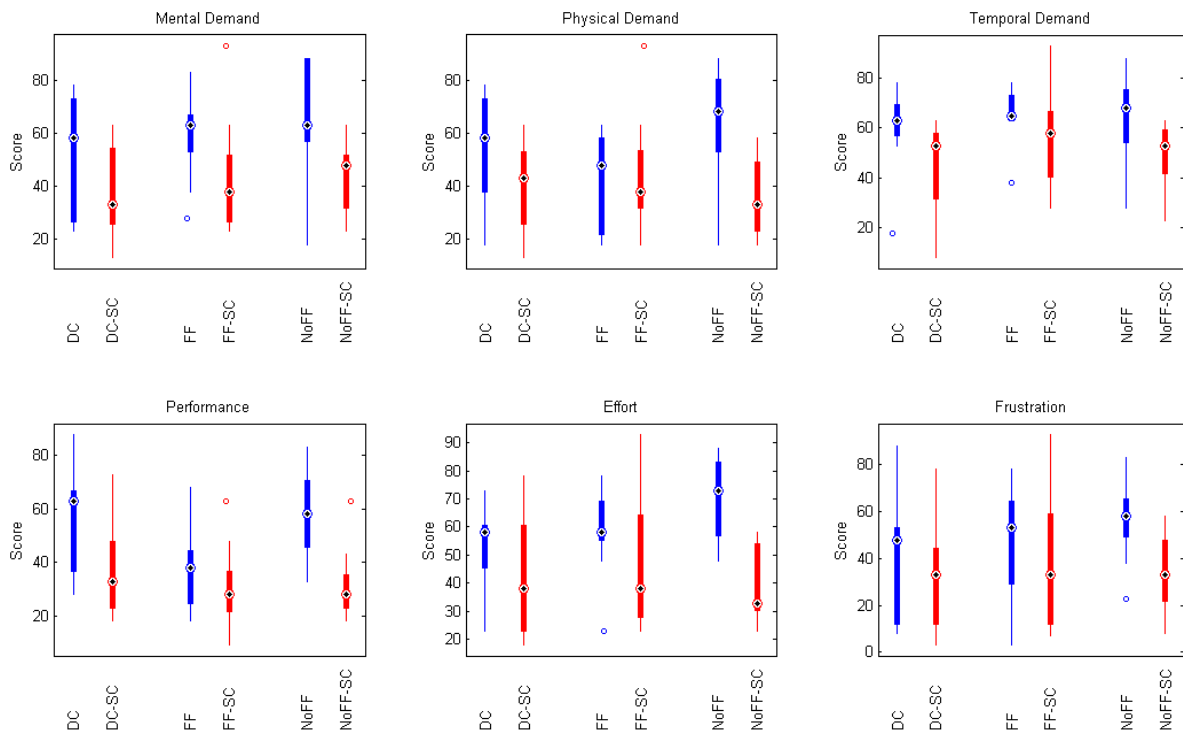


Figure 84: Self reported workload [ML1] for the total task (TT), subdivided into the six measures (normal scores) (No SC: blue / SC: red).

NASA TLX Workload subdivided into the six measures (relative ratings: the average score of each person was subtracted from all data for each person to normalize the data (subjective reference level)):

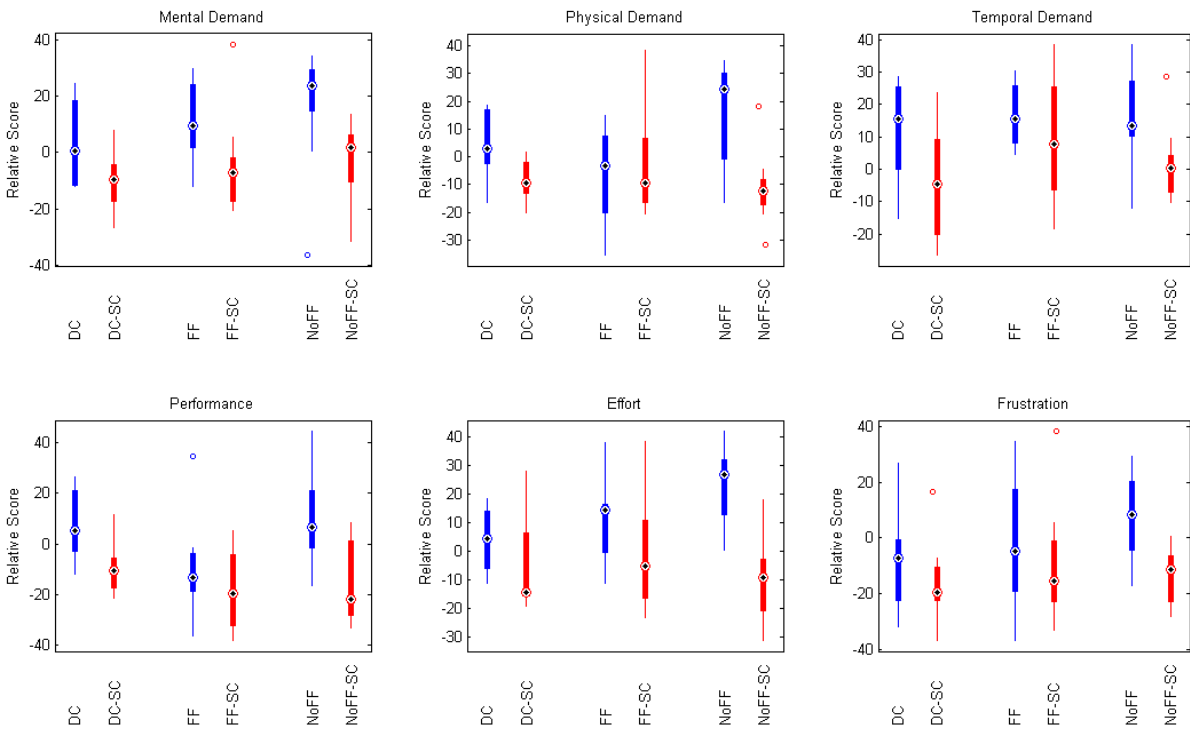


Figure 85: Self reported workload [ML1] for the total task (TT), subdivided into the six measures (Relative scores: normalised to subject means) (No SC: blue / SC: red).

D4.7 – Additional results

Fault rate (relative amount of trials containing a fault in the task execution)

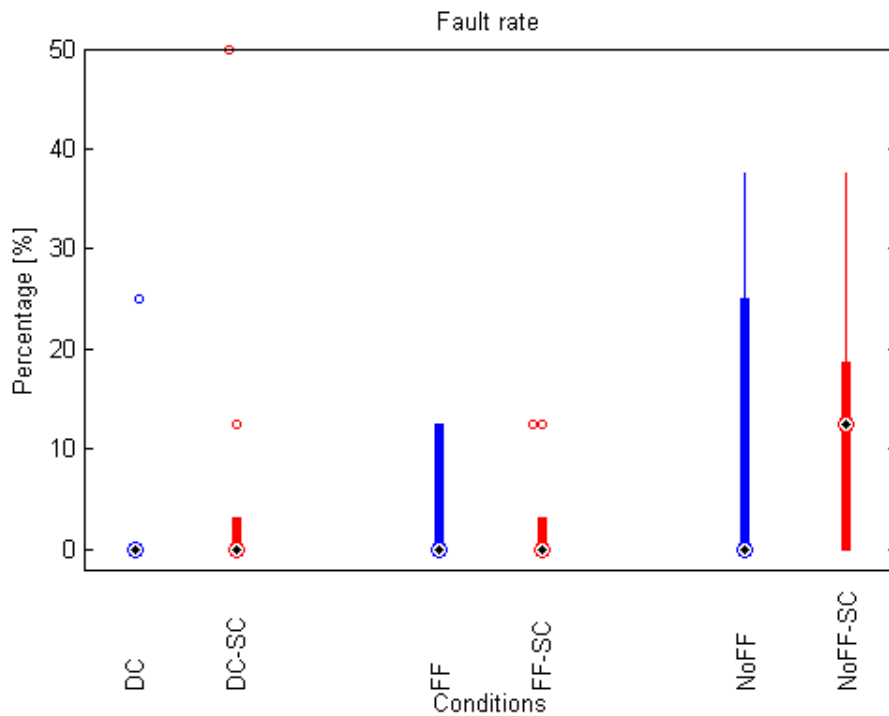


Figure 86: Fault rate; relative number of trials containing a fault in the task execution (*No SC: blue / SC: red*).

Counteractive behaviour between operator and haptic shared control.

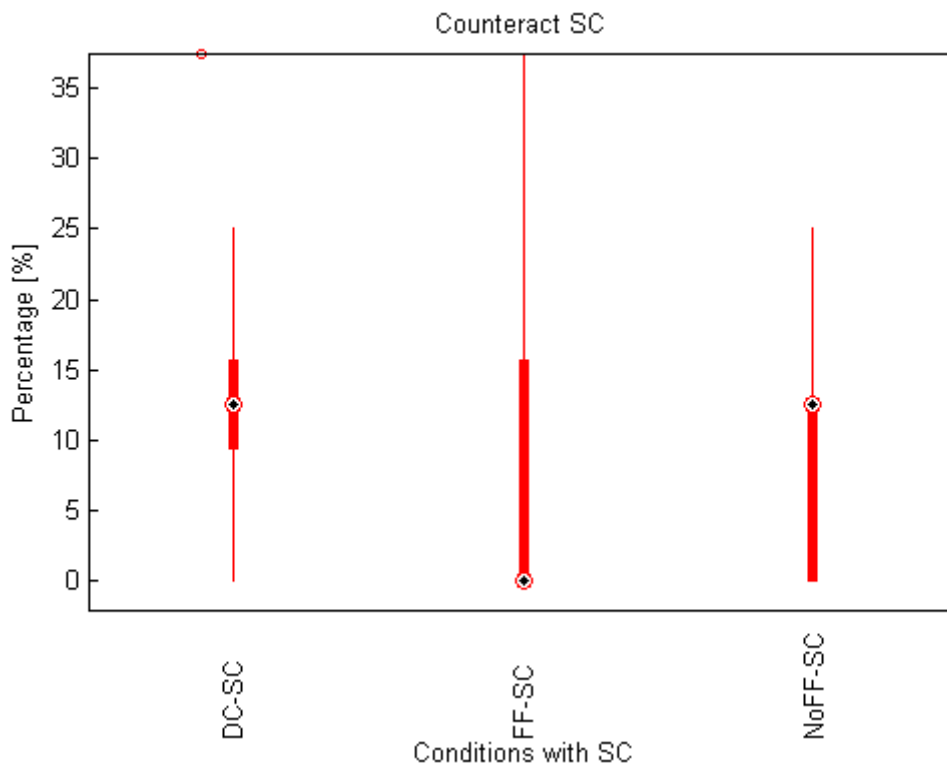


Figure 87: Relative number of trials containing counteracting control behaviour between human and shared control (*SC: red*).

Overview of master trajectories for the 6 conditions (6 x 8 trials):

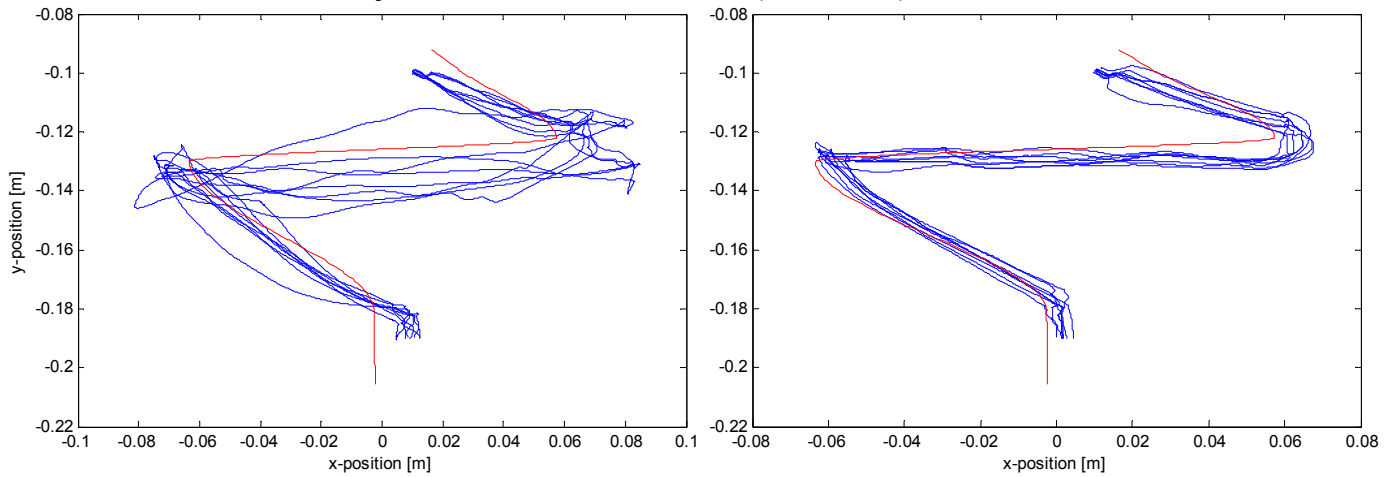


Figure 88: Master trajectories during **Direct Control (DC)** for a typical subject; no Shared control (left), Shared Control (right).

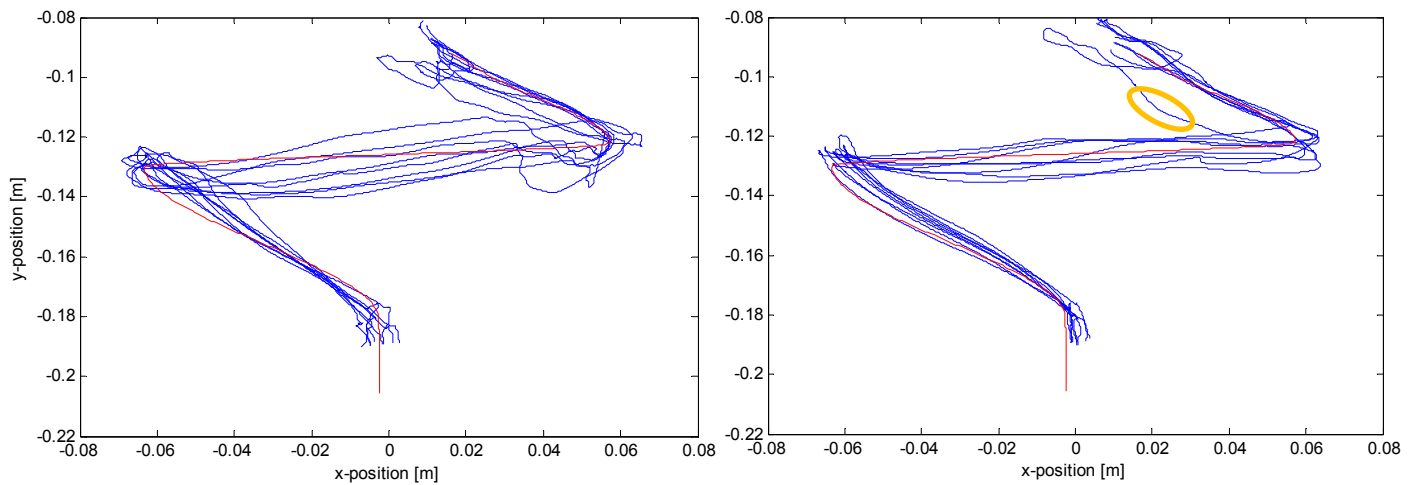


Figure 89: Master trajectories during **Force Feedback (FF)** for a typical subject; no Shared control (left), Shared Control (right). Orange encircled a counteractive behaviour between operator and SC.

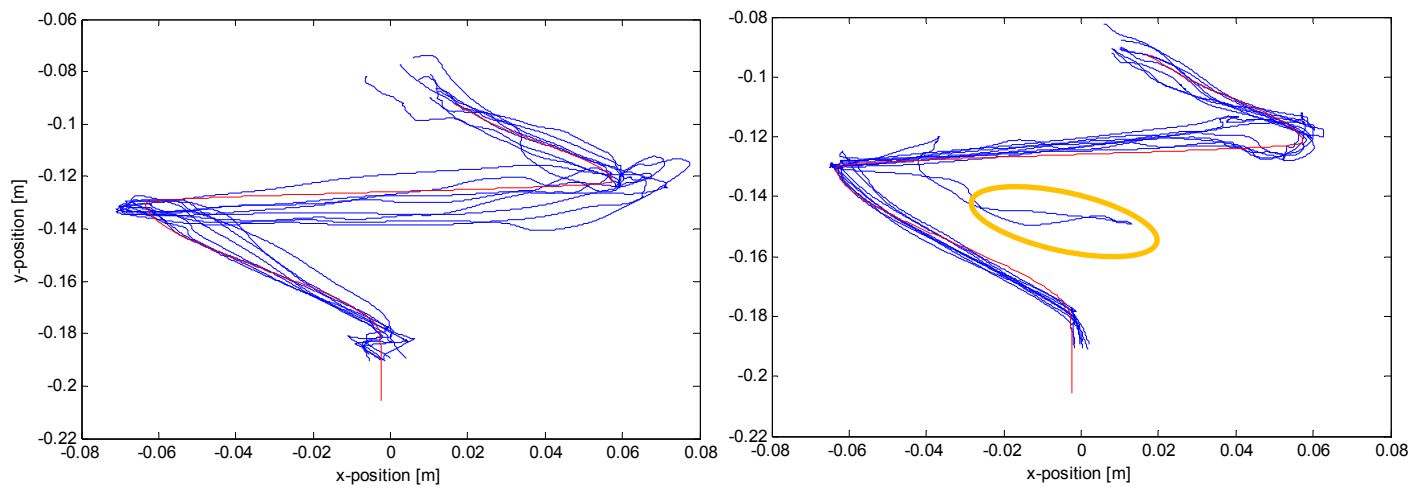


Figure 90: Master trajectories during **No Force Feedback (NoFF)** for a typical subject; no Shared control (left), Shared Control (right). Orange encircled a counteractive behaviour between operator and SC.

Example of haptic shared control forces for a typical subject.

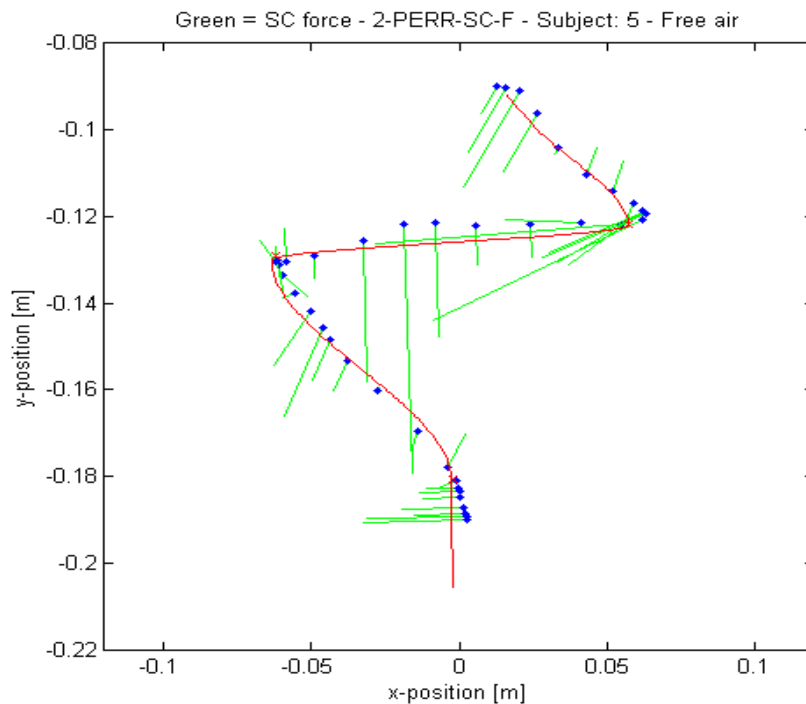


Figure 91: The shared control forces (green; shown with an interval of 1/75 seconds) during the task (until contact with the bolt). Shown the master trajectory, the red line shows the ideal path proposed by the shared controller. **Scale of the forces in the graph: 20 [N/m]**

To illustrate the flexibility of haptic shared control, a small additional test was performed. During the FF-SC condition each subject was asked to perform the task with an obstacle placed at the path. This was only executed once for each subject. The motion trajectory of a typical subject is shown below.

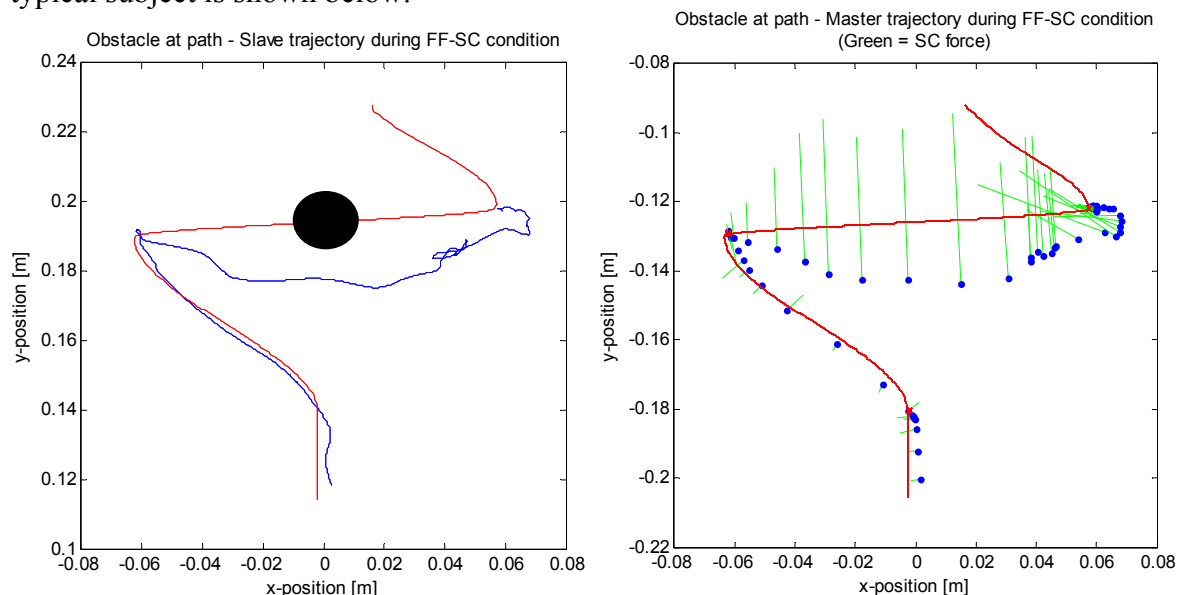


Figure 92: The trajectories of the slave (left) and master (right) during obstacle avoidance (task until point 3). The shared control forces on the master are represented by the green lines (interval 1/75 seconds). The red line shows the ideal path proposed by the shared controller. **Scale of the forces in the graph: 50 [N/m]**

The maximal haptic shared control force during the obstacle avoidance was 2.53 N.

Appendix E – Conference paper WHC

A summarized paper was submitted to the World Haptics Conference (<http://www.haptics2011.org/en/default.asp>). The conference will take place 22-24 June 2011, in Istanbul, Turkey.

Notification of paper acceptance: 1st of March, 2011.

Haptic shared control improves tele-operated task performance towards performance in direct control

Henri Boessenkool*
Delft University of Technology
Heemskerk Innovative
Technology

David A. Abbink†
Delft University of Technology

Cock J.M. Heemskerk‡
Heemskerk Innovative Technology

Frans C.T. van der Helm§
Delft University of Technology

ABSTRACT

In tele-operation, haptic feedback from the remote environment to the human is often limited, which has been shown to negatively influence the performance and required time of tasks. The conventional research focus is on improving the quality of the haptic feedback (transparency), which may have led to significant improvement, but is still imperfect, with many unresolved issues. The present study presents an alternative approach to improve tele-operated tasks: by offering haptic shared control in which both operator and support system apply the required forces at the input (master) device. It is hypothesized that virtual forces from well-designed shared control will improve required time and accuracy, with less control effort, and that these benefits exist for perfect transparency but even more so for imperfect transparency. In an experimental study haptic shared control was designed to aid operators (n=9) with performing a simple bolt-spanner task using a planar (2D, 3DOF) tele-operator setup. Haptic shared control was compared to normal operation for three types of control: the baseline condition of direct control at the master (perfect transparency), teleoperation with a simple PERR controller, and a PERR controller with feedback gains set to zero (no transparency). The experimental results provided evidence for the hypotheses, showing that the tested tele-manipulation task benefits from haptic shared control, for all three levels of transparency. Essentially, the presence of haptic shared control allows for a worse transparency without compromising required time, and can even improve required time during perfect transparency.

Index Terms: Tele-operation, haptic guidance, haptic shared control, transparency, task performance, human factors experiment

1 INTRODUCTION

Human beings are intelligent and dexterous and are able to perform many complex (manipulation) tasks like surgery, (dis-)assembly and maintenance. Though many complex tasks can be taken over by robots, one of the unique abilities of humans remains their ability to deal well with unexpected circumstances and changing environments. There are circumstances where the abilities of both human and robots are needed. One might think of complex tasks that need to be executed in unpredictable environments where human can not directly interact, due to for example the hostile nature of the environment (such as deep sea and nuclear or toxic environments) or due to dimension constraints (such as micro-assembly or mini-

mal invasive surgery). In such cases issues like safety, responsibility [24], and costs restrict the usability of full automation, and the human-in-the-loop approach using tele-manipulation robots is commonly used [10], [21]. Figure 1 shows a schematic representation of the total system of human operator, telemanipulator and environment, which will be referred to as the Connected Tele-manipulator System (CTS)[6].

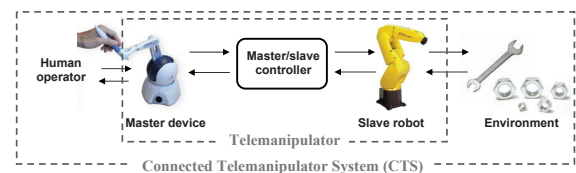


Figure 1: The five components of the Connected Tele-manipulation System (CTS), adapted from [6]

Tele-manipulation robots essentially extend the human's sensorimotor facilities to a remote location, which should give the sensation of actually being at that location performing the task (telepresence [23]). Good telepresence is achieved by accurate visual and audio representation of the (interaction with the) remote location, but also by translating the human's interaction forces on the master device to interaction forces between the remote environment and slave robot, and vice versa.

One of the main challenges in the field remains the accurate rendition of these forces, often called transparency. Previous research showed that providing force feedback from the environment to the human improves task performance [9],[14] and reduces cognitive workload [25]. However, the quality of the provided force feedback is often limited due to technical issues. Great efforts have been made over the past decades to improve transparency, and although substantial progress has been made [15],[16],[8],[5] and [6], optimal transparency is not yet realized. Another approach is then not to focus on achieving optimal transparency but to focus on optimal task performance. This approach was initially used by Rosenberg [22], presenting virtual fixtures which worked as a virtual ruler assisting a tele-manipulated peg-in-hole task. The addition of artificial guiding forces resulted in a large improvement in task performance. This research laid foundation for further research in haptic shared control, combining automation and manual control. The main application of shared control that is found in current literature is on operational assistance; guiding to a certain reference position [28],[22],[8], protecting areas [25],[6] and disturbance reduction [4],[23]. An example is the continuous haptic guiding during car following [4] and curve negotiation [23] proposed by Abbink and Mulder. These studies show that haptic shared control solutions look very promising for tele-manipulation. Most of this research is however limited to 1 or 2 degrees of freedom and/or focused on motions in free air. Furthermore continuous guiding seems promising,

*e-mail: h.boessenkool@student.tudelft.nl

†e-mail: d.a.abbink@tudelft.nl

‡e-mail: c.heemskerk@heemskerk-innovative.nl

§e-mail: f.c.t.vanderhelm@tudelft.nl

but is not often applied yet.

An ideal way of control should be continuous haptic shared control between the human operator and an intelligent control system. Ideally it should be implemented in such a way that the control can shift smoothly between human and machine, optimizing the human-machine interaction. A metaphor of haptic shared control is horse-riding [12]. The rider is in control, and guides the horse. But the horse can find a way by itself in case the rider loosens his or her control for a moment. Through the forces on the reins, control authority is switched smoothly back and forth between horse and rider.

To implement continuous haptic shared control on more degrees of freedom, this research proposes a haptic shared control for tele-manipulation based on the principle used by Abbink and Mulder [3]. The haptic shared control system is an intelligent system which calculates the ideal control action based on sensor information (e.g. about the slave robot, and the environment it interacts with). This ideal control action is presented as a force on the master device, so the operator continuously feels the optimal control action. The system will help the operator to execute this optimal action, but the operator can always resist the assisting forces if he does not agree with the system. A general scheme of the proposed haptic shared control is illustrated in figure 2.

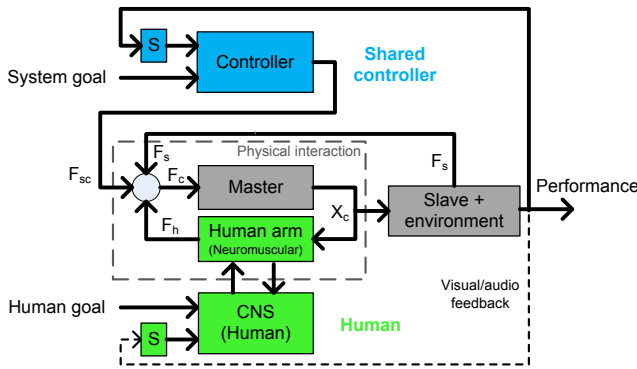


Figure 2: A schematic representation of haptic shared control. The guiding system receives feedback by sensors (S) and uses a control model to continuously calculate the optimal guiding force F_{sc} , which is presented at the master side. The control input to the master (X_c) is affected by the feedback forces from the slave (F_s) and may now be simultaneously influenced by both the human (F_h) and the shared control system (F_{sc}) [adapted from Abbink [3]].

When designing a haptic shared control system, it is important to understand that human tune their visual and haptic feedback differently and use a different control strategy for every different type of motion. The design of a proper haptic shared control system should consider these different types of motion. Based on Aliaga [5] Wildenbeest proposed four fundamental types of motion [26]. For each of these fundamental motion types a different guiding strategy was proposed:

1. *Free Air Movement*. The slave robot has no interaction with the environment. Proposed guiding strategy for haptic shared control: Guiding of tool position and orientation to the *ideal* path.
2. *Contact Transition*. The slave robot moves close to a surface and makes contact. Proposed guiding strategy for haptic shared control: Position and orientation guiding. Guiding prevents hard collision by an artificial damping.
3. *Constrained Position Movement*. One or more degrees of freedom of the slave robot are constrained (e.g. moving over a

Table 1: Hypotheses about the effect of shared control on task performance for different levels of transparency. Direct control is taken as baseline (denoted as '0').

	Ideal <—	Transparency	—> No
F1:	<i>Direct Control</i>	<i>Teleoperation - Force Feedback</i>	<i>Teleoperation - No Force Feedback</i>
F2:	<i>No Shared Control</i>	0	--
	<i>Shared Control</i>	+	+

surface, coaxial sliding of pipes). Proposed guiding strategy for haptic shared control: Guiding of tool position and orientation.

4. *Constrained Force Movement*. A motion in which forces/torques have to be controlled in one or more degrees of freedom (e.g. polishing a pipe, cutting human tissue). Proposed guiding strategy for haptic shared control: Guiding places rotation/compliance center at the bolt origin (only guiding forces perpendicular to the force movement).

Figure 2 shows that both human and the haptic shared control system have a *goal* input. Ideally, the haptic shared control system should be able to figure out the human goal (intention and strategy) and adapt to this goal. The shared control system used in the current study deviates from the system shown in figure 2 in that the shared control system determines the goal (e.g. the ideal path), and shows this visually to the human. This "ideal" path is chosen and is not optimized to human motions.

The main objective of this research was to provide evidence that appropriately designed haptic shared control results in larger improvements in human-in-the-loop task performance than improving transparency. To test this, an experiment was designed using a simple bolt-and-spanner task [26], containing the four fundamental motion types. The subjects had to execute the task for three different levels of transparency: Direct Control (perfect transparency), tele-manipulation with force feedback and tele-manipulation without force feedback (no transparency). These conditions were tested with and without haptic shared control. It was hypothesized that reducing transparency will degrade task performance, while appropriate haptic shared control will increase task performance with respect to Direct Control, independent of the level of transparency (see table 1). Since Direct Control is the golden standard in transparency oriented research, it is defined here as baseline condition.

2 METHODS

2.1 Subjects

The proposed shared control was tested on a group of 9 male subjects. The mean age of the subjects was 26.1 (1.05) year. All subjects were right handed and master students of the department Mechanical Engineering at the Delft University of Technology. None of the subjects had experience with teleoperators. The subjects participated voluntarily and did not receive a financial compensation for their efforts.

2.2 Task description

The subjects were asked to take place in front of the master device and hold the interface of the master device like a normal spanner. Subsequently the following bolt-and-spanner task had to be executed (see also figure 3); start at the lower y-limit, move to points 1, 2 and 3, move to the bolt, slide the spanner over the bolt, and

rotate the bolt to the visible reference angle. The locations of these points were respectively: $(x, y, \theta) = (0m, 0m, 0^\circ)$, $(0m, 0.02m, 0^\circ)$, $(-0.06m, 0.07m, 0^\circ)$, $(0.06m, 0.08m, 65^\circ)$ and the bolt position $(x, y) = (0m, 0.12m)$. The task instruction was; execute the task as fast as possible.

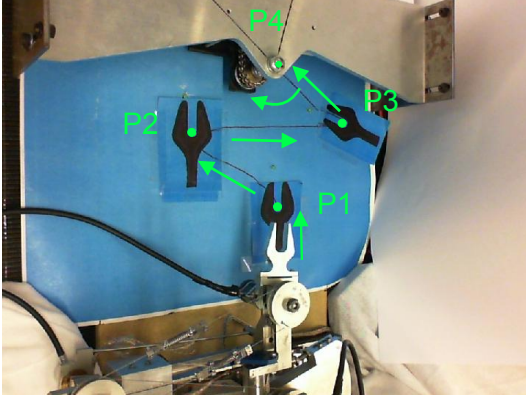


Figure 3: Cameraview (tilted) from the environment at the slave side

These instructions were handed out to the subjects and were verbally explained in addition by the experiment leader before the start of the experiment.

2.3 Experimental setup

The haptic shared control experiment was performed using a 3-DOF planar telemanipulation system. The system consists of a parallel force-redundant master device (see fig. 4) and a serial slave device (see fig. 5)

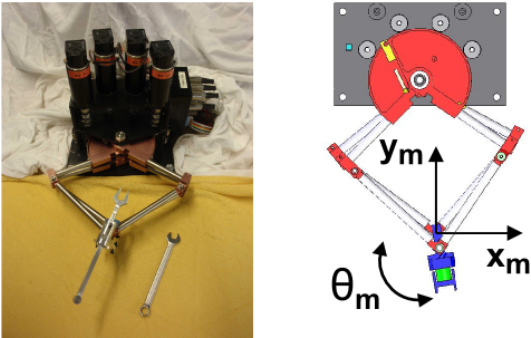


Figure 4: A picture (left) and a schematic drawing (right) of the master device

The controller ran on a Mathworks xPC Target real time operating system at 1kHz. The positional accuracy was 0.03mm and the minimal time delay between master and slave was estimated at 1.5ms (1ms measurement interval and 0.5 due to the zero-order hold of the analogy output [7]). The design of this telemanipulator is discussed in detail by Christiansson [6].

The device performance and stability was evaluated in by Wildenbeest [26] using the two-port network modeling framework [13]. The column *Force Feedback* in table 2 shows a summary of the most important analytic performance metrics for the teleoperator in PERR mode. The other two columns show the deduced values for the other transparency modes.

The setup was equipped to perform a bolt and spanner task. Both master and slave were equipped with a spanner interface. The

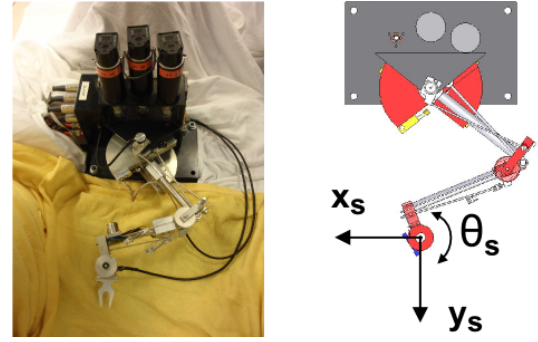


Figure 5: A picture (left) and a schematic drawing (right) of the slave device

Table 2: Numerical Performance Metrics for the different levels of transparency

Analytic Metrics	Ideal <—	Transparency	—> No
	Direct Control	Teleoperation - Force Feedback	Teleoperation - No Force Feedback
free air m [kg]	0.23	0.14	0.23
free air b [Ns/m]	4.5	11	4.5
free air k [N/m]	0	0.027	0
stiff contact m [kg]	~inf	0.23	0.23
stiff contact b [Ns/m]	~inf	4.5	4.5
stiff contact k [N/m]	~inf	400	0
transparency error [-]	0	68	~ inf
Zwidth [-]	~ inf	31	~ 0

slave device was actuated using the series-elastic-actuation principle which provides the ability of estimating interaction forces at the slave side. Furthermore an accelerometer was mounted at the tip of the slave to measure the high frequency contact forces.

The (remote) environment consisted of a construction with an M6 bolt (figure 3). This construction could be placed at the slave or the master side. The torque required to rotate the bolt was artificially created by a friction force induced by a spring. The tightening torques to overcome static and dynamic friction were estimated to be respectively 35.7 (2.0) Nmm and 31.6 (6.0) Nmm. The rotation of the bolt was measured with an angle sensor.

2.4 Haptic shared control design

The haptic shared control design could be based on two fundamentally different types of guiding; *attractive* guiding [17],[18], creating guiding forces towards an ideal path and *repulsive* guiding [22],[4], preventing users to enter forbidden regions by presenting repulsive forces. Attractive motion guiding can be done in a *passive* or in an *active* way: passive guiding will not induce a motion by itself, active guidance however actively pushes the master to the (sub)goal and will induce a motion when the operator releases the master. A variety of shared control designs, partly based on the literature that was discussed above, was implemented and tested during a pilot experiment. Passive guiding based on an ideal path showed the best performance and was chosen for this experiment. This chosen guiding is not necessarily the optimal guiding and neither totally optimized, though suitable for a proof of principle.

The haptic shared control used for the experiments is described below per subtask:

1. *Free Air Movement.* A smooth path between the target points

Table 3: The six experimental conditions

	Ideal <—	Transparency	—> No
F1:	<i>Direct Control</i>	<i>Teleoperation - Force Feedback</i>	<i>Teleoperation - No Force Feedback</i>
F2:	DC	FF	NoFF
	<i>No Shared Control</i>	DC-SC	FF-SC
	<i>Shared Control</i>	DC-SC	FF-SC

was chosen as ideal path (see red line in figure 3). The guiding forces were based on the 'look ahead' path error (E_2 in figure 6) [18], which is defined as the path error at an estimated position in future based on the current velocity vector and a look ahead time of 0.1s.

$$F_{shared-control} = -\vec{E}_2 * k_2 \quad (1)$$

The shared control stiffness was $k_2 = 120[N/m]$. Within a radius of 0.04m of the target points 1 to 3, guiding of the tool orientation was linear increased to a stiffness of 0.5 [Nm/rad].

2. *Contact Transition.* Within a radius of 0.05m of the bolt, the tool orientation guiding was linear increased to a stiffness of 0.5 [Nm/rad]. An artificial damping prevented hard collision.
3. *Constrained Position Movement.* The spanner was guided to the right orientation with a stiffness of 0.5 [Nm/rad]. Furthermore a snap-feature was introduced close to the bolt.
4. *Constrained Force Movement.* The presented guiding force was only perpendicular to the force movement. The snap-feature was active to ensure that the spanner stayed on the bolt head. In the *No Force Feedback* (NoFF) condition, the shared control system introduced a virtual rotation/compliance centre at the bolt origin.

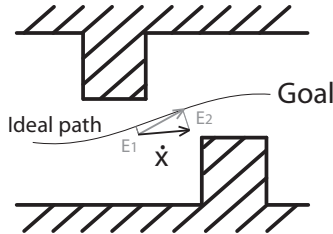


Figure 6: Shared control design for free air movement. E_1 shows the current path error and E_2 the look ahead path error based on the current velocity \dot{x} and a defined look-ahead-time. The guiding force is based on the look ahead path error (E_2), adapted from [18].

2.5 Experiment design

2.5.1 Experimental conditions

The two main factors of the experiment were two different types of haptic information: (F1) the level of transparency, and (F2) with/without haptic shared control. These factors were combined into six experimental condition (see table 3).

Transparency was defined as how transparent the interaction forces were transmitted to the operator. The two extremes of these factor were *Direct Control* (DC), which gives perfect transparency, and *No Force Feedback* (NoFF), which gives no transparency. A

third condition in between was *Force Feedback* (FF) using a classical PERR-controller. The FF and the NoFF conditions were tested in tele-manipulation configuration. The NoFF condition was tested by setting the PERR slave-to-master PD-gains to zero. For the DC condition, the environment was placed at the master side and the task was executed hands on using the spanner mounted at the master.

The experiment contained 8 repetitions of each of the six conditions per subject. Every subject started with the *Force Feedback* (FF) condition, to have a reference for the subjective measures. The remaining conditions were presented randomly to minimize learning effects during the experiment.

All subjects did have training sessions for each new condition in advance of the actual experiment.

2.5.2 Controlled variables

Visual feedback Visual feedback from the remote environment is very important during tele-manipulation tasks and is usually achieved by camera views. Yet in many cases the often hazardous environments limit the quality and available dept information, which increase the difficulty of the task for the human operator.

For all conditions of the experiment, the subjects were dependent on visual feedback from the (remote) environment by a camera view (see figure 3). This camera view had a limited resolution (960 x 544 pixels) and was displayed on a 14 inch laptop screen next to the setup. The camera was placed under an angle of 45 degrees with respect to the horizontal and could be placed at the slave or master side. This tilt of the camera was done to make the task more difficult (and realistic) by introducing dept effects.

Task instruction Upon executing a task human always have a (subconscious) preference for certain control strategies. In most cases, this control strategy has to do with a trade-off between energy consumption, accuracy and/or time. During the training trials preceding the experiments the subjects got an explicit instruction to perform the task with one of the two following control strategies:

1. *Accurate*; perform the task as accurate as possible. This would lead to optimisation of strategy towards low forces and positional accuracy.
2. *Fast*; perform the task as fast as possible. This would lead to optimisation of strategy towards time duration.

During the pilot study it appeared that testing both strategies on each subject resulted in a high burden on the subjects. Hence, during the actual experiments the subjects were instructed to perform the task *as fast as possible* for all conditions.

2.6 Measured variables & Metrics

To analyse the effect of shared control on tele-operated task performance, a vast amount of variables were recorded during the measurements, all sampled at 1 kHz. Based on the recorded data, a number of metrics were calculated to determine the performance. In this paper we will focus on the metric time-to-complete for the total bolt-and-spanner task.

2.7 Data analysis

A univariate analysis of variance (ANOVA) was used to determine the statistical significance between the six experimental conditions. Because of the large variance between subjects, a multi-way ANOVA was considered as most suitable for further analyses. A two-way ANOVA was used to analyse the effects of shared control separately for the three different *transparency* conditions. The two factors in this two-way ANOVA were the experimental factor *haptic shared control* (F2), and the *between-subject variation* (F3).

Table 4: ANOVA results from the factors F2 and F3 on time-to-complete, shown for each F1 condition. All results are significant.

F1:	DC	FF	NoFF
F2 - With/without SC	F[14.15] p=0.006	F[42.85] p=0.0002	F[12.57] p=0.008
F3 - Subject var.	F[4.79] p=0.02	F[14.12] p=0.0006	F[4.33] p=0.027

Normality assumption was checked on all dependent variables ($p = 0.05$) to ensure the applicability of the statistical tests.

Results were regarded as statistical significant when $p \leq 0.05$.

3 RESULTS

The performance, expressed in time-to-complete for the total bolt-and-spanner task, is shown in figure 7. The data is presented in box plots; the central mark is the median, the edges of the box are the 25th and 75th percentiles and the whiskers extend to the most extreme datapoint within 1.5 times interquartile range. The data was first compared using a one-way ANOVA, which showed a difference between the six conditions ($p < 0.001$). This means that the time-to-complete is influenced by the experimental conditions. Results of the two-way ANOVA are shown in figure 7 and table 4.

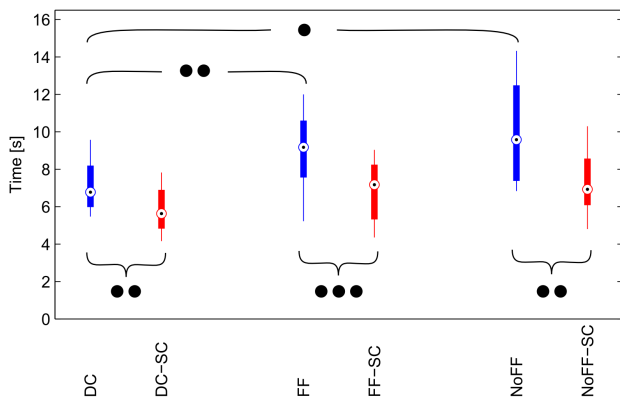


Figure 7: Time-to-complete for the entire bolt-and-spanner task (9 subjects, 8 repetitions), shown for six conditions. Marks (●●●), (●●), (●) denote the significance of $p \leq 0.001$, $p \leq 0.01$ and $p \leq 0.05$ respectively

With respect to transparency, it shows that the baseline (DC/perfect transparency) yields the shortest time to complete. Compared to DC, the FF and NoFF conditions showed an increased time-to-complete of respectively 24% ($p=0.0013$) and 48% ($p=0.0104$). Haptic shared control resulted in an improved time-to-complete of 19.7% ($p = 0.006$), 24.2% ($p = 0.0002$) and 31.9% ($p = 0.008$) for respectively the DC, FF and NoFF condition (see table 4). Subject did not show a significant difference ($p=0.692$) in time performance between perfect transparency (DC) and shared control without transparency (NoFF-SC).

The significance in the second row (F3) of table 4 shows the large variance between subjects.

4 DISCUSSION

The experimental results showed that the tele-manipulation task benefits from shared control, for all three levels of transparency.

In fact, the presence of shared control allowed for a worse transparency without compromising required time. Moreover shared control could even improve required time.

The association between time-performance and transparency was as expected; a lower transparency yields to a higher time-to-complete. These findings correspond with existing literature. For example Draper [9] and Hannaford [14] reported an improved performance when providing force reflection. The relative small difference between the NoFF and FF condition represents the limited force feedback quality of the used tele-manipulator. This was due to the simple PERR controller that was used. The difference in performance between FF and DC shows the room for improvement when focussing on improvement of telemanipulator transparency. Shared control resulted in an improved time-to-complete for all transparency conditions. These effects were higher for imperfect transparency. Even without any force feedback from the environment shared control resulted in task execution approximately as fast as in Direct Control.

It is interesting to note that the effects mentioned above were also present in pilot experiments with the task instruction to "perform as accurately as possible".

The proposed haptic shared control requires the availability of information about the environment, the task and the human intention, since the control system needs to define an ideal path. In most tele-manipulation situations this environmental information could be deduced from a virtual (CAD) model or be obtained by sensors, and since tele-manipulation is mostly used in controlled environments with closely monitored task sequences, the general task sequences are known. Operator intention and operator motion planning also play an important part, but is much harder to track. The experimental results showed the importance of including human intention and motion planning into a haptic shared control design. A limitation of the used shared control implementation was the fact that 9-14% of the executed trials contained counteracting control behaviour between the human and the shared control system. These counteracting actions were caused by a mismatch of intentions between the human and the control system: e.g. in some cases subjects intended to move from point 2 to point 3, while the shared control system expected a movement from point 2 to point 1. The subjects were able to detect and solve these conflicts with guiding forces quite fast, and note that even with this limitation shared control resulted in an improved performance.

The experimental task was a two dimensional three degree of freedom (3DOF) bolt-and-spanner task, containing two translations and one rotation. Performing this similar task in a three dimensional environment using a 6DOF tele-manipulator would make the task considerably harder, mainly due to the need of three dimensional visual information. 3D vision is still a subject of research and is often not practically realizable in tele-manipulation situations. In conventional tele-operation a combination of different (perpendicular) camera views is used to deduce the dept information. In that situation an operator has to track multiple camera views simultaneously, which is quite hard. The problem of receiving depth information when going from 2D to 3D is inherent to the visual channel. The same transition from 2D to 3D does not have such an implication for the haptic channel. Since shared control supports the operator via the haptic channel, improvements by shared control are expected to be even higher for 3D 6DOF manipulation, than for the tested planar situation.

It is interesting to look into more detail on the different roles of transparency and haptic shared control with respect to execution of tasks. In this experimental setup haptic shared control could totally replace transparency; with no transparency subjects were still able to reach a performance comparable to DC. This result implies that tasks containing movement do not require transparency, but can be improved more effectively by addition of haptic shared control.

However, shared control should ideally be combined with transparency for two reasons. First of all, real force tasks require a certain level of transparency, since human need at least an indication of the exerted forces. The force task used in this experiment is actually not a real force task, as there is movement involved. During a real force task the amount and direction of the exerted force can not be approximately deduced from a resulting motion, as was the case during the experiment. Secondly, unexpected situations also require transparency, as the operator will not be able to trust on shared control.

An interesting possibility of the haptic shared control, as proposed earlier [3], is the option to gradually shift between human control and automation [1]. A low stiffness of the shared control system allows the operator to easily over-rule the guiding forces, whereas a high controller stiffness forces the operator to a certain path or even a motion. In this way the shared control stiffness system defines the autonomy level of the shared control system. Marayong [17] showed experimental results which indicate that the level of operator support should be adjusted to the task. In normal situations a low compliance of the guiding was found optimal, however for tasks such as off-path targeting and obstacle avoidance a higher compliance resulted in the best task performance. To support an operator during tele-manipulation tasks the gradual scaling of the amount of shared control depending on the task, as well as the operator's intention and possibly the criticality of the situation are very promising. To develop shared control to such a level, a thorough understanding of human motion control and the human dynamics is required. Knowledge about the physical behaviour of the human arm is important to optimize shared control, as the human arm admittance influences the response to forces. A way to measure and include the highly adaptable human neuromuscular dynamics in a haptic design is proposed by [20] and [2].

Future research could further improve haptic shared control by resolving the conflicting guiding force issues discussed above. This could be done by focusing on a better matching of the guiding to natural control behaviour of the human. Available research in the field of human motion as [11], providing a mathematical model about coordination of arm movement and [19] which focussed on the prediction of movement profiles, can provide more insight in path planning and control intention of humans. Furthermore it is important to include neuromuscular analyses in the shared control design process, as a better insight in human control behaviour and human response to forces is essential to optimize haptic shared control towards the human operator.

5 CONCLUSION

Haptic shared control was investigated as a means of supporting operators with performing a tele-operated bolt-and-spanner task. The effect of the designed shared control system was investigated for three different levels of tele-operator transparency. For all three levels of transparency, shared control allowed subjects to significantly and substantially improve their time-to-complete.

For the experimental conditions studied, shared control influenced task performance much more than transparency: even with the worst possible transparency, shared control allowed subjects to perform just as well as with perfect transparency, as provided by direct control. The experimental results imply that - at least for tasks that contain movement - focusing on haptic shared control may be more beneficial to operators than focussing on improving transparency.

REFERENCES

- [1] D. Abbink and M. Mulder. Exploring the dimensions of haptic feedback support in manual control. *Journal of Computing and Information Science in Engineering*, 9(1), 2009.
- [2] D. A. Abbink. *Neuromuscular analysis of haptic gas pedal feedback during car following*. PhD thesis, TU Delft, 2006.
- [3] D. A. Abbink and M. Mulder. Neuromuscular analysis as a guideline in designing shared control. *Advances in Haptics*, 109:499–516, 2010.
- [4] J. J. Abbott and A. M. Okamura. *Virtual fixture architectures for tele-manipulation*. 2003.
- [5] I. Aliaga, J. Rubio, and E. Sanchez. Experimental quantitative comparison of different control architectures for master-slave teleoperation. *IEEE Transactions on Control Systems Technology*, 12(1):2–11, 2004.
- [6] G. Christiansson. *Hard Master Soft Slave Haptic Teleoperation*. PhD thesis, Delft University of Technology, 2007.
- [7] G. Christiansson. The low-stiffness teleoperator slave - a trade-off between performance and stability. *International Journal of Robotics Research*, 26(3):287–301, 2007.
- [8] R. W. Daniel and R. R. McAree. Fundamental limits of performance for force reflecting teleoperation. *International Journal of Robotics Research*, 17(8):811–830, 1998.
- [9] J. V. Draper, W. E. Moore, J. Herndon, and W. B. S. Effects of force reflection on servomanipulator task performance. In *International topical meeting on remote systems and robotics in hostile environments*, Pasco, WA, pp. 654–660, 1986.
- [10] P. Fischer, R. Daniel, and K. V. Siva. Specification and design of input devices for teleoperation. 1990.
- [11] T. Flash and N. Hogan. The coordination of arm movements: An experimentally confirmed mathematical model. *Journal of Neuroscience*, 5(7):1688–1703, 1985.
- [12] K. H. Goodrich, P. C. Schutte, F. O. Flemisch, and R. A. Williams. Application of the h-mode, a design and interaction concept for highly automated vehicles, to aircraft. In *AIAA/IEEE Digital Avionics Systems Conference - Proceedings*, 2006.
- [13] B. Hannaford. A design framework for teleoperators with kinesthetic feedback. *IEEE Trans. on Robotics and Automation*, 5(4):426–434, 1989.
- [14] B. Hannaford, L. Wood, D. A. McAfee, and H. Zak. Performance evaluation of a six-axis generalized force-reflecting teleoperator. *IEEE Trans. Syst., Man, Cybern.*, 1991.
- [15] J. Dudragne. A generalized bilateral control applied to master-slave manipulators. In *Proc of the 20th ISIR*, pages 435–442, 1989.
- [16] D. A. Lawrence. Stability and transparency in bilateral teleoperation. *IEEE Transactions on Robotics and Automation*, 9(5):624–637, 1993.
- [17] P. Marayong, A. Bettini, and A. Okamura. Effect of virtual fixture compliance on human-machine cooperative manipulation. In *IEEE International Conference on Intelligent Robots and Systems*, 2002.
- [18] M. Mulder, D. A. Abbink, and E. R. Boer. The effect of haptic guidance on curve negotiation behavior of young, experienced drivers. In *Conference Proceedings - IEEE International Conference on Systems, Man and Cybernetics*, pages 804–809, 2008.
- [19] H. Nagasaki. Asymmetric velocity and acceleration profiles of human arm movements. *Experimental Brain Research*, 74(2):319–327, 1989.
- [20] R. Pintelon and J. Schoukens. *System Identification: A Frequency Domain Approach*. IEEE, New York, 2001.
- [21] A. C. Rolfe. A perspective on fusion relevant remote handling techniques. *Fusion Engineering and Design*, 82(15-24):1917–1923, 2007.
- [22] L. B. Rosenberg. Virtual fixtures: Perceptual tools for telerobotic manipulation. In *Virtual Reality Annual International Symposium, 1993.*, 1993 IEEE, 1993.
- [23] T. B. Sheridan. Telerobotics. *Automatica*, 25(4):487–507, 1989.
- [24] T. B. Sheridan. *Humans and Automation: System Design and Research Issues*. WileyBlackwell, 2002.
- [25] H. S. Vitense, J. A. Jacko, and V. K. Emery. Multimodal feedback: An assessment of performance and mental workload. *Ergonomics*, 46(1-3):68–87, 2003.
- [26] J. Wildenbeest. Improving the quality of haptic feedback yields only marginal improvements in teleoperated task performance. Master's thesis, Delft University of Technology, 2010.
- [27] B. Xie and G. Salvendy. Prediction of mental workload in single and multiple tasks environments. *International Journal of Cognitive Ergonomics*, 4:213–242, 2000.

Appendix F – Epilogue

Discussions and exchange of ideas with my coaches and other people have made an important contribution to this research, resulting in inspiration, new viewpoints and fresh ideas. I want to conclude this thesis with two important insights gained during this research period.

During one of the progress meetings an interesting shared control analogy came into our minds, originating from human physiology. Human motion control is most of the time feed forward. In known situations, a human does not use feedback from his exteroceptive and proprioceptive sensors to control his motion, but he applies feed forward based control. This is possible since he is able to include the dynamics of for example his arms into his control model. Only in unknown situations, for example when walking in complete darkness, the human shifts to the much slower feedback based control. In this feedback based control a human directly reacts on his sensor signals.

When applying this idea of feedback and feed forward control to the field of tele-manipulation, it appears that current research mainly focus on tele-manipulators working in ‘feedback’ mode. Tele-manipulators are designed as ‘feedback systems’, not including any information about its dynamics and environment in its control, and purely relying on sensor information. Tele-manipulator performance could be much higher when it should be possible to shift to ‘feed forward’ control in known situations. Here we find the analogy with ideal haptic shared control; shared control can function as a kind of ‘feed forward’ during tele-manipulation, using available information from the environment.

Later another shared control parallel came into my mind, not related to this technical research, but to faith. It starts with the God from the bible, Who wants to live with us. He made it possible for us to become as we were meant to be. Not by posting constraints from the outside (e.g. by law), but by living in us and changing us from the inside; a kind of ‘shared control’. This is well described in the bible verse below:

“I am crucified with Christ: nevertheless I live; yet not I, but Christ liveth in me: and the life which I now live in the flesh I live by the faith of the Son of God, who loved me, and gave himself for me.” [Gal. 2:20, Bible (KJV)]

Similar to shared control proposed in tele-manipulation, the human stays in control.

The nice thing of analogies is that they can give more insight in situations or systems. Highlighting some new aspects. And although the latter one has nothing to do with technical research, I think both analogies are worth some consideration.

References

- D. A. Abbink. *Neuromuscular analysis of haptic gas pedal feedback during car following*. PhD thesis, TU Delft, 2006.
- D. A. Abbink, E. R. Boer, and M. Mulder. *Motivation for continuous haptic gas pedal feedback to support car following*. In IEEE Intelligent Vehicles Symposium, Proceedings, pages 283–290, 2008.
- D. A. Abbink and M. Mulder. *Neuromuscular analysis as a guideline in designing shared control*. Advances in Haptics, 109:499–516, 2010.
- I. Aliaga, Rubio, and E. Sinchez. *Experimental quantitative comparison of different control architectures for master-slave teleoperation*. IEEE Transactions on Control Systems Technology, 12(1):2–11, 2004.
- H. Boessenkool. Literature survey; *Shared control in master-slave manipulation during maintenance at ITER. An overview and classification of shared control*. TU Delft, 2009
- G. Christiansson. *Hard Master Soft Slave Haptic Teleoperation*. PhD thesis, Delft University of Technology, 2007a.
- G. Christiansson. *The low-stiffness teleoperator slave - a trade-off between performance and stability*. International Journal of Robotics Research, 26(3):287–301, 2007b.
- D. T. McRuer and H. R. Jex, “A Review of Quasi-Linear Pilot Models, IEEE Trans. Human Factors in Eletronics,” Vol. 3, pp. 231-208, 1967.
- M. Mulder, D. A. Abbink, and E. R. Boer. *The effect of haptic guidance on curve negotiation behavior of young, experienced drivers*. In Conference Proceedings - IEEE International Conference on Systems, Man and Cybernetics, pages 804–809, 2008.
- R. Penrose, “A generalized inverse for matrices,” Proceedings of the Cambridge Philosophical Society , pp.406–413, 1955
- G.A. Pratt and M.M. Williamson, “Series elastic actuators,” IEEE International Conference on Intelligent Robots and Systems, Vol. 1, pp. 399-406, 1995.
- L. B. Rosenberg. *Virtual fixtures: Perceptual tools for telerobotic manipulation*. In Virtual Reality Annual International Symposium, 1993.
- E. de Vlugt, A.C. Schouten and F.C.T. van der Helm, “Quantification of intrinsic and reflexive properties during multi-joint arm posture,” Journal of Neuroscience Methods 155, pp. 328–349, 2006
- J. Wildenbeest. *Improving the quality of haptic feedback yields only marginal improvements in teleoperated task performance*. Master’s thesis, Delft University of Technology, 2010.